

Downloaded from UvA-DARE, the institutional repository of the University of Amsterdam (UvA)  
<http://dare.uva.nl/document/81670>

---

File ID        81670  
Filename      Thesis

---

SOURCE (OR PART OF THE FOLLOWING SOURCE):

Type            Dissertation  
Title            Dynamics of Gauge Fields at High Temperature  
Author          B.J. Nauta  
Faculty         Faculty of Science  
Year            2000  
Pages           128

FULL BIBLIOGRAPHIC DETAILS:

<http://dare.uva.nl/record/88056>

---

*Copyright*

*It is not permitted to download or to forward/distribute the text or part of it without the consent of the author(s) and/or copyright holder(s), other than for strictly personal, individual use.*

---

**Dynamics of Gauge Fields  
at  
High Temperature**

**Bert-Jan Nauta**

**Dynamics of Gauge Fields  
at  
High Temperature**



Print: Offsetdrukkerij Ridderprint B.V., Ridderkerk

# Dynamics of Gauge Fields at High Temperature

Academisch Proefschrift

ter verkrijging van de graad van doctor  
aan de Universiteit van Amsterdam,  
op gezag van de Rector Magnificus  
prof. dr. J.J.M. Franse

ten overstaan van een door het college voor promoties ingestelde  
commissie, in het openbaar te verdedigen in de Aula der Universiteit  
op woensdag 8 november 2000, te 14.00 uur

door

**Barend Jan Nauta**

geboren te Utrecht

Promotor: Prof. dr. C. van Weert

Promotiecommissie: Prof. dr. ir F.A. Bais  
Prof. dr. G. 't Hooft  
Prof. dr. J. H. Koch  
Dr. E. L. M. P. Laenen  
Prof. dr. C. J. M. Schoutens  
Prof. dr. J. Smit  
Dr. J. C. Vink

Faculteit der Natuurwetenschappen, Wiskunde en Informatica

# Contents

<b>1</b>	<b>Introduction</b>	<b>1</b>
1.1	Early universe . . . . .	1
1.2	Some dynamical processes in the early universe . . . . .	2
1.3	Classical approximation . . . . .	3
1.4	Preview . . . . .	6
<b>2</b>	<b>Classical field theory</b>	<b>9</b>
2.1	Introduction . . . . .	9
2.2	Thermal field theory . . . . .	9
2.3	Soft and hard modes . . . . .	11
2.4	High-temperature behavior . . . . .	13
2.5	Dimensional reduction . . . . .	16
2.6	Classical theory . . . . .	18
2.7	Hot, classical Feynman rules . . . . .	21
<b>3</b>	<b>Hard thermal loops</b>	<b>27</b>
3.1	Introduction . . . . .	27
3.2	HTL self-energy . . . . .	28
3.3	Vlasov equation . . . . .	31
3.4	Statistical HTL theory . . . . .	33
3.5	Stochastic HTL equation . . . . .	35
3.6	Consistency of stochastic HTL theory . . . . .	38
3.7	Non-Abelian HTL's . . . . .	40
3.8	Plasmons . . . . .	41
3.9	Non-perturbative excitations . . . . .	43
3.10	Summary . . . . .	46
<b>4</b>	<b>Divergence structure of hot, real-time classical field theory</b>	<b>49</b>
4.1	Introduction . . . . .	49

4.2	One-loop . . . . .	50
4.2.1	Linear divergences: classical HTL's . . . . .	50
4.2.2	No logarithmic divergences . . . . .	51
4.2.3	Classical self-energy: explicit result . . . . .	54
4.3	Two-loop and beyond . . . . .	55
4.3.1	Degree of divergence . . . . .	55
4.3.2	Two-loop self-energy diagrams . . . . .	57
4.3.3	Higher-order vertex functions . . . . .	61
4.3.4	Other gauges . . . . .	65
4.4	Discussion . . . . .	66
4.5	Transversality of the log divergent part of the self-energy . . . . .	67
4.6	Conclusion . . . . .	70
4.A	Gauge invariant cut-off in the classical theory . . . . .	71
4.B	Classical one-loop $SU(N)$ self-energy: explicit calculation . . . . .	72
4.C	Two loop naively linear divergent contributions . . . . .	73
<b>5</b>	<b>Counterterms for linear divergences</b>	<b>77</b>
5.1	Introduction . . . . .	77
5.2	Cut-off dependence . . . . .	78
5.3	Effective theory with counterterms . . . . .	80
5.4	Continuum . . . . .	81
5.5	Perturbative renormalization on a lattice . . . . .	83
5.5.1	Static . . . . .	83
5.5.2	Real-time . . . . .	84
5.6	Two stable lattice models . . . . .	87
5.6.1	Model with lattice dispersion relation . . . . .	87
5.6.2	Model with a continuum dispersion relation . . . . .	91
5.7	Conclusion . . . . .	94
<b>6</b>	<b>Baryon-number generation in the broken phase</b>	<b>95</b>
6.1	Introduction . . . . .	95
6.2	Sakharov requirements . . . . .	97
6.3	Sphaleron transitions . . . . .	99
6.3.1	Including a baryon density . . . . .	101
6.4	Effect of CP-violation on the rate . . . . .	102
6.4.1	Asymmetry . . . . .	105
6.4.2	Alternative derivation . . . . .	108
6.4.3	Numerical check . . . . .	109
6.4.4	Some remarks on an asymmetric distribution function . . . . .	111

*Contents*

vii

6.4.5 Fokker-Planck equation . . . . .	112
6.5 Baryon-number generation . . . . .	113
6.6 Conclusion . . . . .	116
6.A Chern-Simons number of the sphaleron . . . . .	117
6.B Simple example of asymmetry generation . . . . .	118
<b>Bibliography</b>	<b>119</b>
<b>Samenvatting</b>	<b>123</b>
<b>Dankwoord</b>	<b>127</b>



# 1 Introduction

## 1.1 Early universe

In the 1920's it was discovered that the universe is not static, but that it expands. The observed expansion lies at the basis of standard cosmology. A very successful model for the evolution of the universe is the hot Big Bang model [19, 73], which states that the universe is not infinitely old but came into existence 10-20 billion years ago. The universe started out extremely hot and dense after which it expanded and cooled down, to the present state. During its evolution and cooling down a number of interesting events took place, which we review with increasing temperature and therefore anti-chronologically (we prefer to start from the known and go towards the unknown).

At a temperature  $T = 0.3 \text{ eV} = 3575 \text{ K}$  (we use units where Boltzmann's constant  $k_B = 1$ ), about 200,000 years after the Big Bang, electrons combined with protons and photons decoupled from the plasma. The observed cosmic microwave background radiation (CMBR) is a relic of this event. The CMBR has a thermal spectrum at a temperature of about 2.7 K. This provides a direct observation of the thermal nature of matter in the early universe.

Direct observational evidence that supports the hot Big Bang model extends back to the epoch of primordial nucleosynthesis  $t = 0.01 - 100 \text{ sec}$  after the Big Bang at temperatures of about  $T = 0.1 - 10 \text{ MeV}$ . The observed light-element abundances are in agreement with what would be synthesized in a hot expanding universe. Theoretical calculations of the abundances requires one input parameter, the baryon to photon ratio. From the comparison of such calculations with observational data the baryon to photon density may be inferred [101]

$$\frac{n_B}{n_\gamma} = (1.55 - 4.45) \times 10^{-10}, \quad (1.1)$$

with the baryon-number density  $n_B$  and photon density  $n_\gamma$ .

From the knowledge of particle physics up to energies of about a few hundred GeV it is possible to extrapolate the model further back in time. There are at least two more interesting events that are then encountered. The deconfinement-confinement phase transition at  $T \approx 150$  MeV. Before this phase transition, quarks and gluons were not bounded but moved freely in the so-called quark gluon plasma (QGP). The existence of this new state of matter may have been experimentally confirmed at CERN last year.

Another event of interest in the early universe is the electroweak phase transition at  $T \approx 100$  GeV =  $10^{15}$  K, about  $t = 10^{-10}$  sec after the Big Bang. After the phase transition, the particles in the standard model acquire their masses through the Higgs mechanism. Before the transition, the Higgs expectation value is zero and particles are massless. (This is rather imprecise, since the particles form a plasma and we cannot consider them as free particles; in the plasma particles acquire thermal masses.)

The electroweak phase-transition forms the border between well-known cosmology and more speculative ideas about the universe. This may be illustrated by the phase transition itself. In the minimal standard model for experimentally allowed Higgs masses there is not a phase transition but instead a cross-over. However, a standard scenario for baryogenesis requires a first-order electroweak phase-transition. In extensions of the standard model, such as the minimal supersymmetric standard model, the transition may be first-order. It is possible to severely constrain the parameters of such models by the requirement that sufficient baryons are generated. This is an example, where cosmological observations are used to constrain particle-physics theories.

Finally, the evolution of the universe before the electroweak phase transition depends on the particle model (GUT, supersymmetric extensions of the standard model,...) that is valid for these higher energies. In general, more symmetry-breaking phase-transitions may have occurred.

## 1.2 Some dynamical processes in the early universe

An important motivation for the study of gauge fields at high temperatures comes from electroweak baryogenesis [105,106]. This deals with the question why the baryon-photon ratio has the value (1.1). One would like to explain this value without assumptions about the initial condition. Let us sketch here a standard scenario for electroweak baryogenesis due to Cohen, Kaplan and Nelson [40,100]. As we mentioned before, this scenario requires a first-order

electroweak phase-transition. At the phase-transition, bubbles will nucleate with in the interior the broken Higgs phase and outside the symmetric phase. These bubbles will expand and collide until the entire universe is in the broken phase.

A useful ingredient for this scenario is that baryon-violating processes in the broken phase are much slower than in the symmetric phase. For a strong enough phase transition, effectively no baryon-violating processes occur in the interior of the bubbles. These processes tend to wash out a non-zero baryon or anti-baryon-number density.

The expanding bubbles together with the baryon-number violating processes can be used to generate a resulting baryon number as follows. If one assumes particles and anti-particles scatter differently off the bubble wall there may be a net baryon-number density inside the bubble wall and an opposite net anti-baryon-number density outside the bubble wall (more precisely net number of left-handed baryons or anti-baryons). Outside the net anti-baryon density will be washed out by baryon-number violating processes. But the net baryon density inside the bubble will remain, leaving a non-zero baryon number density as the bubbles have filled out the universe.

In chapter 6 we will discuss some aspects of baryogenesis more in detail and suggest a different complementary scenario for baryon-number generation.

Another interesting dynamical process in the early universe is the formation of defects in symmetry breaking phase-transitions by the Kibble mechanism [70]. Topological stable configurations of gauge and Higgs fields exist as domain walls, cosmic strings and monopoles. These topological defects may affect the evolution of the universe, provide a dark matter candidate or, and may provide information over the earliest stages of the universe [73].

### 1.3 Classical approximation

There are a number of important processes in the early universe that involve dynamical Bose fields, such as bubble nucleation, the motion of a bubble wall, baryon-number violating processes and defect formation. These processes are difficult if not impossible to deal with perturbatively. An effective theory for the dynamics of Bose fields at high temperature is required.

An effective description of dynamical Bose fields is provided by the classical approximation [1, 2, 12, 13, 25, 36, 89, 95, 113]. Grigoriev and Rubakov

[50] were the first to use a classical approximation to study a dynamical process (soliton anti-soliton pair production) at high temperatures. The essential observation is that the processes of interest (for instance those listed at the beginning of this section) involve Bose fields that have a spatial size large compared to the inter-particle distance  $\hbar/T$ . This implies that the typical momentum is small compared to the temperature. The classical theory is expected to be a good approximation at low-energy because the classical limit  $\hbar \rightarrow 0$  and the low-energy limit of the Bose-Einstein distribution function  $n$  yield the same result:

$$n(\omega_{\mathbf{k}}) = \frac{1}{\exp(\beta\hbar\omega_{\mathbf{k}}) - 1} \rightarrow \frac{1}{\beta\hbar\omega_{\mathbf{k}}} \equiv n_{\text{cl}}(\omega_{\mathbf{k}}), \quad \hbar\omega_{\mathbf{k}} \ll T, \quad (1.2)$$

where  $\omega_{\mathbf{k}} = \sqrt{\mathbf{k}^2}$  is the frequency at wave-number  $\mathbf{k}$ ,  $\beta = 1/T$  the inverse temperature, and  $n_{\text{cl}}$  the ‘‘classical’’ distribution function. The classical approximation has been applied to calculate non-perturbative phenomena such as the Chern-Simons diffusion rate [6, 7, 86, 91, 115] (relevant for theories of baryogenesis [105, 106]) and the dynamics of the electroweak phase transition [85], as well as real-time (plasmon) properties of hot non-Abelian gauge theories [116].

However the classical approximation is not without problems. It has been well known since the work of Rayleigh, Einstein, and Jeans that in a classical description of a hot photon gas the free energy is ultraviolet divergent. For example, consider the Planck formula for the energy density for a gas of scalar bosons

$$E = \int \frac{d^3k}{(2\pi)^3} \frac{\hbar k}{e^{\beta\hbar k} - 1} = \frac{\pi^2 T^4}{30 \hbar^3}. \quad (1.3)$$

The classical limit (1.2) of the energy density is severely divergent

$$E_{\text{cl}} = \int \frac{d^3k}{(2\pi)^3} T = \frac{T}{6\pi^2} \Lambda^3, \quad (1.4)$$

where we introduced a UV-cut-off  $\Lambda$  on the integration. Hence, we cannot use the classical approximation for the calculation of the free energy. This is not surprising since the typical momentum of particles that contribute to the energy (1.3) is of the order of the temperature. For these momenta the classical approximation (1.2) is not expected to work anyway.

However, one might hope that for processes involving soft Bose fields the classical approximation is correct. An example of such a process is Chern-Simons number diffusion. Which is of interest for electroweak baryogenesis,

since it is related to the rate of baryon-number non-conservation [54, 75]. In the symmetric phase, the fields that have a typical momentum of order  $g^2T$ , with  $g$  the small gauge coupling, dominate the contribution to the rate [9]. In the broken phase, the typical momentum is of order  $gv$ , with  $v$  the Higgs expectation value. Close enough to the electroweak phase-transition the typical momentum of the fields is small compared to the temperature. Then, in both cases, one may expect that the classical approximation should provide a good estimate for the diffusion rate. Around 1995-1996, classical lattice simulations have been used for the calculation of the rate by Ambjørn and Krasnitz [6], Moore [84], and Smit and Tang [115]. However around the same time, it was argued by Bödeker, McLerran, and Smilga [25] that to really compute the Chern-Simons diffusion rate, hard thermal loop (HTL) corrections have to be included. HTL corrections were introduced, already around 1990, in the vocabulary of thermal field theory by Braaten and Pisarski [31]. They argued that bare perturbation theory breaks down in the calculation of soft amplitudes. To obtain a consistent expansion in the coupling  $g$  the HTL's have to be resummed.

A very relevant paper appeared in 1996, where Arnold, Son, and Yaffe [12] showed that the naive classical estimate for the diffusion rate in the symmetric phase  $\Gamma_{CS} \sim (g^2T)^4$ , changes to

$$\Gamma_{CS} \sim g^2\hbar(g^2T)^4, \quad (1.5)$$

when HTL effects are taken into account. Their analysis made clear that the dynamics of non-perturbative soft gauge fields is affected by hard modes. One consequence of this is, as they argued, that the classical rate is sensitive to the cut-off  $\Lambda$ .

Later it was shown by Bödeker [27], that the estimate (1.5) is not entirely correct in the small coupling limit, since scattering effects give a logarithmic correction to the Chern-Simons diffusion rate

$$\Gamma_{CS} \sim g^2\hbar(g^2T)^4 \log(1/g^2\hbar). \quad (1.6)$$

In his derivation, Bödeker started with an effective classical theory, where HTL corrections were included. From the above examples, it is clear that the classical approximation plays an important role in understanding non-perturbative processes at high temperature.

We end with some inspiring questions, that form a guideline for this thesis. Are there (non-perturbative) infrared processes independent of the cut-off? If not, what is the cut-off dependence? Can such a cut-off dependence

be removed by counterterms? Do we need to include quantum corrections into an effective classical theory? If so, how do these change the classical dynamics? What is the proper  $\hbar$ -expansion of the quantum theory at high temperature?

## 1.4 Preview

The main subject of this thesis is to improve classical field theory, that is, to include the dominant quantum corrections and to add counterterms for the Rayleigh-Jeans divergences. This will all be based on perturbation theory. Since the classical theory is intended for calculations where perturbation theory is of no use, this requires some explanation. The point is that for hard modes (modes with energy of the order of the temperature:  $\hbar\omega_{\mathbf{k}} \sim T$ ), for which the classical approximation (1.2) breaks down, perturbation theory is expected to work. This is confirmed by many explicit results, among which we mention the next-to-leading order calculations of Schulz [109] and Rebhan [104] and calculations presented in chapter 4 in this thesis. A pedagogical review of the argument that supports this viewpoint is given by Arnold in [14].

In chapter 2 we review some basic concepts and techniques of thermal field theory both for quantum and classical field theories. The tadpole resummation of Dolan and Jackiw [42], dimensional reduction [8, 33, 63, 80, 93], and classical thermal field theory [2, 102] are discussed. Also for some simple quantities the classical results are compared with the quantum results. We find the expected result that the classical contributions may be identified with the contributions of the soft modes.

In chapter 3, we turn to dominant quantum corrections, the well known hard thermal loops [31]. After a diagrammatic calculation of the HTL photon self-energy in QED, a kinetic formulation of HTL's is given, following the work of Blaizot and Iancu [20–22]. This formulation allows the HTL's to be included in a classical statistical theory, as was shown by Iancu [56]. We will show that the classical HTL equation of motion is consistent with the classical statistical theory, provided a random noise term is added. We review some of the physics included in HTLs, with a focus on the plasmon and non-perturbative excitations in the non-Abelian plasma. In particular, we will discuss the typical time scale for non-perturbative excitations is estimated, as was found by Arnold, Son, and Yaffe [12]

In chapter 4, we shall argue that, both in  $SU(N)$  gauge theory and in scalar field theory with a  $\phi^4$  interaction term, the divergences are restricted

to one- and two-loop (sub)diagrams [4]. This implies that the proof of Aarts and Smit [1,2] that local mass counterterms render classical  $\phi^4$ -theory finite up to two loops, may be extended to any number of loops. It will be shown that classical one-loop diagrams that correspond to HTL's in the quantum theory lead to linear divergences; all other one-loop diagrams are finite in the classical theory. Also we present a general argument that two-loop diagrams can at most give logarithmic divergences. This is explicitly verified for two-loop self-energy corrections in  $SU(N)$  and scalar theories. We also use the Ward identities to show that the logarithmic divergence in the  $SU(N)$  self-energy is transverse [16].

In chapter 5 we introduce counterterms for the linear divergences [98]. It was already expected that for linear divergences a subtraction in the plasmon frequency is sufficient to render the theory free of linear divergences at one loop [3, 56]. We will confirm this and, using the results of chapter 4, conclude that also beyond one loop, linear divergences will be absent. Furthermore, we will investigate the introduction of counterterms for classical lattice theories. In a sense, as explained there, we will find that to match a classical to a quantum theory is less complicated than to match a lattice theory to a continuum one. Nevertheless, in the latter case approximate counterterms may be given by a lattice generalization of the model in [56].

In the final chapter, we turn to a different topic, namely the problem of explaining the baryon asymmetry (1.1). Usually the required CP-violation is included in a model by an effective dimension-six operator [47,111]. We study the effect of dimension-eight CP-violating operators on sphaleron transitions [99]. We will argue that in a pure gauge theory in equilibrium the distribution function of the Chern-Simons number (that is related to the baryon number) will develop an asymmetry. Also a scenario for baryogenesis is presented where this effect is utilized.



## 2 Classical field theory

### 2.1 Introduction

The complicated nature of the dynamics of interacting thermal field theories has motivated the search for a regime where these theories simplify in some sense. It is generally believed that the high-temperature limit provides such a regime applying to physical quantities that are mainly determined by the low-energy and low mass  $\hbar\omega, m \ll T$  modes of the theory. This would simplify the description of many phenomena that are pertinent to the study of the early universe, the quark gluon plasma, and the electroweak phase-transition.

The traditional formulation of thermal field theory is based on the imaginary-time formalism. In this approach a  $d$ -dimensional system in equilibrium at temperature  $T = 1/\beta$  is encapsulated in a  $d + 1$ -dimensional box, with Euclidean extension  $\hbar\beta$ . In this picture the Euclidean time dimension is squeezed to zero in the high-temperature limit and the system is effectively confined to a  $d$ -dimensional space. In this dimensionally reduced space the system behaves classically because the high-temperature limit is at the same time the classical limit  $\hbar \rightarrow 0$ . If this classical approximation applies, non-linear physics would be amenable to classical methods.

In this chapter we will study the high-temperature limit for some specific quantities, and discuss the validity of the classical approximation. We confine ourselves to a scalar field theory and some heuristic reasoning. In chapter 4 we will take up a systematic study of the divergence structure of the classical theory. In general we will set  $\hbar = 1$ , except where the explicit dependence on  $\hbar$  is essential for the discussion. We generally follow the conventions of Itzykson and Zuber [58].

### 2.2 Thermal field theory

We start here with a short reminder of thermal quantum field theory; for reviews we refer to [18,79]. The situation we have in mind is a quantum system

with Hamiltonian  $H$  in equilibrium at temperature  $T = \beta^{-1}$ . Generally, one is interested in the thermal average of some observable  $O$

$$\langle O \rangle = Z^{-1} \text{Tr } O e^{-\beta H}, \quad (2.1)$$

or the partition function

$$Z(\beta, V) = \text{Tr } e^{-\beta H}, \quad (2.2)$$

as a function of the temperature and the volume  $V$  of the system; the trace is taken over a full set of states.

The practical calculation of such static thermal quantities derives from the observation that the Boltzmann weight  $e^{-\beta H}$  is the evolution operator that evolves a state from time  $t = 0$  to the imaginary time  $t = -i\beta$ , as first noted by F. Bloch in 1932. It allows the partition function (2.2) to be represented as an Euclidean functional integral over fields  $\phi(\tau, \mathbf{x})$  defined on the Euclidean time interval  $t = -i\tau$ , with  $\tau$  real  $0 < \tau < \beta$ :

$$Z = \int \mathcal{D}\phi(\tau, \mathbf{x}) e^{-\int_0^\beta d\tau L_E[\phi]}. \quad (2.3)$$

The Euclidean Lagrangian is related to the Lagrangian density  $\mathcal{L}$  in Minkowski space through

$$L_E = - \int d^3x \mathcal{L}(-i\tau, \mathbf{x}), \quad (2.4)$$

with the time  $t$  analytically continued to  $-i\tau$ . The trace restriction on the the states in (2.2) requires the fields to satisfy either periodic or antiperiodic boundary conditions

$$\phi(0, \mathbf{x}) = \pm \phi(\beta, \mathbf{x}). \quad (2.5)$$

Bosonic, fermionic, and Faddeev-Popov ghost fields satisfy periodic, anti-periodic, and periodic boundary conditions, respectively.

In momentum space the transition to Euclidean space is effected by the substitution  $k_0 \rightarrow i\omega_n$  to discrete Matsubara frequencies  $\omega_n = 2\pi nT$  for bosonic (and ghost) fields and  $\omega_n = \pi(2n + 1)T$  for fermionic fields, with  $n$  integer. By expanding Euclidean fields in Matsubara modes

$$\phi(\tau, \mathbf{x}) = \sum_n \phi_n(\mathbf{x}) e^{i\omega_n \tau}, \quad (2.6)$$

one obtains the propagators in momentum space. The propagator for bosons at temperature  $T$  reads

$$D(\omega_n, \mathbf{k}) = \frac{1}{\omega_n^2 + \mathbf{k}^2 + m^2}. \quad (2.7)$$

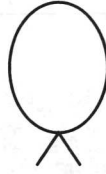


**Figure 2.1:** Tadpole contribution to the self-energy.

The great advantage of the Euclidean formulation of thermal field theory is that the Feynman rules are the same as at zero temperature except for the discrete frequencies in the propagator and the minus signs resulting from the change to a Euclidean metric  $K^2 = -\omega_n^2 - \mathbf{k}^2$  with an overall change of sign. In the next section some sample calculations are performed for a scalar theory.

### 2.3 Soft and hard modes

With regard to high-temperature field theory, it is useful to distinguish between long and short-wavelength excitations. We will illustrate this for scalar  $\lambda\phi^4$ -theory with Lagrangian density

$$\mathcal{L} = \frac{1}{2}(\partial\phi)^2 - \frac{1}{2}m^2\phi^2 - \frac{1}{4!}\lambda\phi^4, \quad (2.8)$$

at temperature  $T \gg m$ . We consider the contribution of the soft and hard modes to static (1PI) vertex functions at zero momentum. The one-loop self-energy represented by the tadpole diagram in fig. 2.1, is given by

$$\Sigma = \frac{1}{2}\lambda T \sum_n \int \frac{d^3k}{(2\pi)^3} \frac{1}{\omega_n^2 + \mathbf{k}^2 + m^2}, \quad (2.9)$$

with the sum running over the Matsubara frequencies  $\omega_n = 2\pi nT$ . The summation yields

$$\Sigma = \frac{1}{2}\lambda \int \frac{d^3k}{(2\pi)^3} \frac{1}{2\omega_{\mathbf{k}}} [1 + 2n(\omega_{\mathbf{k}})], \quad (2.10)$$

where  $n(\omega_{\mathbf{k}})$  is the Bose distribution as a function of the energy  $\omega_{\mathbf{k}}, \omega_{\mathbf{k}}^2 = \mathbf{k}^2 + m^2$ . The "1" in the square brackets corresponds to the zero-temperature contribution, which is quadratically UV-divergent. It may be renormalized

as at zero temperature, with a temperature-independent counterterm. It is a general feature of renormalizable quantum field theories that at non-zero temperature the zero-temperature counterterms suffice to make the theory finite [18]. Here and in the following, we will assume that the vacuum divergences are absorbed by temperature-independent counterterms. Then at high-temperature, the vacuum part may be ignored and the dominant terms in the high-temperature expansion of (2.10) are [42]

$$\Sigma = \frac{1}{24}\lambda T^2 - \frac{1}{8\pi}\lambda mT + \mathcal{O}(\lambda m^2). \quad (2.11)$$

Let us now distinguish between contributions from hard modes and soft modes to the self-energy (2.9). We may regard the sum over Matsubara frequencies as a sum over an infinite number of particles with increasing masses  $\omega_n$ . In the high-temperature limit  $m \ll T$  there is one light mode with mass  $\omega_0 = 0$  and an infinite number of heavy modes with masses  $\omega_1 = 2\pi T, \omega_2 = 4\pi T$  etc.

It is now natural to make a division into soft and hard-modes, by separating into zero and non-zero Matsubara modes [80]. The zero-mode contribution to the self-energy is

$$\begin{aligned} \Sigma_{n=0} &= \frac{1}{2}\lambda T \int \frac{d^3k}{(2\pi)^3} \frac{1}{\mathbf{k}^2 + m^2}, \\ &= \frac{1}{4\pi^2}\lambda\Lambda T - \frac{1}{8\pi}\lambda mT, \end{aligned} \quad (2.12)$$

where  $\Lambda$  is an UV cut-off. The linear divergence indicates that the integration in (2.12) is not dominated by low momenta, as might be expected naively. Later on we will comment on the significance of this divergence. The dominant contribution of the non-zero modes is

$$\Sigma_{n \neq 0} = \frac{1}{24}\lambda T^2 - \frac{1}{4\pi^2}\lambda\Lambda T + \mathcal{O}(\lambda m^2), \quad (2.13)$$

which contains the same divergent term. It drops out of the sum of the two last expressions which gives back the result (2.11) for the self energy as it should.

Let us continue with the one-loop four-point function at zero momentum, see diagram (a) in fig. 2.2. It reads

$$\Gamma^{(4)} = \frac{1}{2}\lambda^2 T \sum_n \int \frac{d^3k}{(2\pi)^3} \frac{1}{(\omega_n^2 + \mathbf{k}^2 + m^2)^2}. \quad (2.14)$$

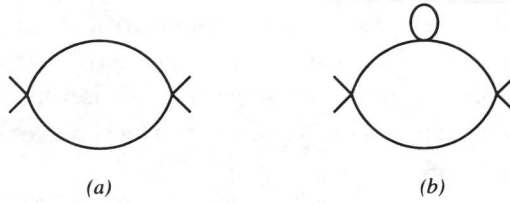


**Figure 2.2:** One loop (a) and a two-loop (b) contribution to the four-point function.

Again we consider the zero-mode and non-zero modes separately. The zero mode contributes

$$\Gamma_{n=0}^{(4)} = \frac{1}{16\pi} \lambda^2 \frac{T}{m}, \quad (2.15)$$

and the sum over non-zero modes

$$\Gamma_{n \neq 0}^{(4)} = \frac{1}{16\pi^2} \lambda^2 \log \left( \frac{T}{m} \right) + \mathcal{O}(\lambda^2). \quad (2.16)$$

It may be noted that both expressions are finite.

For higher-point functions the leading high-temperature behavior for zero- and non-zero modes is

$$\Gamma_{n=0}^{(2N)} \sim \lambda^N \frac{T}{m^{2N-3}} \quad N \geq 3, \quad (2.17)$$

$$\Gamma_{n \neq 0}^{(2N)} \sim \lambda^N \frac{1}{T^{2N-4}} \quad N \geq 3. \quad (2.18)$$

From the last expression we conclude that the contribution of the non-zero modes to higher-point vertex functions,  $N \geq 3$ , are subdominant.

## 2.4 High-temperature behavior

In this section we take a closer look at the sample calculations above. A number of important observations can be made with regards to the high-temperature behavior of thermal field theories:

1. We note that for  $m \rightarrow 0$  the one-loop contribution of the zero-modes to four and higher-point functions diverges. Also in that limit, two-loop diagrams dominate over one-loop diagrams. Consider for instance diagram (b) in fig. 2.2, it can be estimated to be of order  $\lambda^3 T^3 / m^3$ , hence

$$\Gamma^{(4),2l} \sim \Gamma^{(4),1l} \times \frac{\lambda T^2}{m^2}. \quad (2.19)$$

We see that when  $\lambda T^2/m^2 \gg 1$ , the two-loop contribution dominates over the one-loop one. Hence, the perturbation expansion is not valid. The solution to this problem is well known since the work of Dolan and Jackiw [42]: daisy diagrams have to be resummed. This amounts to the replacement of the vacuum mass by the thermal mass,

$$m_T^2 = m^2 + \frac{\lambda}{24} T^2, \quad (2.20)$$

in the Lagrangian (2.8) (and the subtraction of  $\lambda T^2/24$  as a mass counterterm to avoid overcounting). The one-loop results of the resummed theory may be obtained by the replacement  $m \rightarrow m_T$  in the previous formulas (2.11-2.18).

We note that only zero-mode contributions are affected by this replacement. The resummation of the tadpole in the propagator for the non-zero modes will only give subleading corrections, since  $\lambda T^2 \ll \omega_{n \neq 0}^2 \sim T^2$ . In a systematic expansion the resummation of thermal corrections to the mass is only necessary in the zero-mode propagator [10]. The hard-mode contributions are perturbatively calculable without resummation.

2. In the resummed theory there is, besides the usual expansion parameter  $\lambda$ , another one:

$$\lambda T/m_T \sim \lambda^{1/2}. \quad (2.21)$$

For instance, when we compare the one-loop contribution to the four-point function from the zero modes (2.15) with the tree-level contribution,  $\lambda$ , we find this expansion parameter. More generally, the occurrence of this expansion parameter can be seen as follows. We consider a diagram and add a loop to it, while we keep the number of external lines fixed. This brings in an extra interaction  $\lambda$ , an extra integration  $T \int d^3k$ , and two extra propagators  $(k^2 + m_T^2)^{-2}$ . Provided the integrations give a finite result, the typical scale of the momentum is given by the mass  $m_T$ . The total result is the expansion parameter  $\lambda T/m_T$ . Another way to see this is to note that besides a "bare"  $\lambda$  at finite temperature, there also appears a "dressed" coupling  $\lambda n(\omega_{\mathbf{k}})$ . Again, provided the integration is finite, we have  $k \sim m_T$  and  $\lambda n(\omega_{\mathbf{k}}) \sim \lambda T/m_T$ .

3. The zero-mode contributions are classical. Consider for instance the self-energy (2.10). The classical limit  $1 + 2n(\omega_{\mathbf{k}}) \rightarrow 2n_{\text{cl}}(\omega_{\mathbf{k}}) = 2T/\omega_{\mathbf{k}}$  gives the zero-mode contribution (2.12). Note that if we include  $\hbar$ 's in (2.10), we get one overall factor of  $\hbar$ , since it is a one-loop diagram. In the classical limit there occurs also an  $\hbar$  in the denominator from the classical distribution function  $n_{\text{cl}} = T/\hbar\omega_{\mathbf{k}}$ . The result is  $\hbar$ -independent and classical indeed.

4. The classical divergence (2.12) and dominant hard contribution (2.13) are the same for  $\Lambda \sim T$ . This may be understood by realizing that

in the quantum contribution the integration over momenta is cut-off by the Bose-Einstein distribution function at temperature  $T$ . Hence a similar result when the classical cut-off is taken to be of the order of the temperature may be expected. Later on, we will find that the correspondence between classical divergences and quantum hard-mode contributions holds in much more complicated cases.

As an aside we may note that a particular regularization exists, for which the classical contributions exactly equal the thermal quantum contributions for  $\Lambda = T$ . Namely, the regularization of the classical theory by

$$n_{\text{cl}} \rightarrow n_{\text{cl}} f(\Lambda, k, m, T), \quad (2.22)$$

with regularization function  $f = (\omega_{\mathbf{k}}/\Lambda)[\exp(\omega_{\mathbf{k}}/\Lambda) - 1]^{-1}$  (in (2.12), we have used  $f = \Theta(\Lambda - k)$ ). For  $\Lambda = T$  the regularized classical distribution is the Bose-Einstein distribution function. Hence, as far as thermal effects are concerned, the classical theory with this special regularization is equivalent to the quantum theory. However, the above regularization can only be implemented in perturbation theory. Since, the classical theory is eventually intended to be used for non-perturbative calculations, we will in the following not make use of this equivalence.

5. Finally, we will comment on a different way to divide the hard and soft-mode contributions. Namely one could introduce an intermediate scale  $\Lambda_{\text{int}}$  in between the mass and the temperature  $m \ll \Lambda_{\text{int}} \ll T$  [25, 49]. Modes are called hard when they have momenta  $k > \Lambda_{\text{int}}$  and soft when  $k < \Lambda_{\text{int}}$ . The soft contribution to the self-energy is then

$$\Sigma_{\text{soft}} = \frac{1}{4\pi^2} \lambda \int_0^{\Lambda_{\text{int}}} dk k^2 \frac{1}{2\omega_{\mathbf{k}}} [1 + 2n(\omega_{\mathbf{k}})]. \quad (2.23)$$

Due to the restriction on the integration over  $k$ , we have the inequality  $\omega_{\mathbf{k}} \ll T$ . Therefore the integrand may be expanded in  $\beta\omega_{\mathbf{k}}$ . This yields

$$\Sigma_{\text{soft}} = \frac{1}{4\pi^2} \lambda \Lambda_{\text{int}} T - \frac{1}{8\pi} \lambda m T + \frac{1}{144\pi^2 T} \lambda \Lambda_{\text{int}}^3 + \mathcal{O}(T^{-2} \Lambda_{\text{int}}^4). \quad (2.24)$$

We compare this with the zero-mode contribution (2.12). The cut-off  $\Lambda$  in (2.12) was introduced to regularize the linear divergence. When we take this cut-off small compared to the temperature  $m \ll \Lambda \ll T$ , the results (2.12) and (2.24) agree. In that case, there is no essential difference in the two ways to separate hard from soft modes. The advantage of the division into zero and non-zero Matsubara modes is that the cut-off may also be taken large compared to the temperature.

## 2.5 Dimensional reduction

The first important observation of the previous section was that for a small mass perturbation theory breaks down. We also remarked that this can be cured by a resummation of the thermal mass in the propagator for the zero modes. Here we will discuss a systematic method to perform this and more advanced resummations that goes under the name of dimensional reduction. In thermal field theory the dimensional reduction technique has been used to calculate the free energy of  $\lambda\phi^4$ -theory and QCD [33, 34], and properties of the electroweak phase-transition [45, 63].

The basic idea is to construct an effective theory for the soft mode field  $\phi_0(\mathbf{x})$ , which lives on 3D Euclidean space [8, 93], by integrating out the heavy modes  $\phi_n(\mathbf{x})$ ,  $n \neq 0$  in the path integral (2.3). If all influence of the hard modes is ignored, the weight factor in the path integral reduces to a classical Boltzmann factor

$$\exp -\hbar^{-1} \int_0^{\hbar/T} d\tau L_E \rightarrow \exp -\beta E_{\text{cl}} \quad (2.25)$$

with the energy of the three-dimensional theory

$$E_{\text{cl}} = \int d^3x \left[ \frac{1}{2} (\nabla\phi_0)^2 + \frac{1}{2} m^2 \phi_0^2 + \frac{1}{4!} \lambda \phi_0^4 \right]. \quad (2.26)$$

In the high-temperature limit  $T \rightarrow \infty$  this dimensionally reduced theory is purely classical. One may note that we do not include here a factor  $\sqrt{T}$  in the fields, as is common in the literature.

The effective 3D theory can be improved by systematic inclusion of thermal corrections that arise from the non-zero Matsubara modes. Following [45, 63], we restrict the effective theory to contain only local superrenormalizable (in three dimensions) operators

$$\mathcal{L}_{\text{eff}} = \frac{1}{2} (\nabla\phi_3)^2 + \frac{1}{2} (m_3^2 - \delta m^2) \phi_3^2 + \frac{1}{4!} \lambda_3 \phi_3^4. \quad (2.27)$$

The field  $\phi_3$  is the zero mode of the original 4D theory, including perturbative corrections:  $\phi_3 = \sqrt{Z_3} \phi_{n=0}$  with  $Z_3 = 1 + \mathcal{O}(\lambda^2)$ . The parameters of the effective theory should be chosen such that the correlation functions of the effective theory reproduce as good as possible the static correlation functions of the 4D quantum theory at low momenta. The accuracy that in general can be obtained by a proper choice of the coefficients may be given by the relative error in the correlation functions calculated with the effective theory [63].

For the effective theory (2.27) the relative error is  $\mathcal{O}(\lambda^{\frac{3}{2}})$  [65]. For particular quantities, such as the free energy, a higher accuracy can be obtained [33].

For our purpose it is sufficient to illustrate this for an effective theory that is accurate up to leading order, since a higher accuracy will not survive the generalization from static to non-static correlation functions that we are interested in. To leading order, the effective coupling is simply given by  $\lambda_3 = \lambda$ . For the mass and the counterterm, one has to include one and two-loop thermal corrections

$$m_3^2 = m^2 + m_{1l}^2 + m_{2l}^2, \quad (2.28)$$

$$\delta m^2 = \delta m_{1l}^2 + \delta m_{2l}^2. \quad (2.29)$$

At one loop

$$m_{1l}^2 = \frac{\lambda}{24} T^2, \quad (2.30)$$

$$\delta m_{1l}^2 = \lambda \frac{\Lambda}{8\pi^2} T. \quad (2.31)$$

This is nothing but the tadpole correction from the non-zero Matsubara modes (2.13) split up in a finite part and a divergent counterterm. The inclusion of this correction in the effective theory for the zero modes, is another way to implement the tadpole resummation discussed in section 2.4.

The two-loop correction

$$m_{2l}^2 = -\lambda^2 T^2 \frac{1}{16\pi^2} (\log(T/m) + \dots), \quad (2.32)$$

is subdominant. However, at two-loop there is also a divergence in the self-energy that needs to be renormalized

$$\delta m_{2l}^2 = -\lambda^2 T^2 \frac{1}{16\pi^2} \log(\Lambda/m) + \text{"finite"}. \quad (2.33)$$

Note the equivalence of the hard mode contribution (2.32) and the classical divergence (2.33) when  $\Lambda \sim T$ .

The conclusion is that static correlation functions can be calculated to leading order with an effective classical theory when this theory includes the dominant hard mode contribution and counterterms for the linear and logarithmic divergence [33, 63].

## 2.6 Classical theory

The dimensionally reduced theory for the zero-mode field  $\phi_3(\mathbf{x})$  defined by the effective Lagrangian (2.27) is in essence a classical theory. Omitting the subscript on the field, we may write the corresponding Hamiltonian as

$$H = \int d^3x \left( \frac{1}{2} \pi^2 + \frac{1}{2} \mu^2 \phi^2 \right) + H_{\text{int}}, \quad (2.34)$$

where  $\mu$  is the effective mass and  $H_{\text{int}}$  the interaction Hamiltonian, which may include any local  $n$ -point coupling that respects the symmetries of the system [33]. As discussed in the preceding section, these couplings are determined by matching correlation functions of the effective theory:

$$\langle \phi(\mathbf{x}_1) \phi(\mathbf{x}_2) \dots \rangle = Z^{-1} \int D\pi D\phi \phi(\mathbf{x}_1) \phi(\mathbf{x}_2) \dots e^{-\beta H[\pi, \phi]}, \quad (2.35)$$

$$Z = \int D\pi D\phi e^{-\beta H[\pi, \phi]}, \quad (2.36)$$

to the static correlation functions of the full quantum theory.

It is straightforward to extend the classical field theory defined by the procedure of dimensional reduction to time-dependent fields; for a review of classical field theory see e.g. [102]. We prescribe Hamiltonian equations of motion

$$\dot{\phi} = \frac{\delta H}{\delta \pi}, \quad (2.37)$$

$$\dot{\pi} = -\frac{\delta H}{\delta \phi}, \quad (2.38)$$

with initial conditions imposed at some initial time  $t_{\text{in}}$

$$\phi(t_{\text{in}}, \mathbf{x}) = \phi_{\text{in}}(\mathbf{x}), \quad (2.39)$$

$$\pi(t_{\text{in}}, \mathbf{x}) = \pi_{\text{in}}(\mathbf{x}). \quad (2.40)$$

Time-dependent correlation functions are calculated by first solving the equations of motion with initial conditions (2.40). This gives a solution  $\phi(t, \mathbf{x}, [\pi_{\text{in}}, \phi_{\text{in}}])$  that depends on time and the initial fields. Correlation functions are then obtained by a thermal average over initial fields:

$$\langle \phi(t_1, \mathbf{x}_1) \phi(t_2, \mathbf{x}_2) \dots \rangle = \quad (2.41)$$

$$Z^{-1} \int D\pi_{\text{in}} D\phi_{\text{in}} \phi(t_1, \mathbf{x}_1, [\pi_{\text{in}}, \phi_{\text{in}}]) \phi(t_2, \mathbf{x}_2, [\pi_{\text{in}}, \phi_{\text{in}}]) \dots e^{-\beta H[\pi_{\text{in}}, \phi_{\text{in}}]}.$$

As an example we consider the two-point function for a free scalar theory. After a spatial Fourier transform we easily find the solution of the the equations of motion in terms of the initial conditions (2.38) as

$$\phi_0(t, \mathbf{k}, [\pi_{\text{in}}, \phi_{\text{in}}]) = \phi_{\text{in}}(\mathbf{k}) \cos \omega_{\mathbf{k}}(t - t_{\text{in}}) + \frac{\pi_{\text{in}}(\mathbf{k})}{\omega_{\mathbf{k}}} \sin \omega_{\mathbf{k}}(t - t_{\text{in}}), \quad (2.42)$$

with frequency  $\omega_{\mathbf{k}}$ ,  $\omega_{\mathbf{k}}^2 = \mathbf{k}^2 + \mu^2$ , and wave-number  $\mathbf{k}$ . This solution may be substituted into (2.41). The thermal average over the initial conditions can be calculated as

$$\langle \phi_{\text{in}}(-\mathbf{k}) \phi_{\text{in}}(\mathbf{k}) \rangle_0 = \frac{T}{\omega_{\mathbf{k}}^2}, \quad \langle \phi_{\text{in}}(-\mathbf{k}) \pi_{\text{in}}(\mathbf{k}) \rangle_0 = 0, \quad \langle \pi_{\text{in}}(-\mathbf{k}) \pi_{\text{in}}(\mathbf{k}) \rangle_0 = T, \quad (2.43)$$

which yields the free classical two-point correlation function

$$S_0(t_1 - t_2, \mathbf{k}) = \langle \phi_0(t_1, -\mathbf{k}) \phi_0(t_2, \mathbf{k}) \rangle_0 = \frac{T}{\omega_{\mathbf{k}}^2} \cos \omega_{\mathbf{k}}(t_1 - t_2). \quad (2.44)$$

When interactions are included in the classical theory, one may perform a perturbation expansion for small coupling. For definiteness, let us consider a three- and a four-point coupling

$$H_{\text{int}} = \int d^3x \left( \frac{1}{3!} g \phi^3 + \frac{1}{4!} \lambda \phi^4 \right). \quad (2.45)$$

In terms of the solution (2.42) of the free problem, a perturbative solution of the equations of motion

$$(\partial_t^2 - \nabla^2 + \mu^2) \phi = -\frac{\delta H_{\text{int}}}{\delta \phi}, \quad (2.46)$$

is constructed with the help of the free retarded Green function  $G_0^R(x)$ , as

$$\phi(x) = \phi_0(x) + \int d^4x' G_0^R(x - x') \frac{\delta H_{\text{int}}[\phi_0]}{\delta \phi_0(x')} + \dots, \quad (2.47)$$

to first order in the coupling constants. The procedure may be iterated to higher orders. In spatial and temporal momentum space the retarded free propagator is

$$G_0^R(K) = \frac{1}{\omega_{\mathbf{k}}^2 - (k^0 + i\epsilon)^2} = \sum_{s=\pm} \frac{1}{2\omega_{\mathbf{k}}} \frac{s}{k^0 + i\epsilon + s\omega_{\mathbf{k}}}, \quad (2.48)$$

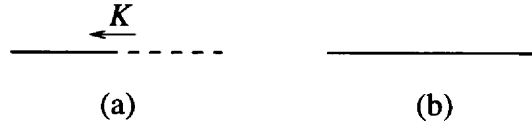


**Figure 2.3:** Propagators, (a)  $G_0^R(K) = G_0^A(-K)$ , (b)  $iS_0(K)$ .

By inserting the expansion (2.47) into  $\langle \phi(x_1)\phi(x_2) \rangle$ , and by ordering according to the power of the coupling constants, the perturbative expansion of the correlation function is constructed. The thermal information is carried by the thermal propagator obtained by a temporal Fourier transform of (2.44)

$$\begin{aligned} S_0(K) &= \hbar n_{\text{cl}}(k^0) \epsilon(k^0) 2\pi \delta(k_0^2 - \omega_{\mathbf{k}}^2) \\ &= \sum_{s=\pm} \hbar n_{\text{cl}}(s\omega_{\mathbf{k}}) \frac{1}{2\omega_{\mathbf{k}}} 2\pi s \delta(k^0 - s\omega_{\mathbf{k}}), \end{aligned} \quad (2.49)$$

$$n_{\text{cl}}(k^0) = \frac{T}{\hbar k^0}, \quad \omega_{\mathbf{k}} = \sqrt{\mathbf{k}^2 + \mu^2}, \quad \epsilon(k^0) = \theta(k^0) - \theta(-k^0). \quad (2.50)$$

Note that the combination  $\hbar n_{\text{cl}}$ , which occurs in the thermal propagator  $S_0$ , is independent of  $\hbar$ . The (free) retarded and (free) thermal two-point function are related by the classical KMS condition [2, 102]

$$iS_0(K) = \hbar n_{\text{cl}}(k^0) [G_0^R(K) - G_0^A(K)], \quad (2.51)$$

where  $G_0^A(K) = G_0^R(-K)$  is the free advanced Green function.

The perturbative terms may be represented by diagrams in the following way [1, 2]. Lines in the diagrams are either  $G_0^R$  lines coming from the solution (2.47), or  $S_0$  lines coming from the thermal average of products of initial fields  $\phi_{\text{in}}$ . In figure 2.3 the dashed-full line represents the retarded and advanced Green functions and the full line the thermal propagator  $iS_0$ . The retarded and advanced Green functions are distinguished by the direction of the momentum flow through the propagator, as indicated by the arrow. Classical loop integrals containing these two-point functions arise from the spacetime integral(s) in (2.47). From the structure of the interaction term it may be deduced that the interaction vertices have always one retarded (advanced) propagator attached; see fig 2.4.

In principle one can go on and find all possible diagrams in this way. However, explicitly solving the equations of motion perturbatively and making all possible contractions becomes rather cumbersome at higher order in the coupling constants. Therefore, in the next section a general procedure



**Figure 2.4:** Classical vertices

is given for obtaining the complete set of rules from the classical limit of the underlying quantum perturbative approach.

In a perturbation expansion for  $\lambda\phi^4$ -theory one encounters the same linear and logarithmic divergences as in the dimensional reduced theory. Hence, one expects that the effective Lagrangian (2.27) which includes the resummed thermal mass and counterterms for the linear and logarithmic divergences will lead to finite results. It has been shown in [1, 2] that this works. The classical field theory with effective Lagrangian (2.27) is finite up to two loops and gives the same results as the quantum theory in leading order. This will be further discussed in the next chapter.

The situation for a scalar field theory can be summarized as follows: the dominant hard mode contribution, the tadpole mass, must be included in the classical theory. This corresponds to the resummation of daisy diagrams. Furthermore, linear as well as logarithmic divergences in the classical self-energy can be removed by the inclusion of mass counterterms. The resulting classical correlation functions are finite and give the leading order to the full quantum result. To extend this effective classical theory to gauge theories will be the goal of the following three chapters.

Before we turn to gauge theories we discuss the diagrammatics of the classical theory.

## 2.7 Hot, classical Feynman rules

In this section we discuss the diagrammar of classical perturbation theory, i.e. the classical Feynman rules at finite temperature, in scalar field theory. As we will show, classical perturbation theory can be derived as the  $\hbar \rightarrow 0$  limit

of the well-known closed-time-path (CTP) formulation of the quantum field theory [68, 79, 110]. The CTP method involves a time-contour  $\mathcal{C}$  that consists of two branches, the upper branch  $\mathcal{C}_+$  that runs up the real-time axis and the lower branch  $\mathcal{C}_-$  that runs back in time. This leads to a doubling of the fields, denoted as  $\phi_+, \phi_-$  to indicate on which branch they live. As a consequence, the propagator takes a matrix form

$$\mathbf{G}(x - x') = \begin{pmatrix} G^{++}(x - x') & G^{+-}(x - x') \\ G^{-+}(x - x') & G^{--}(x - x') \end{pmatrix}, \quad (2.52)$$

where the different superscripts specify the possible positions on and orderings along the contour. From the definition one deduces that the components satisfy the identity

$$G^{++} - G^{+-} - G^{-+} + G^{--} = 0, \quad (2.53)$$

the so-called largest-time equation. The interaction terms in the action also double

$$\begin{aligned} S_{\text{int}} &= - \int_{\mathcal{C}} dt H_{\text{int}} \\ &= - \int d^4x \left( \frac{1}{3!} g \phi_+^3 - \frac{1}{3!} g \phi_-^3 + \frac{1}{4!} \lambda \phi_+^4 - \frac{1}{4!} \lambda \phi_-^4 \right), \end{aligned} \quad (2.54)$$

with the minus sign coming from the negative orientation of the lower branch of the contour.

For the purpose of taking the classical limit, a convenient variation is the Keldysh formalism, which involves a change of basis from  $\phi_{+,-}$  to a "classical" field  $\phi_1$  and a "quantum" field  $\phi_2$ :

$$\begin{pmatrix} \phi_1 \\ \phi_2 \end{pmatrix} = \begin{pmatrix} (\phi_+ + \phi_-)/2 \\ (\phi_+ - \phi_-)/\hbar \end{pmatrix}, \quad (2.55)$$

such that the (free) matrix propagator takes the form [2]

$$\mathbf{G}_0(x - x') \rightarrow \begin{pmatrix} F_0(x - x') & iG_0^R(x - x') \\ iG_0^A(x - x') & 0 \end{pmatrix}. \quad (2.56)$$

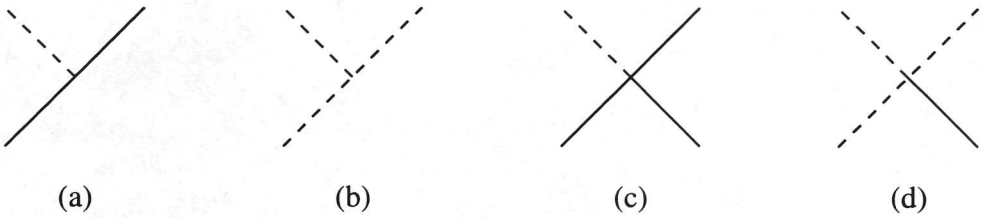


**Figure 2.5:** Vertices, (a)  $\frac{1}{2}g\phi_1^2\phi_2$ , (b)  $\hbar^2\frac{1}{4!}g\phi_2^3$ , (c)  $\frac{1}{3!}\lambda\phi_1^3\phi_2$ , (d)  $\hbar^2\frac{1}{4!}\lambda\phi_1\phi_2^3$ .

Here the free retarded and advanced Green function are given in momentum space by the (classical) expression (2.48), and the quantum thermal two-point function in momentum space reads

$$F_0(K) = \hbar \sum_{s=\pm} [n(s\omega_{\mathbf{k}}) + \frac{1}{2}] \frac{1}{2\omega_{\mathbf{k}}} 2\pi s \delta(k^0 - s\omega_{\mathbf{k}}), \quad n(\omega_{\mathbf{k}}) = \frac{1}{\exp(\beta\hbar\omega_{\mathbf{k}}) - 1}, \quad (2.57)$$

which reduces to the classical propagator (2.49) in the classical limit. The (free) retarded and thermal two-point functions are related by the KMS condition

$$F_0(K) = i\hbar n(k^0) [G_0^R(K) - G_0^A(K)]. \quad (2.58)$$

We note that the inclusion of the factor  $\hbar$  in (2.55) is essential to obtain the proper classical limits.

Feynman rules appear when the interaction part along the closed time path contour (2.54) is written in terms of the  $\phi_{1,2}$  fields [43]

$$S_{\text{int}} = -\hbar \int d^4x \left( \frac{1}{2}g\phi_1^2\phi_2 + \frac{\hbar^2}{4!}g\phi_2^3 + \frac{1}{3!}\lambda\phi_1^3\phi_2 + \frac{\hbar^2}{4!}\lambda\phi_1\phi_2^3 \right). \quad (2.59)$$

The vertices are presented pictorially in fig. 2.5. The  $\phi_1$  field is denoted by a full line and the  $\phi_2$  field by a dashed line.

We now discuss the  $\hbar \rightarrow 0$  limit of these real-time quantum Feynman rules. This limit affects the diagrams in two ways. The first one is obvious, the thermal propagator  $F_0$  has to be replaced by  $S_0$ . The second one leads to a drastic simplification: because of the relative order in  $\hbar$ , only the vertices (a) and (c) in fig. 2.5 contribute in the classical limit, and the two other vertices (b) and (d) can be neglected.

This can also be seen as follows: vertices (b) and (d) can only appear in a diagram with retarded (or advanced) Green functions attached to the

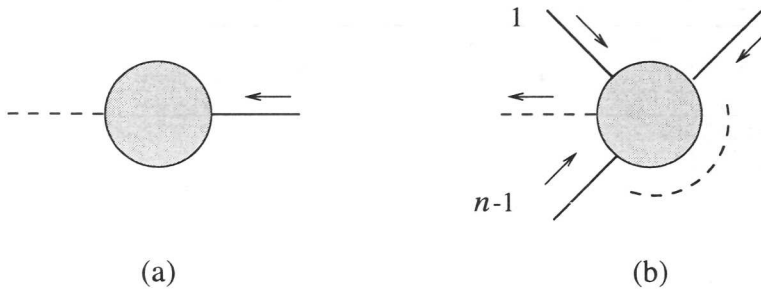


**Figure 2.6:** (a) Retarded self-energy, (b) generalized retarded  $n$ -point vertex functions.

three dashed legs. After attaching these Green functions, the resulting outer lines (which either still have to be attached to another vertex or are external lines) are always full lines. However, such a configuration can be constructed as well with vertices (a) and (c): these vertices have two full legs where (b) resp. (d) have two dashed legs. By attaching two thermal two-point functions on these legs, the external lines are full as well, and the vertices can be part of a diagram in exactly the same manner. But each classical thermal two-point contains one distribution function and therefore a relative factor  $1/\hbar$ . Diagrams with vertex (a) or (c) have two more thermal two-point functions than the corresponding diagrams with vertex (b) or (d). Hence, the first class of diagrams is relatively stronger in the classical limit with respect to the second class by a factor  $1/\hbar^2$ .<sup>1</sup> In other words, vertices (b) and (d) will be  $\mathcal{O}(\hbar^2)$  suppressed with respect to vertices (a) and (c).

We surmise that classical Feynman rules follow from the quantum ones by taking  $\hbar$  to zero, which results in the following rules:

1. Correlation functions have  $n$  full external ‘legs’.
2. The retarded self energy and the so-called generalized retarded  $n$ -point vertex functions [43] have one dashed ‘leg’ and  $n - 1$  full ‘legs’. These are shown in fig. 2.6. Arrows denote the momentum flow of the external momenta.
3. To calculate these quantities in the classical limit, draw all diagrams as in the quantum case, but use only vertices (a) and (c).
4. Replace the thermal propagator  $F_0$  by its classical counterpart  $S_0$ .

An explicit check of these rules (by a comparison with the results obtained by perturbatively solving the equations of motion and averaging over the initial

1. Negative powers of  $\hbar$  will of course be canceled by positive powers coming from loop counting.

conditions) can be found in [2] for the case of  $\lambda\phi^4$ -theory for the two-point function up to two loops and the four-point function to one loop .



## 3 Hard thermal loops

### 3.1 Introduction

Around 1988 the following problem arose in thermal field theory: one-loop calculations of the gluon damping rate in the high-temperature limit turned out to be gauge dependent, see e.g. [38] and references therein, although it was generally believed that this physical quantity should be gauge independent (as was proven later [72]). The problem was even more accentuated by the fact that in certain gauges the damping rate turned out to be negative, which would indicate the instability of the quark gluon plasma. The cause of the problem is that at one-loop the dominant contribution to the integration over soft momenta is of order  $gT$ . For these momenta there are higher-loop corrections that are not suppressed. This situation is similar to the one in section 2.3 (as discussed particularly in remark 1. in section 2.4), where for a small mass  $m \ll T$  loop corrections exist that are unsuppressed also. The solution to the damping rate problem is that these unsuppressed contributions need to be resummed. The resummed one-loop contribution to the damping rate is gauge independent and positive [32].

The terms that need to be resummed to obtain a consistent perturbation theory are called hard thermal loops (HTL's). By definition the hard thermal loops are loop-contributions from the integration region  $K \sim T$  that are as large as the tree-level contribution for (external) momenta  $P \sim gT$  [31].

We have encountered already an example of a hard thermal loop, namely the tadpole self-energy in  $\lambda\phi^4$ -theory, see section 2.3. We recall that the tadpole self-energy is of order  $\lambda T^2 \sim g^2 T^2$ , setting  $\lambda \sim g^2$ . The tree-level part of the two-point vertex function is  $P^2 - m^2$ . For  $P, m \sim gT$ , the tadpole self-energy is as large as the tree-level part. Hence, it is a hard thermal loop. This is the only hard thermal loop that occurs in  $\lambda\phi^4$ -theory. The need for resummation of this contribution was already discussed in section 2.4; see remark 1..

In this chapter we will review the hard thermal loops for gauge theories. We start with a diagrammatic calculation of the HTL self-energy in QED.

### 3.2 HTL self-energy

As an interesting example of a hard thermal loop, we consider the photon self-energy in QED. The HTL contribution comes from the one-loop diagram. Since the loop consists of fermion lines, the diagram does not depend on the gauge. However, for a non-Abelian theory the one-loop gluon self-energy is generally gauge dependent, and only after the HTL approximations, that will be discussed below, a gauge independent result is obtained.

Again, we will compare the self-energy with the tree-level two-point vertex, which for soft momenta  $P \sim eT$  is estimated as

$$\Gamma^{(2)}(P) \sim P^2 \sim e^2 T^2. \quad (3.1)$$

We now look for terms in the photon self-energy that are of the same order. At one-loop the self-energy reads

$$\begin{aligned} \Pi_{\mu\nu}(P) = 4e^2 \int \frac{d^3\mathbf{k}}{(2\pi)^3} \{ & A_{\mu\nu} I^1(\omega_{\mathbf{k}}) \\ & + B_{\mu\nu}(\mathbf{k}, P) [I^2(p_0, \omega_{\mathbf{k}}, \omega_{\mathbf{p}-\mathbf{k}}) + I^3(p_0, \omega_{\mathbf{k}}, \omega_{\mathbf{p}-\mathbf{k}})] \}, \end{aligned} \quad (3.2)$$

with the tensors

$$\begin{aligned} A_{\mu\nu} &= 2g_{\mu 0} g_{\nu 0} + g_{\mu\nu}, \\ B_{\mu\nu}(\mathbf{k}, P) &= 2\bar{K}_\mu \bar{K}_\nu - P_\mu \bar{K}_\nu - \bar{K}_\mu P_\nu - g_{\mu\nu} \bar{K} \cdot P. \end{aligned} \quad (3.3)$$

Here we defined the on-shell four-vector  $\bar{K}^\mu = (\omega_{\mathbf{k}}, \mathbf{k})$ ,  $\omega_{\mathbf{k}} = \sqrt{\mathbf{k}^2 + m_e^2}$  with electron mass  $m_e$ . The remaining terms in the integrand read

$$\begin{aligned} I^1 &= \frac{1}{2\omega_{\mathbf{k}}} [1 - 2\tilde{n}(\omega_{\mathbf{k}})], \\ I^2 &= \frac{1}{4\omega_{\mathbf{k}}\omega_{\mathbf{p}-\mathbf{k}}} [1 - \tilde{n}(\omega_{\mathbf{k}}) - \tilde{n}(\omega_{\mathbf{p}-\mathbf{k}})] \times \\ &\quad \left( \frac{1}{p_0 + i\epsilon + \omega_{\mathbf{k}} + \omega_{\mathbf{p}-\mathbf{k}}} - \frac{1}{p_0 + i\epsilon - \omega_{\mathbf{k}} - \omega_{\mathbf{p}-\mathbf{k}}} \right), \\ I^3 &= \frac{1}{4\omega_{\mathbf{k}}\omega_{\mathbf{p}-\mathbf{k}}} [\tilde{n}(\omega_{\mathbf{k}}) - \tilde{n}(\omega_{\mathbf{p}-\mathbf{k}})] \times \\ &\quad \left( \frac{1}{p_0 + i\epsilon + \omega_{\mathbf{k}} - \omega_{\mathbf{p}-\mathbf{k}}} - \frac{1}{p_0 + i\epsilon + \omega_{\mathbf{k}} - \omega_{\mathbf{p}-\mathbf{k}}} \right), \end{aligned} \quad (3.4)$$

with  $\tilde{n} = (e^{\beta\omega_{\mathbf{k}}} + 1)^{-1}$  the Fermi-Dirac distribution at zero chemical potential. The  $\epsilon$ -prescription used in (3.4) gives the retarded self-energy. Time-ordered, advanced, symmetric or other self-energies are related to the retarded one by the KMS condition [18, 79].

The HTL contribution is obtained from the full one-loop expression (3.2) by a number of approximations that are discussed below. Let us start with the first term in (3.2). It contains a  $T = 0$  contribution, coming from the "1" between square brackets in the expression for  $I^1$  (3.4), and a thermal contribution that comes from the distribution function. In the high-temperature limit, the thermal contributions dominate over the  $T = 0$  quantum contributions, hence the "1" in  $I^1$  may be neglected. Furthermore, the temperature is taken to be much larger than the electron mass. Since the internal momentum is of the order of the temperature  $\mathbf{k} \sim T \gg m_e$ , one may use the approximation  $\omega_{\mathbf{k}} \approx k$ , with  $k = |\mathbf{k}|$ . With these approximations, the integral that is needed for the first term in the self-energy reads

$$\int \frac{d^3k}{(2\pi)^3} \frac{1}{k} \tilde{n}(k) = \frac{T^2}{24}. \quad (3.5)$$

Next, we consider the HTL approximation for the tensor  $B_{\mu\nu}$ . Since the external momentum  $P \sim eT$  is small compared to the internal momentum  $\bar{K} \sim T$ , one may write

$$B_{\mu\nu} \approx 2\bar{K}_\mu \bar{K}_\nu \approx 2k^2 V_\mu V_\nu, \quad (3.6)$$

where in the last member we used that  $\omega_{\mathbf{k}} \approx k$ . Further, the four velocity  $V^\mu = (1, \mathbf{v})$ , with  $\mathbf{v} = \mathbf{k}/k$ , was introduced. Also in the factor  $I^2$  the electron mass and external momentum may be neglected, which gives

$$I^2 \approx \frac{1}{k^3} \tilde{n}(k). \quad (3.7)$$

The factor  $I^3$  is more interesting, since in the denominators the external momentum cannot simply be neglected. For instance, for  $p_0, \mathbf{p} \ll k$  one has

$$\frac{1}{p_0 + i\epsilon - \omega_{\mathbf{k}} + \omega_{\mathbf{p}-\mathbf{k}}} \approx \frac{1}{p_0 + i\epsilon - \mathbf{p} \cdot \mathbf{v}}. \quad (3.8)$$

Hence, for small external momenta the factor  $I^3$  becomes

$$I^3 = \frac{1}{4k^2} \tilde{n}'(k) \mathbf{p} \cdot \mathbf{v} \left( \frac{1}{\hat{V} \cdot P + i\epsilon} - \frac{1}{V \cdot P + i\epsilon} \right), \quad (3.9)$$

with the notation  $\hat{V}^\mu = (1, -\mathbf{v})$  and  $\tilde{n}'(k) = d\tilde{n}(k)/dk$ . Note that in (3.9) the dependence on the radial and angular part of the integration variable  $\mathbf{k}$  is factorized. Since the other factors in the self-energy after the HTL approximation only depend on the radial component  $k$ , the angular and radial integration can be performed separately. The radial integration gives [112]

$$\Pi_{\mu\nu,\text{HTL}} = 3\omega_{\text{pl}}^2 \int \frac{d\Omega}{4\pi} \left( \frac{V_\mu V_\nu p_0}{V \cdot P + i\epsilon} - g_{0\mu} g_{0\nu} \right), \quad (3.10)$$

where  $d\Omega$  indicates the angular integration over  $\mathbf{v}$  and  $\omega_{\text{pl}} = eT/3$  the plasmon frequency.

The self-energy can be decomposed with respect to two tensors

$$\Pi_{\mu\nu,\text{HTL}} = \Pi_{L,\text{HTL}} L_{\mu\nu} + \Pi_{T,\text{HTL}} T_{\mu\nu}, \quad (3.11)$$

given by

$$L_{\mu\nu} = g_{\mu\nu} - \frac{P_\mu P_\nu}{P^2} - T_{\mu\nu}, \quad (3.12)$$

$$T_{\mu\nu} = g_{\mu i} g_{\nu j} \left[ \delta_{ij} - \frac{p_i p_j}{p^2} \right]. \quad (3.13)$$

The tensors  $L_{\mu\nu}$  and  $T_{\mu\nu}$  are longitudinal and transverse with respect to  $\mathbf{p}$ , respectively. Both tensors are transverse with respect to the four-momentum  $P_\mu$ . The longitudinal and transverse self-energies read

$$\Pi_{L,\text{HTL}} = -3\omega_{\text{pl}}^2 \frac{P^2}{p^2} \left[ 1 - \frac{p_0}{p} Q \left( \frac{p_0}{p} \right) \right], \quad (3.14)$$

$$\Pi_{T,\text{HTL}} = \frac{3}{2} \omega_{\text{pl}}^2 \frac{p_0}{p} \left[ \left( 1 - \frac{p_0^2}{p^2} \right) Q \left( \frac{p_0}{p} \right) + \frac{p_0}{p} \right], \quad (3.15)$$

with the Legendre function

$$Q \left( \frac{p_0}{p} \right) = \frac{1}{2} \ln \left| \frac{p_0 + p}{p_0 - p} \right| - \frac{i\pi}{2} H(p^2 - p_0^2) \quad (3.16)$$

and the Heaviside function  $H$ . In sections 3.8 and 3.9, we will discuss some of the consequences of the self-energies (3.14), (3.15) for gauge excitations in a plasma.

The important point is that the HTL self-energy is as large as the tree-level two-point vertex at momenta  $P \sim eT$ . As was explained in the introduction, this self-energy has to be included in the propagator when the

integration over soft momenta dominates the momentum integration of a given diagram (for instance in the calculation of the damping rate). This means that the HTL self-energy also appears in the effective equation of motion of the classical theory for soft modes:

$$(\partial^2 g_{\mu\nu} - \partial_\mu \partial_\nu) A^\nu(x) = \int d^4x' \Pi_{\mu\nu, \text{HTL}}^R(x-x') A^\nu(x'), \quad (3.17)$$

where  $\Pi_{\mu\nu, \text{HTL}}^R$  is the retarded self-energy.

There are two problems concerned with the inclusion of the self-energy in this way. Firstly, the HTL self-energy (3.14),(3.15) contains an imaginary part coming from Landau damping. This implies that (3.17) has decaying solutions. Since we started out with a QED plasma in equilibrium this is not consistent. It is well known how to resolve this problem, namely by the introduction of a stochastic force. This will be discussed in section 3.5. The second problem is the non-locality of the HTL self-energy. Fortunately, as shown by Blaizot and Iancu [21], there exists a local formulation of the HTL effective equations of motion. This is the subject of the next section.

### 3.3 Vlasov equation

The local formulation of the HTL equation (3.17) takes the form of the linearized Vlasov equation well known from kinetic theory. It describes a collisionless plasma of charged particles in the presence of dynamical electromagnetic fields. In the Vlasov theory, the gauge fields satisfy Maxwell's equations

$$(\partial^2 g_{\mu\nu} - \partial_\mu \partial_\nu) A^\nu(x) = j_\mu(x), \quad (3.18)$$

with the current induced by the charged particles written as

$$j_\mu(x) = 2e \int \frac{d^3k}{(2\pi)^3} V_\mu [\delta N_+(x, \mathbf{k}) - \delta N_-(x, \mathbf{k})]. \quad (3.19)$$

The auxiliary fields  $\delta N_\pm$  are the deviation from equilibrium of the electron (+) and positron (-) particle distribution function at time-space point  $x = (t, \mathbf{x})$ , for particles of momentum  $\mathbf{k}$ . They satisfy the Vlasov equation

$$(\partial_t + \mathbf{v} \cdot \nabla) \delta N_\pm(x, \mathbf{k}) = \mp e \mathbf{v} \cdot \mathbf{E}(x) \tilde{n}'(k), \quad (3.20)$$

where we use the velocity  $\mathbf{v} = \mathbf{k}/|\mathbf{k}|$ . Equation (3.20) describes the evolution of the electron and positron distribution functions in the presence of an electric field  $\mathbf{E}$ .

It is well known that the induced current (3.19) generates the retarded HTL self-energy:

$$\Pi_{\mu\nu,\text{HTL}}^R(x-x') = \frac{\delta}{\delta A^\nu(x')} j_\mu(x). \quad (3.21)$$

To show this, one has to solve (3.20) for the particle distribution functions. The dependence of the solution on an initial particle distribution function is not of interest to us, since it drops out in (3.21). It is convenient to demand that the gauge fields and particle distribution functions vanish for  $t \rightarrow -\infty$  as  $\exp(-\epsilon t)$ . Then we may take a Fourier transform of (3.20), which gives

$$\delta N_\pm(P, \mathbf{k}) = \pm \frac{\mathbf{v} \cdot [p_0 \mathbf{A}(P) - \mathbf{p} A^0(P)]}{p_0 + i\epsilon - \mathbf{v} \cdot \mathbf{p}} \tilde{n}'(k). \quad (3.22)$$

Inserting the last equation into (3.19) gives

$$j_\mu(P) = 4e^2 \int \frac{d^3k}{(2\pi)^3} \tilde{n}'(k) \left( \frac{V_\mu V_\nu p_0}{P \cdot V + i\epsilon} - \delta_{\mu 0} \delta_{\nu 0} \right) A^\nu(P). \quad (3.23)$$

The radial integration is decoupled and can be performed; after partial integration we may use (3.5). This leads to the result

$$j_\mu(P) = 3\omega_{\text{pl}}^2 \int \frac{d\Omega}{4\pi} \left( \frac{V_\mu V_\nu p_0}{P \cdot V + i\epsilon} - \delta_{\mu 0} \delta_{\nu 0} \right) A^\nu(P). \quad (3.24)$$

At the right-hand side we recognize the retarded HTL self-energy (3.10) times the gauge field. Hence the induced source (3.19) generates indeed the retarded HTL self-energy.

The Vlasov equation (3.18-3.20) may be derived from the Dyson-Schwinger equations for QED [21]. To understand the physics of the HTL-approximation it is of interest to discuss some of the basic assumptions that are involved in this derivation. First, in the high-temperature limit the mass is small compared to the typical momenta:  $\mathbf{k} \sim T \gg m_e$ . This allows the approximation that the particles move at the speed of light:  $|\mathbf{v}| = 1$ . Next, consider the right-hand side of (3.20). In the non-linear Vlasov equation the force term has the form

$$e(\mathbf{E} + \mathbf{v} \times \mathbf{B}) \cdot \nabla_{\mathbf{k}} N(x, \mathbf{k}), \quad (3.25)$$

with  $N(x, \mathbf{k}) = \tilde{n}(\omega_{\mathbf{k}}) + \delta N(x, \mathbf{k})$ . The assumption is now that the deviation from equilibrium is small  $\delta N \ll \tilde{n}$ . Since the Lorentz force vanishes in equilibrium, one may then neglect deviations from equilibrium  $\delta N(x, \mathbf{k})$

to linear order. As a consequence, because the equilibrium distribution is rotationally invariant, the term including the magnetic field vanishes. The result is the right-hand side of (3.20). Furthermore, the collision term has been neglected, since it gives only contributions that are higher order in the coupling  $e$ . Diagrammatically these contributions would correspond to rung diagrams that start at two loops; see [60, 61] for detailed calculations in a scalar field theory.

An essential approximation is the treatment of fermionic excitations as classical particles. This implies that the dispersion of wave-packets of hard (fermionic) excitations is neglected [13]. Dispersion would be described by a term of the form  $\nabla^i \partial_{\mathbf{k}}^i v^j \nabla^j N_{\pm}(x, \mathbf{k})$ . The idea is that the fields and particle densities change slowly in space and time, typically  $\nabla \sim eT$  [21]. Then the inequality  $\nabla^i \partial_{\mathbf{k}}^i v^j \nabla^j \ll \mathbf{v} \cdot \nabla$  holds and the dispersion of fermionic wave packets may be neglected. In the diagrammatic HTL-calculation of the previous section this corresponds to the approximation (3.8).

A final remark is the following: the equivalence of the HTL equation of motion (3.17) and the Vlasov equation (3.18-3.20) has been shown for initial conditions where the fields vanish for  $t \rightarrow -\infty$ . When initial conditions are to be specified at a finite initial time, the Vlasov equations require an additional initial condition for the particle distribution functions. Such an initial condition is not given by specifying the initial gauge field. To deal with this extra freedom, one may introduce an ensemble average over initial values of  $\delta N$ . As will be discussed in the next section, it is possible to define such an average within a consistent statistical HTL-theory.

### 3.4 Statistical HTL theory

Before we discuss the statistical ensemble, we first specify the initial conditions for the Vlasov equation (3.20). Following Blaizot and Iancu [23], we introduce the new field

$$W(x, \mathbf{v}) = -[\delta N_+(x, \mathbf{k}) - \delta N_-(x, \mathbf{k})] / 2e\tilde{n}'(k), \quad (3.26)$$

that satisfies the equation

$$(\partial_t + \mathbf{v} \cdot \nabla) W(x, \mathbf{v}) = \mathbf{v} \cdot \mathbf{E}(x). \quad (3.27)$$

The auxiliary field  $W$  has suggestively been written as a function of the velocity  $\mathbf{v}$  instead of the momentum  $\mathbf{k}$ , since the last equation involves only

the velocity. However, this requires that also the initial conditions for  $W$  are independent of  $|\mathbf{k}|$ . In the present section we will assume this to be the case. After expressing the current (3.19) in terms of the new fields  $W$ , the integration over the radial component of  $\mathbf{k}$  can be performed. The result is

$$j_\nu = 3\omega_{\text{pl}}^2 \int \frac{d\Omega}{4\pi} V_\nu W(x, \mathbf{v}). \quad (3.28)$$

Following Iancu [56], we will formulate the classical statistical theory for QED including the HTL self-energy. Essential is that the Vlasov equations (3.18), (3.27), and (3.28) have a conserved energy [23, 94]

$$H = \int d^3x \frac{1}{2} \left[ \mathbf{E}^2 + \mathbf{B}^2 + 3\omega_{\text{pl}}^2 \int \frac{d\Omega}{4\pi} W(x, \mathbf{v}) W(x, \mathbf{v}) \right]. \quad (3.29)$$

Remarkably enough, in the  $A_0 = 0$  gauge, the energy acts also as a Hamiltonian. Poisson brackets  $\{, \}$  can be defined for which the canonical equations  $\partial_t \mathbf{A} = \{H, \mathbf{A}\}$ ,  $\partial_t \mathbf{E} = \{H, \mathbf{E}\}$ , and  $\partial_t W = \{H, W\}$  together with the Gauss' constraint

$$G = \nabla \cdot \mathbf{E}(x) - 3\omega_{\text{pl}}^2 \int \frac{d\Omega}{4\pi} W(x, \mathbf{v}) = 0 \quad (3.30)$$

are the Vlasov equations (3.18) and (3.27), with (3.28) [56, 94]. Therefore, it is natural to define a statistical HTL theory by a path integral over initial values of the gauge field  $\mathbf{A}$  its conjugate momentum  $\mathbf{E}$ , and the auxiliary field  $W$ . Let the fields at some initial time  $t_{\text{in}}$  be denoted as

$$\begin{aligned} \mathbf{A}(t_{\text{in}}, \mathbf{x}) &= \mathbf{A}_{\text{in}}(\mathbf{x}), \\ \mathbf{E}(t_{\text{in}}, \mathbf{x}) &= \mathbf{E}_{\text{in}}(\mathbf{x}), \\ W(t_{\text{in}}, \mathbf{x}, \mathbf{v}) &= W_{\text{in}}(\mathbf{x}, \mathbf{v}), \end{aligned} \quad (3.31)$$

The partition function for the HTL-theory may then be written as

$$Z = \int \mathcal{D}\mathbf{A}_{\text{in}} \mathcal{D}\mathbf{E}_{\text{in}} \mathcal{D}W_{\text{in}} \delta(G[\mathbf{E}_{\text{in}}, W_{\text{in}}]) \exp -\beta H, \quad (3.32)$$

where the Gauss law is imposed on the initial conditions. It is essential that integration measure in (3.32) is time independent.

In [57] it was shown that this statistical theory yields the transverse HTL two-point function

$$\langle A_\mu(-P) T^{\mu\nu}(P) A_\nu(P) \rangle = \frac{T}{p_0} \rho_{\text{HTL}}^T(P). \quad (3.33)$$

The tensor  $T^{\mu\nu}$  has been specified in (3.13) and the spectral density  $\rho_{\text{HTL}}^T(P)$  is related to the HTL-retarded and advanced Green functions in the standard way, see formulae (3.39) and (3.41) in the next subsection. The result (3.33) is the correct classical HTL two-point function. Also it has been verified that the longitudinal two-point function comes out correctly. Without the ensemble average over initial conditions the two-point function would (bilinearly) depend on the initial fields, and certainly not give the correct thermal behavior (3.33).

### 3.5 Stochastic HTL equation

Let us return to the HTL equation (3.17). We already discussed the non-thermal behavior of this equation. The solution was also indicated, namely the introduction of a stochastic force. This is consistent with the picture of the hard modes forming a 'heat bath' in which the soft gauge fields evolve. Physically, the stochasticity arises because the hard scales which are integrated out in the HTL scheme and are responsible for Landau damping will also provide random kicks to the soft degrees of freedom [30].

Let us first consider the introduction of a stochastic force for a scalar field

$$(\partial^2 + m^2)\phi + \int d^4x' \Sigma_R(x-x')\phi(x') = \xi(x). \quad (3.34)$$

The main effect of integrating out the hard modes, is encoded in the dissipative kernel given by the retarded self-energy as in (3.17) and a stochastic source term in the generalized Langevin equation (3.34). We assume the source to be Gaussian

$$\langle \xi(x) \rangle_\xi = 0, \quad (3.35)$$

$$\langle \xi(x)\xi(x') \rangle_\xi = \Sigma_C(x-x'), \quad (3.36)$$

where  $\Sigma_C$  is the symmetric self-energy, which is related to the dissipative kernel via the fluctuation dissipation relation

$$\begin{aligned} \Sigma_C(P) &= [1 + 2n(p_0)] \text{Im}\Sigma_R(P) \\ &\rightarrow 2\frac{T}{p_0} \text{Im}\Sigma_R(P). \end{aligned} \quad (3.37)$$

In the second line we have taken the classical limit.

We may use the requirement of proper thermalization as a consistency check on the form of the noise correlator (3.36) [66]. We know that in thermal equilibrium the two-point function of the fields reads [18]

$$\langle \phi(P)\phi(-P) \rangle = \frac{T}{p_0} \rho(P), \quad (3.38)$$

with the spectral density

$$\rho(P) = -i [G_R(P) - G_A(P)] \quad (3.39)$$

expressed in terms of the retarded and advanced propagators

$$G_R(P) = \frac{1}{-(p_0 + i\epsilon)^2 + \mathbf{p}^2 + m^2 + \Sigma_R}, \quad (3.40)$$

$$G_A(P) = G_R^*(P) = G_R(-P), \quad (3.41)$$

with  $p_0 = \text{Re}(p_0) + i\epsilon$ . We expect that the system thermalizes and that after a sufficiently long time it is entirely independent of the initial state. In this long-time limit the stochastic equation (3.34) can simply be solved with the (retarded) initial condition that the field vanishes for  $t \rightarrow -\infty$ . In Fourier space the solution reads

$$\phi(P) = G_R(P)\xi(P). \quad (3.42)$$

The two-point function of the fields is then related to the noise two-point correlation function by

$$\langle \phi(P)\phi(-P) \rangle = G_R(P)G_A(P)\langle \xi(P)\xi(-P) \rangle_\xi. \quad (3.43)$$

From (3.41) one immediately infers the relation

$$G_R(P) - G_A(P) = G_R(P)G_A(P)2i\text{Im}\Sigma_R(P), \quad (3.44)$$

and the comparison of (3.43) with (3.38) yields indeed the noise correlation function (3.36).

A microscopic derivation of stochastic equations like (3.34) is possible with the Feynman-Vernon influence functional approach [46]. For applications of this method to field theories in or near equilibrium we refer to [49, 114].

When the retarded self-energy has the simple form  $\Sigma_R = i\gamma p_0$  the stochastic equation (3.34) reduces to a local Langevin equation with constant coefficients:

$$(\partial^2 + m^2)\phi + \gamma\partial_t\phi = \xi, \quad (3.45)$$

and a Gaussian local white noise term.

Now we turn to QED. For the transverse gauge fields, the stochastic equation has been given by Boyanovsky et al [30]. We keep the the four gauge fields, which allows us to to directly see how the noise term enters the Gauss' law. Including a stochastic source in the effective equations of motion (3.17) yields

$$(\partial^2 g_{\mu\nu} - \partial_\mu \partial_\nu) A^\nu - \int dt' d^3 x' \Pi_{\mu\nu, \text{HTL}}^R(x - x') A^\nu(x') = \xi_\mu(x). \quad (3.46)$$

There is one complication compared to the scalar case, namely the noise is a current and has to be conserved:  $\partial_\mu \xi^\mu = 0$ . This allows us to express the stochastic charge in terms of the vector current and the initial charge density as

$$\xi^0(t, \mathbf{x}) = \int_{t_{\text{in}}}^t dt' \nabla \cdot \xi(t', \mathbf{x}) + \xi_{\text{in}}^0(\mathbf{x}) \quad (3.47)$$

The initial value of the stochastic charge  $\xi_{\text{in}}^0$  may be expressed in terms of the divergence of the initial electric field through the Gauss' law at the initial time. The relation (3.47) ensures then that Gauss' law is satisfied at later times.

As for the scalar case, we will assume  $t_{\text{in}} \rightarrow -\infty$  (and include an infinitesimal damping  $\epsilon$ ), such that the system at finite times is independent of the initial conditions, especially the initial charge density. The spatial component of the stochastic source is then Gaussian:

$$\langle \xi_i(x) \rangle_\xi = 0, \quad (3.48)$$

$$\langle \xi_i(x) \xi_j(x') \rangle_\xi = \Pi_{Cij}(x - x'), \quad (3.49)$$

The relation between the symmetric self-energy and the retarded self-energy is the same as in the scalar case; see (3.37).

From relation (3.47) and the noise correlation functions (3.48) and (3.49), we may infer the correlation functions for the stochastic charge

$$\langle \xi_0(x) \rangle_\xi = 0, \quad (3.50)$$

where we used that  $t_{\text{in}} \rightarrow -\infty$ ; furthermore

$$\langle \xi_0(x) \xi_0(x') \rangle_\xi = \Pi_{C00}(x - x'), \quad (3.51)$$

$$\langle \xi_0(x) \xi_i(x') \rangle_\xi = \Pi_{C0i}(x - x'). \quad (3.52)$$

This ensures a proper thermalization of the system.

When a non-equilibrium system is considered, such as a heavy-ion collision, the initial time should be kept finite. And initial correlations may have to be kept [53]. This means that correlations between fields at a finite time and initial fields need to be included. This is possible as we have worked out in the appendix of [96]. However, then also correlations between initial fields and the stochastic current at later times, as well as correlations between the initial stochastic charge-density and the fields and stochastic current at later times, have to be taken into account.

### 3.6 Consistency of stochastic HTL theory

As discussed before, the linearized Vlasov equations (3.18-3.20) give rise to a statistical HTL theory (3.32). Here we will show the consistency of this classical statistical theory with the stochastic HTL equation (3.46). In particular, we will show that the statistical average of the stochastic source is in fact an integration over the initial auxiliary fields  $W_{\text{in}}$  with the thermal weight of the statistical HTL theory (3.32).

Following [57], we divide the auxiliary field into a induced and fluctuation part

$$W(x, \mathbf{v}) = W_{\text{ind}}(x, \mathbf{v}) + W_{\text{fl}}(x, \mathbf{v}). \quad (3.53)$$

We let the induced part satisfy

$$(\partial_t + \mathbf{v} \cdot \nabla) W_{\text{ind}} = \mathbf{v} \cdot \mathbf{E}, \quad \text{with } W_{\text{ind}}(t_{\text{in}}, \mathbf{x}, \mathbf{v}) = 0. \quad (3.54)$$

The fluctuation part then satisfies the equation of motion

$$(\partial_t + \mathbf{v} \cdot \nabla) W_{\text{fl}} = 0, \quad \text{with } W_{\text{fl}}(t_{\text{in}}, \mathbf{x}, \mathbf{v}) = W_{\text{in}}(\mathbf{x}, \mathbf{v}), \quad (3.55)$$

which involves the unknown initial field  $W_{\text{in}}$ . It is convenient to split also the current into an induced and fluctuation part

$$j^\nu = j_{\text{ind}}^\nu + j_{\text{fl}}^\nu, \quad (3.56)$$

with the induced and fluctuation part given by

$$j_{\text{ind, fl}}^\nu = 3\omega_{\text{pl}}^2 \int \frac{d\Omega}{4\pi} V^\nu W_{\text{ind, fl}}. \quad (3.57)$$

The induced part of the current generates the retarded self-energy in the equation of motion for the gauge field in the manner explained in sect 3.3.

Here we will show that, within the statistical HTL-theory, the fluctuation part of the current may be identified with the stochastic source  $\xi_\mu$  in (3.46). We have already established that the statistical HTL-theory is Gaussian. Hence, what we have to show that in the classical HTL-theory the fluctuation part of the current has the same Gaussian two-point correlation function (3.49) as the stochastic source.

First, we solve equation (3.55) for the fluctuation field:

$$W_{\text{fl}}(t, \mathbf{x}, \mathbf{v}) = W_{\text{in}}(\mathbf{x} - (t - t_{\text{in}})\mathbf{v}, \mathbf{v}). \quad (3.58)$$

Since the initial field  $W_{\text{in}}$  is Gaussian, so are  $W_{\text{fl}}$  and  $j_{\text{fl}}$ . To compare the results with the stochastic system (3.46) of the previous section, we take here also  $t_{\text{in}} \rightarrow -\infty$ , such that the initial divergence of the electric field (the initial charge density) does not contribute to the current expectation value at finite times. Then we obtain

$$\langle j_{\text{fl}}^\mu \rangle = 0, \quad (3.59)$$

where the brackets denote the classical thermal average defined by (3.32).

This leaves us to show that the two-point correlation of the fluctuation part of the current equals the two-point function of the stochastic source (3.49). For this, we have to calculate

$$\langle j_{\text{fl}}^\mu(x) j_{\text{fl}}^\nu(x') \rangle = (3\omega_{\text{pl}}^2)^2 \left\langle \int \frac{d\Omega}{4\pi} V^\mu W_{\text{fl}}(x, \mathbf{v}) \int \frac{d\Omega'}{4\pi} V^\nu W_{\text{fl}}(x', \mathbf{v}') \right\rangle. \quad (3.60)$$

To evaluate the right-hand side we insert the solution (3.58) in (3.60) and perform the Gaussian integration over  $W_{\text{in}}$ . This gives

$$\langle j_{\text{fl}}^\mu(x) j_{\text{fl}}^\nu(x') \rangle = T(3\omega_{\text{pl}}^2) \int \frac{d\Omega}{4\pi} V^\mu V^\nu \delta^3(\mathbf{x} - \mathbf{x}' - (t - t')\mathbf{v}). \quad (3.61)$$

A Fourier transformation yields

$$\langle j_{\text{fl}}^\mu(-P) j_{\text{fl}}^\nu(P) \rangle = T(3\omega_{\text{pl}}^2) \int \frac{d\Omega}{4\pi} V^\mu V^\nu \left( \frac{-i}{p_0 + i\epsilon - \mathbf{p} \cdot \mathbf{v}} + \text{c.c.} \right), \quad (3.62)$$

where we have included an infinitesimal damping  $\epsilon$ . We recognize on the right-hand side of (3.62) the imaginary part of the retarded HTL self-energy (3.10) times the classical distribution function

$$\langle j_{\text{fl}}^\mu(-P) j_{\text{fl}}^\nu(P) \rangle = 2 \frac{T}{p_0} \text{Im} \Pi_R^{\mu\nu}(P). \quad (3.63)$$

Hence, the two-point correlation functions of the fluctuation current (3.63), and the stochastic current (3.49) have been proven to be the same.

We conclude that the statistical theory (3.32) based on the local Vlasov equations and the non-local stochastic HTL equation (3.46) are entirely consistent. To be completely equivalent, the latter should be complemented by an ensemble average over initial gauge and electric fields. In a microscopic derivation this average naturally arises [49].

### 3.7 Non-Abelian HTL's

Let us start with the Vlasov equations for a non-Abelian  $SU(N)$  gauge theory derived by Blaizot and Iancu [22]

$$D_\mu^{ab} F^{\mu\nu b} = j^{\nu a}, \quad (3.64)$$

$$j^{\nu a} = 3\omega_{\text{pl}}^2 \int \frac{d\Omega}{4\pi} V^\nu W^a, \quad (3.65)$$

$$V^\mu D_\mu^{ab} W^b = \mathbf{v} \cdot \mathbf{E}^a, \quad (3.66)$$

where the plasmon frequency is  $\omega_{\text{pl}}^2 = g^2 NT^2/9$ . The field strength is given by  $F^{\mu\nu a} = \partial^\mu A^{\nu a} - \partial^\nu A^{\mu a} - gf_{abc}A^{\mu b}A^{\nu c}$ , and the covariant derivative is  $D_\mu^{ab} = \delta^{ab}\partial_\mu + gf_{abc}A_\mu^c$ , with the structure functions  $f_{abc}$  and  $a, b, c$  adjoint indices. It follows from (3.66) that the induced current is covariantly conserved:

$$D_\mu^{ab} j^{\mu b} = 0. \quad (3.67)$$

The main difference between the Abelian Vlasov equations (3.18)-(3.20) and non-Abelian ones, is that the latter contains interactions through the non-Abelian field strength and the covariant derivative in (3.66). Nevertheless, retarded HTL vertex functions can be extracted from the Vlasov equations in a manner analogous to the case of the Abelian plasma. First solve  $W^a$  from (3.66) for retarded boundary conditions. Then insert the solution into the expression for the current (3.65). Since the current is given by a derivative of the effective action [22]

$$j_\mu^a = \frac{\delta}{\delta A^{\mu a}} \Gamma_{\text{HTL}}[A], \quad (3.68)$$

the HTL vertex functions may be obtained by differentiating the current with respect to the gauge field

$$\Gamma_{\mu_1 \dots \mu_n, \text{HTL}}^{(n) a_1 \dots a_n} = \frac{\delta}{\delta A^{\mu_n a_n}} \dots \frac{\delta}{\delta A^{\mu_2 a_2}} j_{\mu_1}^{a_1}, \quad (3.69)$$

according to the standard definition of vertex functions.

First of all we may notice that for the calculation of the HTL self-energy,  $\Pi_{\mu\nu, \text{HTL}}^{ab} = \Gamma_{\mu\nu, \text{HTL}}^{(2), ab}$ , we may neglect the gauge field in the covariant derivative in (3.66). Except for the different plasmon frequency, the equation for  $W^a$  is the same as in the Abelian case. Hence, the HTL self-energy in a  $SU(N)$  gauge theory is given by the equations (3.10), (3.14), and (3.15) with the proper expression for plasmon frequency. One can generate also higher-point HTL vertex functions (3.69) also. They are schematically given by (see [22, 31] for explicit formulas)

$$\Gamma_{\text{HTL}}^{(n)} \approx \omega_{\text{pl}}^2 g^{n-2} \int d\Omega \frac{p_0}{P^{n-1}} \quad n \geq 3. \quad (3.70)$$

They vanish in the static limit  $p_0 \rightarrow 0$ . For soft momenta  $P \sim gT$ , we have  $\Gamma_{\text{HTL}}^{(n)} \sim g^2 T^{4-n}$ . For the three- and four-point function we can directly compare this to the tree-level estimates  $\Gamma_{\text{tree}}^{(3)} \sim gP \sim g^2 T$ ,  $\Gamma_{\text{tree}}^{(4)} \sim g^2$ . We see that the HTL's are as large as the tree-level vertices. In the calculation of diagrams that are dominated by soft momenta not only the HTL self-energy, but also the HTL vertices, have to be resummed [31].

The non-Abelian Vlasov equations can be incorporated into a classical theory [56] in a similar manner as Abelian equations (section 3.4). (We will not give the formulae for the energy and partition sum; these are the same as for the Abelian theory except for the adjoint index that has to be introduced at appropriate places.) The same consistency checks as for the Abelian theory can be made, namely the Vlasov equations are Hamiltonian and the phase-space measure is conserved.

In the next section we will consider some of the physics included in the HTL's.

### 3.8 Plasmons

In this section we will discuss some properties of the HTL self-energies, especially the existence of collective excitations such as plasmons. But we will start with a static property.

Consider a QED plasma and a local external static charge density  $\rho(\mathbf{x}) = q\delta(\mathbf{x})$ . When this charge density is small, we may use linear response theory for the calculation of the induced electric field

$$\langle \mathbf{E}(\mathbf{x}) \rangle_\rho = \int d^3 x' \nabla_x \langle A_0(\mathbf{x}) A_0(\mathbf{x}') \rangle \rho(\mathbf{x}'), \quad (3.71)$$

where the average of the product of the two temporal gauge fields may be taken at charge density zero. For the potential  $\Phi$  defined by

$$\langle \mathbf{E} \rangle_\rho = \nabla \Phi, \quad (3.72)$$

we get after a Fourier transformation of (3.71) the expression

$$\Phi(\mathbf{x}) = q \int d^3p \frac{e^{i\mathbf{p}\cdot\mathbf{x}}}{\mathbf{p}^2 - \Pi_{00}(p_0 = 0, \mathbf{p})}. \quad (3.73)$$

The leading-order contribution to the self-energy comes from the HTL's. From (3.10), we infer that in the static limit  $\Pi_{00,\text{HTL}}$  is just a constant

$$\Pi_{00,\text{HTL}}(p_0 = 0, \mathbf{p}) = -3\omega_{\text{pl}}^2 = -\frac{1}{3}e^2T^2. \quad (3.74)$$

Expression (3.73) then gives the screened potential

$$\Phi(\mathbf{x}) = \frac{q}{4\pi|\mathbf{x}|} e^{-m_D|\mathbf{x}|}, \quad (3.75)$$

with Debye mass  $m_D^2 = e^2T^2/3$ .

In a similar manner one finds that a local charge in a non-Abelian  $SU(N)$  theory is screened with Debye  $m_D^2 = g^2NT^2/3$ . However, in a non-Abelian theory the induced electric field and the two-point function of temporal gauge fields are not gauge invariant. Nevertheless the Debye mass is a gauge invariant quantity, even beyond the HTL approximation [104]. This is because it is the position of a pole of a propagator [72]. If one is interested in the screening behavior beyond the value of the Debye mass, one has to use a gauge invariant definition. This can be given by the correlation function of two Polyakov loop operators [104].

Let us now consider homogeneous spatial gauge fields  $\mathbf{A}(t, \mathbf{p} = 0)$ . The HTL self-energy (3.10) at zero momentum  $\mathbf{p} = 0$  is again a constant

$$\Pi_{ij,\text{HTL}}(p_0, \mathbf{p} = 0) = -\omega_{\text{pl}}^2 \delta_{ij}. \quad (3.76)$$

Inserting this in the HTL equation (3.17), one finds that the spatial gauge-fields oscillate with frequency  $\omega_{\text{pl}}$  (which is called plasmon frequency for good reason).

For a non-Abelian theory the same result is obtained in the limit of small field amplitudes (so that we may linearize the equation of motion). Here the same remark applies as was made after formula (3.75). Namely, the

plasmon frequency is gauge invariant beyond leading order, since it is the pole of a propagator.

At non-zero momentum, small-amplitude fields also show oscillatory behavior. In a similar manner as above the dispersion relation may be calculated. Within the HTL approximation the frequencies are real and of order  $gT$  for momenta  $p \sim gT$ . The associated propagating gauge excitations in the plasma are often called plasmons. We will see shortly that their interaction strength is small. Therefore, the interactions will not spoil a particle picture of plasmons. This picture is also born out by the calculation of the gluon (better: plasmon) damping rate, which is of order  $g^2T$ . Thus compared to the typical frequency  $\sim gT$  these excitations are long-lived.

This reasoning requires that higher-order corrections are small. Let us consider the accuracy of the HTL resummation. As for a scalar theory (2.21), one can determine an effective expansion parameter

$$g_{\text{eff}}^2 \sim g^2 \frac{T}{m}, \quad (3.77)$$

with  $m$  a typical mass scale. The plasmon frequency and Debye mass are both of order  $gT$ . If these are used as typical mass scales, one gets

$$g_{\text{eff}}^2 \sim g. \quad (3.78)$$

Therefore, the HTL resummed loop expansion is an expansion in  $g$  rather than in  $g^2$ . For example, the next-to-leading contribution to the Debye-mass squared is of order  $g^3T^2 \log m_D/m_m$  [104], with  $m_m$  the magnetic mass which is of order  $g^2T$ . Hence, the next-to-leading order contribution is smaller by a factor  $g \log 1/g$ . In the simple estimate leading to (3.77) (or (2.21) for scalar  $\lambda\phi^4$ -theory), we treat corrections  $\log 1/g \sim \mathcal{O}(1)$ . Then the next-to-leading contribution to the Debye mass is in agreement with the estimate for the effective expansion parameter (3.78). Also the plasmon frequency has been calculated in next-to-leading order [109]. It is a factor  $g \log T/\omega_{\text{pl}}$  smaller than the HTL result, again in agreement with (3.78). The estimate (3.78) also implies that the effective interaction strength between plasmons is small if  $g$  is small.

### 3.9 Non-perturbative excitations

The plasmon excitations are not the full story. In a non-Abelian plasma there are quantities that cannot be perturbatively calculated even in a HTL

resummed theory. This may be illustrated for static quantities, for which we use the dimensionally reduced theory as in 2.5. The static dimensionally reduced theory for a pure  $SU(N)$ -theory reads [63]

$$L_{DR} = \int d^3x \left[ \frac{1}{4} F_{ij}^a F^{ija} + \frac{1}{2} (D_i^{ab} A_0^b)^2 + \frac{1}{2} \mu_0^2 (A_0^a)^2 + \frac{1}{4} \lambda_0 (A_0^a A_0^a)^2 \right]. \quad (3.79)$$

There is one HTL contribution contained in this effective theory, namely in the mass  $\mu_0$  of the temporal gauge field. In the static limit the transverse part of the HTL self-energy vanishes while the longitudinal part reduces to the Debye mass  $m_D^2$  (3.14). Higher-order HTL vertex-functions vanish in the static limit.

The non-perturbative regime that we are interested in appears at momentum scale  $g^2 T$ , as we will see shortly. Thus, we are interested in momentum scales below the scale  $gT$ . Then we may integrate out the temporal gauge field in (3.79), since it has a mass that is large compared to the scale of interest. With the temporal gauge field integrated out the resulting theory reads

$$L_{\text{eff}} = \int d^3x \frac{1}{4} F_{ij}^a F^{ija}. \quad (3.80)$$

This theory is non-perturbative, as can be deduced by a rescaling of the gauge field  $A_i^a \rightarrow g A_i^a$ . This brings out a factor  $1/g^2$  in front of (3.80) and the field strength itself does no longer contain any coupling. In the Boltzmann weight  $\exp -\beta L_{\text{eff}}$ , the factor  $1/g^2$  combines with  $\beta$  in the dimensionful length scale  $1/g^2 T$ . This is the inverse magnetic screening mass  $m_m \sim g^2 T$ .

The theory is non-perturbative: there is simply no dimensionless scale left to expand in. This may be inferred also from the effective expansion parameter (3.77). When we use the magnetic mass  $m_m \sim g^2 T$  as a mass scale in (3.77) we get

$$g_{\text{eff}}^2 = g^2 \frac{T}{m_m} \sim 1. \quad (3.81)$$

So, even though the coupling  $g$  may be very small there is a non-perturbative regime in thermal field theory. This the reason that the contribution of order  $g^6 T^4$  to the free energy is not perturbatively calculable as noted long ago by Linde [81].

Let us consider the dynamics of fields of size  $1/g^2 T$ . It is convenient to add an external current  $j_{\text{ext}}$  to the system and consider the induced gauge field. We decompose the gauge field and the current in longitudinal and

transverse parts using (3.13). Then we have

$$\langle A_L(P) \rangle = \frac{1}{P^2 - \Pi_L(P)} j_{\text{ext},L}(P), \quad (3.82)$$

$$\langle A_T(P) \rangle = \frac{1}{P^2 - \Pi_T(P)} j_{\text{ext},T}(P), \quad (3.83)$$

with retarded propagators and self-energies. We will use the HTL approximation for the self-energies in (3.83). This may be somewhat surprising, since we just argued that at the momentum scale of interest  $p \sim g^2 T$  we enter a non-perturbative regime. Therefore one would expect  $\mathcal{O}(1)$  corrections to the HTL self-energies at these momenta. However, as will be argued later on, the order estimate for the frequency of fields with momenta  $p \sim g^2 T$  will not change by these  $\mathcal{O}(1)$  corrections.

We would like to know the typical time scale for gauge fields of momenta  $p \sim g^2 T$ . We now look for frequencies  $p_0$  of the external current for which the induced gauge field extends over a length scale  $1/g^2 T$ . First consider the longitudinal part. Since  $\Pi_{L,\text{HTL}} \sim g^2 T^2$  for any  $p_0$ , the longitudinal current is screened over a length  $1/gT$ . Hence, no non-perturbative excitations occur in the longitudinal gauge field. For the transverse part we have the same when  $|p_0| > p$ , then  $\Pi_{T,\text{HTL}} \sim g^2 T^2$ . Hence the propagating (transverse) modes are also screened on a length scale  $1/gT$ .

Next we consider the case  $|p_0| < p$  for the transverse self-energy. The small-frequency limit of the transverse self-energy (3.15) is

$$\Pi_{T,\text{HTL}} = -i\pi\omega_{\text{pl}}^2 \frac{p_0}{p}, \quad |p_0| \ll p. \quad (3.84)$$

Note that in the static limit the self-energy vanishes. This is the reason that in the (static) dimensionally reduced theory (3.79) there is no HTL contribution for the spatial gauge fields. On account of (3.84) the induced transverse gauge field (3.83) for momenta  $|p_0| \ll p$  has a pole at

$$p = -i(\pi\omega_{\text{pl}}^2 p_0)^{1/3}. \quad (3.85)$$

This pole determines the spatial size of the induced gauge field. One may read off from (3.85) the frequency that is necessary to induce gauge fields of size  $1/g^2 T$ , namely [12]

$$p_0 \sim \frac{p^3}{\omega_{\text{pl}}^2} \sim g^4 T, \quad (3.86)$$

for  $p \sim g^2 T$ . Hence, gauge fields of size  $1/g^2 T$  have a typical time scale  $1/g^4 T$ .

The non-perturbatively large interactions between the modes with momentum scale  $p \sim g^2 T$  are not expected to change the frequency scale (3.86) simply because they all have the same frequency scale. These interactions do, however, affect the coefficient in front of  $g^4 T$ . This coefficient is therefore not calculable in perturbation theory.

The above result (3.86) was first derived by Arnold, Son, and Yaffe [12]. Before this time, it was generally expected that  $p_0 \sim p \sim g^2 T$ . The slowing down of these large gauge-field fluctuations by the hard modes expressed by (3.86) has some important consequences. For instance the Chern-Simons diffusion in the symmetric phase of the electro-weak theory is carried by fields of spatial size  $1/g^2 T$ . The diffusion rate is the inverse volume times the inverse time-scale of these fields

$$\Gamma_{CS} \sim (tl^3)^{-1} \sim g^{10} T^4. \quad (3.87)$$

Before the analysis of [12] it was expected to be of order  $g^8 T^4$  [9]. Later Bödeker [27] obtained a logarithmic correction to both (3.86) and (3.87). This logarithm occurs from integrating out the momentum scale  $gT$ . For a nice physical explanation of (3.86) and the logarithmic correction we refer to [15].

Another effect of the large time-scale for these non-perturbative excitations is that it slows down some other processes. For instance, they slow down the motion of a bubble wall in a first-order electro-weak phase transition [92].

### 3.10 Summary

Let us review the spectrum of excitations in a non-Abelian plasma. There are hard-mode excitations with energy and momentum of order  $T$ . In the HTL approximation these are treated as classical particles. Then we have plasmons, which are long-lived collective excitations of momentum and frequency of order  $gT$ . The plasmons have an effective interaction strength  $g_{\text{eff}}^2 = g$ . They interact weakly, albeit not as weakly as the hard modes. Finally, there are strongly-interacting excitations of spatial size  $1/g^2 T$ . These mode are non-propagating and have a typical time scale of order  $1/g^4 T$ .

The existence of non-perturbative excitations provides an important motivation for the study of the classical theory. Without them one might in principle use a HTL resummed perturbation expansion for the calculation of the quantity of interest (in practice such a calculation may well be extremely

complicated). However, due to the presence non-perturbative modes certain quantities are simply not calculable perturbatively.

The classical approximation enters this story for the following reasons. Firstly, it well-suited for a non-perturbative treatment by means of lattice simulations, see for recent reviews e.g. [89,113]. Secondly, because the classical approximation is especially well-suited for the non-perturbative modes, since for  $p \sim g^2 T$ , we have that  $\beta p \ll 1$ . However a purely classical theory is not sufficient. As we have seen in this chapter a correct description of the soft modes requires the inclusion of HTL's into an effective classical theory. It was the main subject of this chapter how this may be achieved.

Even if the HTL's are included into an effective classical theory, there remains the problem of the Rayleigh-Jeans divergences in the classical theory. For a scalar theory, we have already encountered a classical divergence in the tadpole mass (2.12). It is the subject of the next chapter to study the divergences that appear in non-Abelian gauge theories in a more systematic manner.



## 4 Divergence structure of hot, real-time classical field theory

### 4.1 Introduction

The replacement

$$n(\omega_{\mathbf{k}}) = \frac{1}{\exp(\beta\hbar\omega_{\mathbf{k}}) - 1} \rightarrow \frac{1}{\beta\hbar\omega_{\mathbf{k}}} \equiv n_{\text{cl}}(\omega_{\mathbf{k}}), \quad \hbar\omega_{\mathbf{k}} \ll T, \quad (4.1)$$

is a good approximation for infrared-dominated diagrams, but it changes the ultraviolet behavior of the theory and introduces classical (Rayleigh-Jeans-type) divergences. When the classical theory is considered as a low-energy effective theory, these divergences can be regularized by introducing a cut-off of the order of the temperature,  $\Lambda \sim T/\hbar$ . Since in a weakly coupled theory the temperature is large compared to dynamically generated energy scales such as  $g^2T$ , the resulting cut-off dependences are a direct reflection of the divergences of the classical theory. The general strategy to improve the effective theory is to include counterterms that reduce the cut-off dependence. In particular, if a complete set of counterterms can be specified, the cut-off may be sent to infinity and the theory is renormalized. It is clear that a knowledge of the divergences is necessary to determine the appropriate counterterms. In the next chapter we will investigate how counterterms can be introduced in a classical gauge theory. We will assume that these divergences are tractable in perturbation theory.

In the case of a  $\lambda\phi^4$  scalar field theory the divergences have been studied in classical perturbation theory for the two-point function up to two loops and the four-point function up to one-loop [1, 2, 36]. It was found that the one-loop resp. two-loop correction to the self-energy is linearly resp. logarithmically divergent, and that the one-loop correction to the four-point function is finite [2]. In  $3+1$  dimensional gauge theories on the other hand, the attention has mainly been restricted to the classical equivalent of the quantum hard thermal loop (HTL) expressions [18, 31, 117], which introduce

linear divergences in the classical theory [12, 13, 25]. Numerical studies using a HTL improved effective theory [25, 55, 56] can be found in [29, 88, 103]. An analysis of the divergences in the classical theory that goes beyond the HTL limit at one-loop, or to higher loops, has not yet been performed for gauge theories. Our aim in this chapter is therefore to give a more complete analysis of the divergence structure of hot, real-time classical field theory.

## 4.2 One-loop

### 4.2.1 Linear divergences: classical HTL's

The one-loop linear divergences of the classical theory are closely related to the (quantum) hard thermal loops discovered by Braaten and Pisarski [31] (see also [112, 117, 118]). For instance, the divergent part of the classical self-energy in  $SU(N)$  gauge theory can be obtained as the classical limit of the HTL self-energy [12, 25]. To be specific, the spatial part of the retarded HTL self-energy reads

$$\Pi_{ij,\text{HTL}}^{ab}(P) = -2\delta^{ab}g^2\hbar N \int \frac{d^3k}{(2\pi)^3} \hat{k}_i \hat{k}_j n'(\omega_{\mathbf{k}}) \frac{p^0}{p^0 - \hat{\mathbf{k}} \cdot \mathbf{p}}, \quad (4.2)$$

with  $\hat{\mathbf{k}} = \mathbf{k}/k$ . Here and in the following the external frequency  $p^0$  is taken real with a small imaginary part to obtain the retarded self-energy, i.e.  $p^0 \equiv \text{Re}(p^0) + i\epsilon$ , and

$$n'(\omega_{\mathbf{k}}) = \frac{dn(\omega_{\mathbf{k}})}{d\omega_{\mathbf{k}}}. \quad (4.3)$$

As usual in the HTL approximation, the radial and angular integration decouple and the radial integration determines the plasmon frequency

$$\omega_{\text{pl}}^2 = -\frac{1}{3\pi^2}g^2\hbar N \int_0^\infty dk k^2 n'(k) = \frac{1}{9}g^2N \frac{T^2}{\hbar}. \quad (4.4)$$

The classical self-energy corresponding to (4.2) is obtained by taking the  $\hbar \rightarrow 0$  limit, before the integration over  $\mathbf{k}$  is performed. This simply amounts to replacing the Bose-Einstein distribution function by the classical distribution function, as in (4.1). The classical self-energy is non-vanishing, since the  $\hbar$  in the prefactor of (4.2) is compensated by the  $\hbar$  in the denominator of the classical distribution function. The resulting radial integral is linearly divergent and to handle this we introduce a cut-off in the classical

distribution function  $n_{\text{cl}}(\omega_{\mathbf{k}}) \rightarrow n_{\text{cl}}(\omega_{\mathbf{k}})\theta(\Lambda - k)$ . This particular way of introducing a momentum cut-off in loop integrals does not lead to problems with gauge invariance. This can be most easily understood from the gauge propagator of Landshoff and Rebhan [77, 78] as is explained in appendix 4.A. The result is a linearly divergent classical plasmon frequency

$$\omega_{\text{pl,cl}}^2 = \frac{2}{3\pi^2} g^2 N T \Lambda. \quad (4.5)$$

The relation between the quantum plasmon frequency (4.4) and the classical analogue (4.5) is that the Bose-Einstein distribution function effectively introduces a cut-off of the order of the temperature on the integration,  $\Lambda \sim T/\hbar$ . Since the angular integration is completely decoupled, the dependence on the external momenta of the linearly divergent contribution to the classical self-energy and HTL self-energy are equal.<sup>1</sup> All of this is well-known [12, 25].

Hard thermal loops are the leading contributions to vertex functions for soft external momenta  $|p^0|, p \sim gT$ . Power counting reveals that one-loop diagrams, with any number of external gauge fields, contain a HTL contribution. The fact that the external momenta are small compared to the internal momentum  $k \sim T$  allows for several simplifications in the calculation of HTL's. As a result all HTL's are proportional to the plasmon frequency squared (4.4) [18, 31].

Divergences in classical field theories have a similar behavior, since here also the internal momenta  $k \sim \Lambda$  are much larger than the external momenta. In fact, all classical HTL's have the proportionality factor (4.5). Therefore, all classical HTL's are linearly divergent.

Other one-loop contributions in the quantum theory are smaller by a factor  $p/k \sim p/T$ . In the classical limit these subleading contributions give a factor  $p/k \sim p/\Lambda$ , which reduces the degree of divergence. Therefore we may conclude that all linear divergences at one-loop are given by the classical HTL's.

#### 4.2.2 No logarithmic divergences

Next we will argue that there are no logarithmic divergences at one-loop in the classical theory. Firstly, we discuss one particular example in  $SU(N)$  gauge theory explicitly, which is the spatial part of the self-energy in the Feynman gauge. A convenient starting point is the expression in the quantum theory,

---

1. At least with a (perturbative) continuum-like regularization as employed here. On a spatial lattice, this is not the case [13, 25, 98].

which reads

$$\begin{aligned}
 \Pi_{ij}^{ab}(P) &= \delta^{ab} g^2 \hbar N \int \frac{d^3k}{(2\pi)^3} \left\{ g_{ij} \frac{2n(\omega_{\mathbf{k}}) + 1}{\omega_{\mathbf{k}}} - \frac{A_{ij}}{4\omega_{\mathbf{k}}\omega_{\mathbf{p}+\mathbf{k}}} \times \right. \\
 &\quad \left( [n(\omega_{\mathbf{k}}) + n(\omega_{\mathbf{p}+\mathbf{k}}) + 1] \left[ \frac{1}{p^0 + \omega_{\mathbf{k}} + \omega_{\mathbf{p}+\mathbf{k}}} - \frac{1}{p^0 - \omega_{\mathbf{k}} - \omega_{\mathbf{p}+\mathbf{k}}} \right] \right. \\
 &\quad \left. \left. + [n(\omega_{\mathbf{k}}) - n(\omega_{\mathbf{p}+\mathbf{k}})] \left[ \frac{1}{p^0 - \omega_{\mathbf{k}} + \omega_{\mathbf{p}+\mathbf{k}}} - \frac{1}{p^0 + \omega_{\mathbf{k}} - \omega_{\mathbf{p}+\mathbf{k}}} \right] \right) \right\}, \quad (4.6)
 \end{aligned}$$

with

$$A_{ij} = \frac{1}{2} [8k_i k_j + 5p_i k_j + 3k_i p_j + 4(p^2 - p_0^2)g_{ij} - 2p_i p_j]. \quad (4.7)$$

This diagram contains of course the HTL self-energy (4.2). As before, the classical expression is obtained by taking  $\hbar$  to zero. The non-thermal contribution from the “1” in the first and second line vanishes as  $\hbar$  goes to zero.

From the previous section we know that contributions to the self-energy (4.6) are at most linearly divergent. The classical limit of the momentum-independent tadpole-like contribution in the first line is indeed linearly divergent. For the contribution proportional to  $A_{ij}$ , it implies that the contributions bilinear in the external momenta, i.e. the terms proportional to  $p_i p_j$  or  $p^2 \delta_{ij}$ , can only give ultraviolet finite contributions, and that the terms linear in the external momenta (terms proportional to  $k_i p_j$  or  $p_i k_j$ ) may give logarithmic divergences. The contributions proportional to  $k_i k_j$  may contain logarithmic divergences besides the linearly divergent contributions as well.

To obtain the linearly and logarithmically divergent contributions we expand the integrand in  $1/k$ , so that we can estimate the ultraviolet behavior of the integrand by power counting. The contribution from the second line reads

$$\begin{aligned}
 &\frac{A_{ij}}{4\omega_{\mathbf{k}}\omega_{\mathbf{p}+\mathbf{k}}} [n_{\text{cl}}(\omega_{\mathbf{k}}) + n_{\text{cl}}(\omega_{\mathbf{p}+\mathbf{k}})] \left[ \frac{1}{p^0 + \omega_{\mathbf{k}} + \omega_{\mathbf{p}+\mathbf{k}}} - \frac{1}{p^0 - \omega_{\mathbf{k}} - \omega_{\mathbf{p}+\mathbf{k}}} \right] \\
 &= \frac{A_{ij}}{4k^2} \left\{ \frac{2}{k} n_{\text{cl}}(k) + (\mathbf{p} \cdot \hat{\mathbf{k}}) \left[ \frac{1}{k} n'_{\text{cl}}(k) - \frac{3}{k^2} n_{\text{cl}}(k) \right] + \mathcal{O}(k^{-4}) \right\}. \quad (4.8)
 \end{aligned}$$

We have to distinguish between the quadratic and linear  $k$  behavior of  $A_{ij}$ . The first term on the second line between the curly brackets that multiplies the quadratic term in  $A_{ij}$ , is part of the HTL contribution. The second term between curly brackets that multiplies the quadratic term in  $A_{ij}$ , and the first

term with the linear term in  $A_{ij}$ , contain the contributions proportional to  $k^{-3}$ . These may give a logarithmic divergence after integration. However, it turns out that these contributions are odd under the transformation  $\hat{\mathbf{k}} \rightarrow -\hat{\mathbf{k}}$  and therefore they vanish upon integration. The other terms, including those indicated with  $\mathcal{O}(k^{-4})$ , are ultraviolet finite by power counting.

Similarly, the third line can be expanded, and after some algebra it can be written as

$$\begin{aligned} & \frac{A_{ij}}{4\omega_{\mathbf{k}}\omega_{\mathbf{p}+\mathbf{k}}} [n(\omega_{\mathbf{k}}) - n(\omega_{\mathbf{p}+\mathbf{k}})] \left[ \frac{1}{p^0 - \omega_{\mathbf{k}} + \omega_{\mathbf{p}+\mathbf{k}}} - \frac{1}{p^0 + \omega_{\mathbf{k}} - \omega_{\mathbf{p}+\mathbf{k}}} \right] \\ &= \frac{A_{ij}}{4k^2} \frac{2\mathbf{p} \cdot \hat{\mathbf{k}}}{p_0^2 - (\mathbf{p} \cdot \hat{\mathbf{k}})^2} \left\{ (\mathbf{p} \cdot \hat{\mathbf{k}}) n'_{\text{cl}}(k) + \frac{1}{2} (\mathbf{p} \cdot \hat{\mathbf{k}})^2 n''_{\text{cl}}(k) \right. \\ & \quad \left. - \frac{1}{k} n'_{\text{cl}}(k) \left[ (\mathbf{p} \cdot \hat{\mathbf{k}})^2 - p_0^2 \frac{p^2 - (\mathbf{p} \cdot \hat{\mathbf{k}})^2}{p_0^2 - (\mathbf{p} \cdot \hat{\mathbf{k}})^2} \right] + \mathcal{O}(k^{-4}) \right\}. \quad (4.9) \end{aligned}$$

The first term on the second line, again with  $A_{ij} \propto k_i k_j$ , is part of the HTL contribution, and is proportional to  $k^{-2}$ . The other terms contain a contribution proportional to  $k^{-3}$ , which after integration could yield a logarithmic divergence. However, just as in the previous case these contributions are odd under the transformation  $\hat{\mathbf{k}} \rightarrow -\hat{\mathbf{k}}$  and they vanish upon integration. The remaining terms are ultraviolet finite.

Therefore, we conclude that there is no logarithmic divergence in the spatial part of the retarded classical self-energy in the Feynman gauge. In a similar manner, we have also verified that the spatial part of the three-point vertex contains no logarithmic divergences.

The reason for the vanishing of possible logarithmically divergent contributions lies in the behavior of the self-energy and the vertex functions under parity (P) and time reversal (T). The spatial part of the self-energy discussed here is invariant under  $\mathbf{p} \rightarrow -\mathbf{p}$ , and  $p^0 \rightarrow -p^0$  in combination with complex conjugation (i.e.  $p^0 + i\epsilon \rightarrow -(p^0 + i\epsilon)$  in (4.6)). The point is that the expansion in  $1/k$  turns out to be an expansion in PT odd (dimensionless) functions of  $p^0$  and  $\mathbf{p}$ . Since the linearly divergent HTL contributions to the self-energy are even under P and T, the logarithmically divergent contributions are odd and should therefore vanish. This argument extends to the temporal part of the self-energy as well as to other vertex functions.

Finally we would like to remark that the vanishing of logarithmic divergences holds in general Coulomb or covariant gauges, since the corresponding

gauge fixing term does not break PT invariance, and the same argument can be applied.

### 4.2.3 Classical self-energy: explicit result

The analysis presented above is useful for a general understanding. However, in some cases it is possible to actually calculate the loop integrals and avoid an expansion in  $1/k$ . Here we give one of those explicit results in  $SU(N)$  theory.

We calculate the diagonal ( $ii$ ) part of the classical one-loop retarded self-energy in the Feynman gauge in appendix 4.B, and the result reads

$$\Pi_{ii,\text{cl}}^{ab}(P) = \delta^{ab} g^2 N \left[ \frac{T\Lambda}{\pi^2} \frac{p^0}{p} \ln \frac{p^0 + p}{p^0 - p} + \frac{T}{4\pi} \left( ip^0 - \frac{3p^2 - 4p_0^2}{2p} i \ln \frac{p^0 + p}{p^0 - p} \right) \right]. \quad (4.10)$$

The real and imaginary parts can be obtained in the usual way, using

$$\ln \frac{p^0 + p}{p^0 - p} = \ln \left| \frac{p^0 + p}{p^0 - p} \right| - i\pi\theta(p^2 - p_0^2). \quad (4.11)$$

The linear divergence is precisely the equivalent of the hard thermal loop contribution, which follows from the replacement  $T\Lambda/\pi^2 \rightarrow T^2/(6\hbar)$ . The finite terms are exactly equal to the terms linear in  $T$  that are obtained in a high temperature expansion in the quantum theory, as can be checked explicitly [35, 118].<sup>2</sup> There are no other terms. The  $p^0 \rightarrow 0$  limit equals the well-known result from the quantum theory in the Feynman gauge [62]

$$\Pi_{ii,\text{cl}}^{ab}(0, \mathbf{p}) = -\delta^{ab} g^2 N \frac{3pT}{8}. \quad (4.12)$$

Note that in this limit the leading-order behavior is completely determined by classical physics.

To conclude the one-loop analysis, the above described situation can be understood also directly by keeping  $\hbar$  in the high-temperature expression of the quantum theory. The high-temperature expansion then has the form [35, 118]

$$\begin{aligned} \Pi_{ii}^{ab}(P) = & \delta^{ab} g^2 N \left[ \frac{T^2}{\hbar} \Pi_{-1}(P) + T \Pi_0(P) + \right. \\ & \left. \left( \hbar \ln \frac{T}{\hbar\mu} \right) \Pi_{\log}(P) + \hbar \Pi_1(P) + \mathcal{O}\left(\frac{\hbar^3}{T^2}\right) \right], \quad (4.13) \end{aligned}$$

2. Up to some typographical errors.

where  $\mu$  is the renormalization scale. The term proportional to  $T^2$  is the HTL part, which turns into the linearly divergent term when  $\hbar \rightarrow 0$ , and the second term in this expansion is the finite term in the classical theory. All the other terms vanish when  $\hbar \rightarrow 0$ . Let us finally remark, that for soft momenta  $P \sim gT$  it is known that the quantum self-energy should be calculated with HTL resummed propagators and vertices, for the classical approximation to be valid in this case, the HTL's should be included in the (then effective) classical theory.

### 4.3 Two-loop and beyond

#### 4.3.1 Degree of divergence

In this section we study the degree of divergence of higher-loop diagrams in the classical theory. In the first part we shall argue that the superficial degree of divergence of the self-energy decreases by one with each loop, starting with the one-loop linear divergence. Then we will check this statement explicitly for a number of diagrams. We shall argue that the same is true for classical vertex functions in section 4.3.3.

To make the argument for the self-energy, we start with the following basic assumption: in the high-temperature limit the retarded self-energy in the quantum theory scales according to its dimension, i.e., the quantum retarded gluon self-energy behaves as

$$\Pi_{\mu\nu}(P) = T^2 \bar{\Pi}_{\mu\nu}(p^0/p, \hat{\mathbf{p}}, g) + T^2 \mathcal{O}(P/T), \quad (4.14)$$

for high temperatures, fixed external momentum and frequency, and a renormalization scale of the order of the temperature  $\mu \sim T$ . This assumption consists of two parts: The contribution of diagrams with hard momenta  $K \sim T$  on all internal lines yields a term proportional to  $T^2$  in the self-energy. Contributions that are excluded in (4.14) are of the form  $g^{2L} T^2 (T/P)^m$  for  $m > 0$  and with  $L$  indicating the number of loops. For *fixed* external momenta and high temperatures such terms become larger than the one-loop (HTL) contribution  $g^2 T^2$ , so they invalidate a loop expansion. Therefore the assumed absence of these contributions can be re-expressed by saying that we assume that hard modes are perturbative. The second part of the assumption is that also diagrams with soft internal momenta give a  $T^2$  contribution. This relies on the belief that infrared divergences are controlled by induced masses which are proportional to the temperature, such as the electric and magnetic masses in  $SU(N)$  gauge theories.

Let us then consider a classical contribution to the self-energy containing  $M$  distribution functions. To be able to compare the degree of divergence of such a contribution with the quantum expression, we regard the temperature in the quantum self-energy as a particular ultraviolet cut-off. Using the assumption (4.14) we count the degree of divergence as 2. Since every classical distribution function gives rise to an extra energy in the denominator when compared to the quantum diagram,<sup>3</sup> the classical contribution to the self-energy with  $M$  distribution functions has then a superficial degree of divergence  $2 - M$ .

To complete the argument, we now use that the number of distribution functions  $M$  can be related to the number of loops  $L$  in the following manner [44, 52]. One way to obtain the retarded self-energy is by using the imaginary-time or Matsubara formalism [18, 67]. One first performs the sums over the discrete loop frequencies and then analytically continues the external frequencies to real values with a small positive part to incorporate the appropriate retarded boundary conditions. In the imaginary-time formalism the number of loops equals the number of Matsubara frequency summations. Using the method of contour integration to perform these sums, each sum gives rise to one ‘coth’ function, either with positive or negative energy. Explicitly, each sum gives a factor [44, 52]

$$\frac{1}{2} \coth \frac{s\hbar\omega}{2T} = n(s\omega) + \frac{1}{2} = s[n(\omega) + \frac{1}{2}], \quad s = \pm. \quad (4.15)$$

Hence, the resulting expressions are of the form of spatial momentum integrals over Bose-Einstein distribution functions, where the number of distribution functions is equal to or less than the numbers of loops. The classical limit can now be taken by replacing  $n(\omega) + \frac{1}{2} \rightarrow T/(\hbar\omega)$ , such that the  $\hbar$ 's counting the loops cancel against the  $1/\hbar$ 's from the distribution functions. After taking the classical limit, only the leading term, which has as many distribution functions as loops, remains and the number of classical distribution functions  $M$  in a given diagram is counted by the number of loops,  $M = L$ . Note that this applies not only to the self-energy diagrams but to vertex functions as well. It follows then that the superficial degree of divergence of a classical diagram is given by  $2 - L$ , such that the classical one-loop contribution to the self-energy is superficially linearly divergent, the two-loop contribution

---

3. In the ultraviolet regime of a loop integral the quantum (Bose) distribution function can be approximated as  $\exp -\beta\hbar\omega$  and acts as a cut-off function. On the other hand, the classical distribution function remains proportional to  $1/\omega$ .

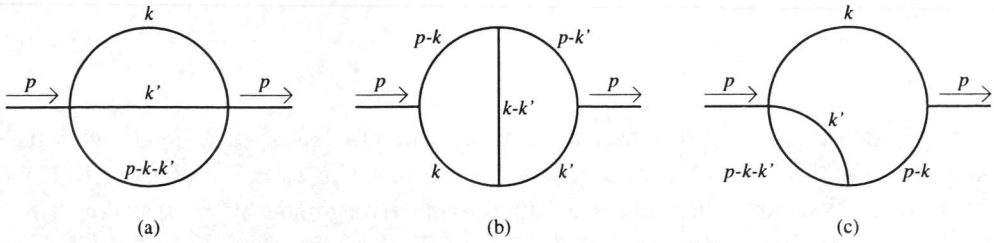


**Figure 4.1:** Two-loop diagrams. The setting sun diagram (a) and diagram (b) are discussed in section 4.3.2, and diagram (c) is treated in appendix 4.C.

is superficially logarithmically divergent, and higher-loop contributions are superficially finite.

### 4.3.2 Two-loop self-energy diagrams

We now want to verify the general argument of the previous section for the two-loop self-energy diagrams appearing in  $SU(N)$  and scalar field theory. We do not discuss diagrams which have a one-loop self-energy subdiagram (and hence also a linear subdivergence), but we concentrate on the two-loop diagrams as shown in fig. 4.1. Furthermore, since we are only interested in the structure of ultraviolet divergences, i.e. in power counting, we do not need to make a distinction between gauge field propagators in the Feynman gauge and ghost propagators in the loops.

Let us, as a first relatively simple example, consider the two-loop setting-sun contribution (a) to the retarded self-energy as it appears in  $\lambda\phi^4$ -theory (with  $\lambda = g^2$ ) and  $SU(N)$  gauge theory. It reads

$$\begin{aligned} \Pi^{(a)}(P) = & \frac{1}{6}(g^2\hbar)^2 \int \frac{d^3k}{(2\pi)^3} \int \frac{d^3k'}{(2\pi)^3} \sum_{ss's_1} \frac{ss's_1}{2^3\omega_{\mathbf{k}}\omega_{\mathbf{k}'}\omega_{\mathbf{k}_1}} \times \\ & \frac{1}{p^0 + s\omega_{\mathbf{k}} + s'\omega_{\mathbf{k}'} + s_1\omega_{\mathbf{k}_1}} \left\{ [1 + n(s\omega_{\mathbf{k}})] [1 + n(s'\omega_{\mathbf{k}'})] [1 + n(s_1\omega_{\mathbf{k}_1})] \right. \\ & \left. - n(s\omega_{\mathbf{k}})n(s'\omega_{\mathbf{k}'})n(s_1\omega_{\mathbf{k}_1}) \right\}, \end{aligned} \quad (4.16)$$

where  $\omega_{\mathbf{k}_1} = \omega_{\mathbf{p}-\mathbf{k}-\mathbf{k}'}$ , and the sum is over all  $s$ 's being  $\pm$ .

Note that the product of three distribution functions drops out. It is then clear that the classical limit of (4.16),

$$\Pi_{\text{cl}}^{(a)}(P) = \frac{1}{6}g^4 \int \frac{d^3k}{(2\pi)^3} \int \frac{d^3k'}{(2\pi)^3} \sum_{ss's_1} \frac{1}{2^3\omega_{\mathbf{k}}\omega_{\mathbf{k}'}\omega_{\mathbf{k}_1}} \times$$

$$\frac{1}{p^0 + s\omega_{\mathbf{k}} + s'\omega_{\mathbf{k}'} + s_1\omega_{\mathbf{k}_1}} \left( s_1 \frac{T^2}{\omega_{\mathbf{k}}\omega_{\mathbf{k}'}} + s' \frac{T^2}{\omega_{\mathbf{k}}\omega_{\mathbf{k}_1}} + s \frac{T^2}{\omega_{\mathbf{k}'}\omega_{\mathbf{k}_1}} \right), \quad (4.17)$$

contains products of two classical distribution functions, in accordance with the statement that the number of loops equals the number of distribution functions. We now estimate the degree of divergence by power counting and take the loop momenta  $k, k' \sim \Lambda$ . The integral measures give two contributions  $\sim \Lambda^3$ , and all single energy denominators  $1/\omega$  give a factor  $1/\Lambda$ . The energy denominator that contains  $p^0$  will produce, for generic large loop momenta  $\mathbf{k}, \mathbf{k}'$ , a hard energy denominator  $\sim 1/\Lambda$ . It can only produce a soft energy denominator when there is a cancellation, which is in the special case that  $\mathbf{k} \simeq \pm \mathbf{k}'$ , depending on the signs of  $s, s'$  and  $s_1$  [31]. However, for these special configurations the integral over phase space is restricted so that this will not alter the degree of divergence. We will use this estimate for energy denominators with three hard energies [31] below as well.

By power counting we therefore establish that this contribution is logarithmically divergent, as expected. This is also the result obtained in [1, 2, 36], where the classical setting sun diagram was analyzed in detail and it was shown that in fact the logarithmic divergence can be separated and is independent of the external momentum and frequency.

It should be noted that the setting-sun diagram (as well as the diagrams discussed below) contains an infrared divergence for vanishing external momentum [11]. For massless  $\lambda\phi^4$  theory, this can be cured by resumming the effective thermal mass, arising from the one-loop tadpole diagram. This has only an effect on the soft infrared modes, and does not interfere with the ultraviolet behavior of the classical diagram we investigated above.

The next example we treat is the two-loop diagram (b) in fig. 4.1, which appears in  $SU(N)$  and in scalar  $\phi^3$ -theory. This particular diagram is more delicate, and it is instructive to carry out the procedure described above in detail. We will verify explicitly that in  $SU(N)$  theory (the spatial part of) this diagram is logarithmically divergent in the Feynman gauge.

Since we are only interested in the degree of divergence of the diagram, we may ignore the color and Lorentz structure of the diagram. The momentum-dependence of the four vertices in the gauge theory results in a fourth-order polynomial in internal and external momenta which we denote by  $(k)_{ij}^4$ . The precise form of the momentum insertions is unimportant for the power counting performed below.

We have found it convenient to calculate this diagram in the imaginary-time formalism, and after performing the sums over the Matsubara frequen-

cies, the diagram can be written as

$$\begin{aligned}
 \Pi_{ij}^{(b)}(P) = & \frac{1}{2}(g^2\hbar)^2 \int \frac{d^3k}{(2\pi)^3} \int \frac{d^3k'}{(2\pi)^3} (k)_{ij}^4 \sum_{ss's_1s_2s_3} \frac{ss's_1s_2s_3}{2^5\omega\omega'\omega_1\omega_2\omega_3} \times \\
 & \frac{1}{p^0 + s'\omega' + s_3\omega_3} \frac{1}{p^0 + s\omega + s_2\omega_2} \left\{ \frac{1}{-s_3\omega_3 + s_2\omega_2 + s_1\omega_1} \times \right. \\
 & \left. \left( [n(s_1\omega_1) + 1][n(s_2\omega_2) + 1]n(s_3\omega_3) - n(s_1\omega_1)n(s_2\omega_2)[n(s_3\omega_3) + 1] \right) \right. \\
 & + \frac{1}{p^0 + s_3\omega_3 + s\omega - s_1\omega_1} \times \\
 & \left. \left( [n(s_3\omega_3) + 1][n(s\omega) + 1]n(s_1\omega_1) - n(s_3\omega_3)n(s\omega)[n(s_1\omega_1) + 1] \right) \right. \\
 & + \frac{1}{p^0 + s'\omega' + s_2\omega_2 - s_1\omega_1} \times \\
 & \left. \left( [n(s'\omega') + 1][n(s_2\omega_2) + 1]n(s_1\omega_1) - n(s'\omega')n(s_2\omega_2)[n(s_1\omega_1) + 1] \right) \right. \\
 & + \frac{1}{s'\omega' - s\omega + s_1\omega_1} \times \\
 & \left. \left. \left( [n(s_1\omega_1) + 1][n(s'\omega') + 1]n(s\omega) - n(s_1\omega_1)n(s'\omega')[n(s\omega) + 1] \right) \right\}, \tag{4.18}
 \end{aligned}$$

where we have used the shorthand notation

$$\omega = \omega_{\mathbf{k}}, \quad \omega' = \omega_{\mathbf{k}'}, \quad \omega_1 = \omega_{\mathbf{k}-\mathbf{k}'}, \quad \omega_2 = \omega_{\mathbf{p}-\mathbf{k}}, \quad \omega_3 = \omega_{\mathbf{p}-\mathbf{k}'}, \tag{4.19}$$

and the sum is over all sign factors  $s = \pm 1$ . Again the products of three distribution functions drop out. The corresponding classical integral  $\Pi_{ij,cl}^{(b)}(P)$  may be obtained by taking the  $\hbar \rightarrow 0$  limit, which amounts to neglecting the constants and single distribution functions and replacing all distribution functions that appear in products of two by classical distribution functions.

We will now consider the large  $k, k' \sim \Lambda$  behavior of the classical diagram as we did for the setting sun diagram, by looking at the various factors in  $\Pi_{ij,cl}^{(b)}(P)$  and naively combine those to obtain an indication for its degree of divergence. First of all, each integration measure contributes  $d^3k \sim \Lambda^3$  and the factor  $(k)_{ij}^4$  is proportional to  $\Lambda^4$ . Each of the energies in the denominator on the first line gives a contribution  $1/\omega \sim 1/\Lambda$ , such that this factor leads to a contribution  $1/\Lambda^5$ . Each classical distribution function gives a factor  $1/\Lambda$  as well.

The other energy denominators require a bit more care. All energy denominators between the curly brackets contain three large energies that will generically not cancel, as in the case of the setting sun diagram. These therefore contribute with a factor  $1/\Lambda$ . The two energy denominators in the second line may produce a ‘soft’ energy denominator for specific combinations of the sign factors, namely for  $s_3 = -s'$ , and  $s_2 = -s$ . For example, the first denominator may give

$$\frac{1}{p^0 + s'(\omega_{\mathbf{k}'} - \omega_{\mathbf{p}-\mathbf{k}'})} \sim \frac{1}{p^0 + s'\hat{\mathbf{k}} \cdot \mathbf{p}} \sim \Lambda^0, \quad (4.20)$$

similar to what happens in the one-loop case. This gives us four possibilities: both energy denominators are soft, only one of them is soft and the other is hard, or both are hard. Putting all these estimates together, we obtain in the first case, with two soft denominators, the naive result  $\Pi_{ij,cl}^{(b)}(P) \sim \Lambda^6 \Lambda^4 \Lambda^{-5} \Lambda^{-2} \Lambda^{-1} \sim \Lambda^2$ , which is a quadratic divergence. With one soft denominator we find  $\Pi_{ij,cl}^{(b)}(P) \sim \Lambda$ , a linear divergence, and with two hard contributions  $\Pi_{ij,cl}^{(b)}(P) \sim \Lambda^0$ , the expected logarithmic behavior. However, from the general argument we expect solely a logarithmic divergence.

The reason for this mismatch is that this naive power counting doesn't treat the distribution functions correctly. In the one-loop (HTL) case, often differences of statistical factors appear. In the classical theory, these lead to a different ultraviolet behavior and hence change the power counting. Therefore we take a closer look at the two-loop diagram to see whether a similar thing occurs here as well. We denote the (naively) quadratically divergent piece, with  $s_3 = -s'$  and  $s_2 = -s$ , by  $\tilde{\Pi}_{ij,cl}^{(b)}(P)$ . To re-estimate the divergence, we put the external momentum in the energy denominator with three large loop-energies (i.e. in the second, fourth and sixth line of (4.18)) equal to zero, since for generic large  $\mathbf{k}, \mathbf{k}'$  the denominator does not vanish.<sup>4</sup> Taking the external momentum equal to zero can in fact be seen as the zeroth order term in an expansion in the external momentum. The first order term, linear in the external momentum, is treated in appendix 4.C. The naively quadratically divergent contribution can now be written, after flipping  $s_1$  to  $-s_1$  in the term on the sixth line, as

$$\tilde{\Pi}_{ij,cl}^{(b)}(P) = \frac{1}{2}(g^2 \hbar)^2 \int \frac{d^3 k}{(2\pi)^3} \int \frac{d^3 k'}{(2\pi)^3} (k)_{ij}^4 \sum_{s s' s_1} \frac{s_1}{2^5 \omega \omega' \omega_1 \omega_2 \omega_3} \times$$

4. Again, the region where it does vanish is only a restricted part of phase space and is excluded in the argument for power counting.

$$\frac{1}{p^0 + s'(\omega' - \omega_3)} \frac{1}{p^0 + s(\omega - \omega_2)} \frac{1}{s'\omega' - s\omega + s_1\omega_1} \times \\ [n_{\text{cl}}(s\omega_2) - n_{\text{cl}}(s\omega)] [n_{\text{cl}}(s'\omega_3) - n_{\text{cl}}(s'\omega')] . \quad (4.21)$$

We redo the power counting for  $\tilde{\Pi}_{ij,\text{cl}}^{(b)}(P)$ . The thing to notice is that indeed two differences of two classical distribution functions have appeared, and for hard loop-momenta

$$[n_{\text{cl}}(s\omega_{\mathbf{p}-\mathbf{k}}) - n_{\text{cl}}(s\omega_{\mathbf{k}})] \sim -s(\hat{\mathbf{k}} \cdot \mathbf{p})n'_{\text{cl}}(\omega_{\mathbf{k}}) \sim \Lambda^{-2}. \quad (4.22)$$

Both differences give one extra power of  $1/\Lambda$ , compared to the naive power counting employed before. The conclusion is therefore that  $\tilde{\Pi}_{ij,\text{cl}}^{(b)}(P)$ , instead of being quadratically divergent, is only superficially logarithmically divergent, as expected by the general argument.

Note that the classical limit of diagram (b) may contain a linear divergence from a HTL (three-point) subdiagram. The linear divergence occurs, e.g. in contribution (4.21), whenever  $(k)_{ij}^4 \sim k^3 k'$  or  $(k)_{ij}^4 \sim k k'^3$ . However, at this stage we are not interested in divergences caused by one-loop subdiagrams since we study only the superficial degree of divergence.

Potentially, there are also superficial linear divergences in the classical limit of (4.18). These are worked out in appendix 4.C. In this appendix we also discuss the other self-energy contribution (c), which is naively linearly divergent as well. It turns out that they are all in fact logarithmically divergent, in accordance with the general argument of the preceding section.

### 4.3.3 Higher-order vertex functions

We now extend the argument to general vertex functions. At zero-temperature we know that the degree of divergence of a Feynman diagram decreases with the number of external lines. In a real-time classical theory at non-zero temperature this is not the case. We already saw that the linear divergences at one-loop occur for diagrams with any number of external gauge field lines. Therefore we do not expect that the two-loop contributions to three- or higher-point functions are finite.

To argue what happens for vertex functions with more loops, we use the real-time Feynman rules which are presented for scalar field theory in section 2.7. We employ Feynman rules in which two type of propagators appear, the temperature-independent retarded propagator  $G_0^R$  and the thermal two-point function  $S_0$  that contains the thermal distribution. It is useful to

recall here their explicit representation (2.48), (2.49)

$$G_0^R(K) = \sum_{s=\pm} \frac{1}{2\omega_{\mathbf{k}}} \frac{s}{k^0 + i\epsilon + s\omega_{\mathbf{k}}}, \quad S_0(K) = \sum_{s=\pm} n_{\text{cl}}(s\omega_{\mathbf{k}}) \frac{2\pi s}{2\omega_{\mathbf{k}}} \delta(k^0 - s\omega_{\mathbf{k}}). \quad (4.23)$$

Starting from the classical retarded self-energy with  $L$  loops (and hence  $M = L$  thermal propagators), generalized retarded  $n$ -point functions with  $L$  loops can be obtained by adding retarded Green functions in the loops, using the vertices (a) and (c) shown in fig. 2.5 of section 2.7. Note that thermal propagators cannot be added in the loops, since then the number of distribution functions  $M$  is no longer equal to the number of loops, which is required by the argument given in section 4.3.1 and is needed to have the cancellation of  $\hbar$  in the classical diagrams. Note that this also implies that all integrals over the zeroth components of the loop momenta can trivially be performed with the help of the on-shell delta functions in the thermal propagators.

To continue, in the case of a gauge theory, every additional (momentum-dependent) three-point vertex gives an additional factor  $K$  (we do not need to be more specific for the power counting argument presented below). Hence the total effect of adding one external line using a three-point vertex is an additional factor  $K$  times a retarded propagator

$$\frac{K}{\omega_{\mathbf{k}}} \frac{s}{k^0 + i\epsilon + s\omega_{\mathbf{k}}}. \quad (4.24)$$

From the viewpoint of power counting, the first factor is of order  $\Lambda^0$ , and the second factor can be of order  $\Lambda^0$  or  $1/\Lambda$ , depending on whether a soft or hard energy denominator results, after the integrals over the on-shell delta functions in the thermal propagators have been performed.

This leads us to give the following general argument: in the case that the propagator in (4.24) is soft, the additional external line will not change the degree of divergence, compared to the diagram without the additional line. On the other hand, when the energy denominator turns out to be hard, when the extra vertex is a 4-point vertex, or in scalar field theory, where the momentum  $K$  in the numerator is absent, additional lines will always lower the degree of divergence. Using the result for the two-point function, this implies that higher-point vertex functions are superficially logarithmically divergent by power counting (at two-loop) or finite (at higher-loop).

There is one slight complication in this general argument. In the self-energy considered in the previous section, the logarithmic divergence was the

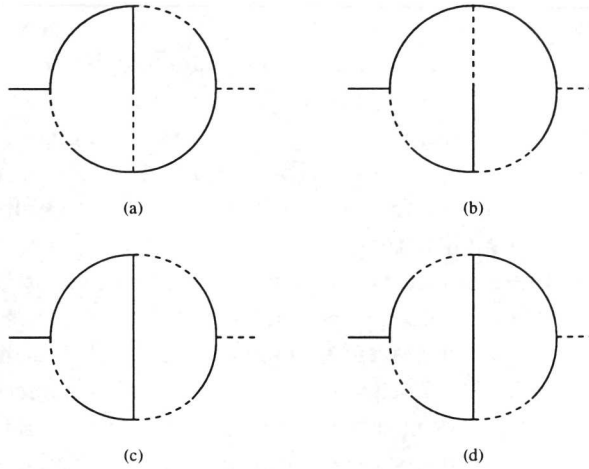


**Figure 4.2:** Two-loop diagrams in the real-time formulation that contribute in the classical limit. Full lines are thermal propagators and dashed-full lines retarded propagators.

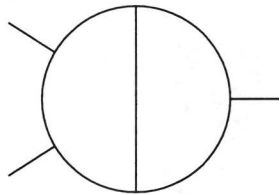


**Figure 4.3:** Two-loop diagram with three external lines.

result of a subtle cancellation between quadratically (and linearly) divergent contributions. The question is whether this subtle cancellation is not spoiled by adding an external line. Although a complete analysis of two-loop vertex functions is beyond the scope of this chapter, we will check explicitly in one particular case that the cancellation indeed still occurs.

This analysis can be done most conveniently using the real-time Feynman rules of section 2.7. We start by presenting in fig. 4.2 the classical two-loop contribution to the self-energy (b) in the real-time formalism. The integral over the zeroth components of the loop momenta can easily be performed using the on-shell delta functions in the thermal propagators, and we have verified that this yields indeed the classical limit of (4.18), which was calculated in the imaginary-time formalism, as expected.

We want to add one external line to obtain a diagram as in fig. 4.3.

In the case of the self-energy that we discussed in the previous section we found that the naively quadratically divergent contribution (4.21) does not contain a distribution function at energy  $\omega_1 = \omega_{\mathbf{k}-\mathbf{k}'}$ . That means that in terms of the real-time diagrams no diagram with a thermal propagator on the line shared by the two loops contributes to (4.21). Hence we do not need to consider the addition of extra lines to the third and fourth diagram. Let's now see how an additional three-point vertex of type (a) in fig. 2.5 and an additional retarded Green function can be added to the first two diagrams in fig. 4.2. It turns out that for each diagram (a) and (b) there are 14 possibilities to do this. A closer look, however, reveals that not all diagrams are needed to establish a cancellation of the naive quadratic divergence. For example, a combination of the two diagrams that are shown in fig. 4.4 is sufficient to obtain a difference between distribution functions that reduces the degree of divergence to a logarithmic one.

Indeed, the sum of the most divergent part of the diagrams in fig. 4.4 yields

$$\Gamma_{ijk,cl}^{(a+b)} = g^5 \hbar^2 \int \frac{d^3 k}{(2\pi)^3} \int \frac{d^3 k'}{(2\pi)^3} (k)_{ijk}^5 \sum_{ss's_1} \frac{ss_1}{2^6 \omega_{\mathbf{k}}^3 \omega_{\mathbf{k}'}^2 \omega_{\mathbf{k}-\mathbf{k}'}} \frac{1}{p_1^0 + s\mathbf{p}_1 \cdot \hat{\mathbf{k}}} \frac{1}{p_2^0 + s\mathbf{p}_2 \cdot \hat{\mathbf{k}}} \frac{1}{q^0 - s'\mathbf{q} \cdot \hat{\mathbf{k}'}} \frac{1}{s_1 \omega_{\mathbf{k}-\mathbf{k}'} - s\omega_{\mathbf{k}} - s'\omega_{\mathbf{k}'}} \frac{1}{[n_{cl}(s\omega_{\mathbf{p}_1-\mathbf{k}}) - n_{cl}(s\omega_{\mathbf{k}})] [n_{cl}(s'\omega_{\mathbf{q}-\mathbf{k}'}) - n_{cl}(s'\omega_{\mathbf{k}'})]}, \quad (4.25)$$

with  $Q = P_1 + P_2$ . The factor  $(k)_{ijk}^5$  has been included to account for the momentum insertions from the vertices in a  $SU(N)$  gauge theory, and the factor  $\hbar^2$  arises from loop-counting. We had to expand also the single energy denominators, such as  $1/\omega_{\mathbf{p}_1-\mathbf{k}}$ , in external momenta. Compared to the self-energy expression (4.21) the vertex function has one extra factor (4.24) with a soft energy denominator as anticipated. After power counting, taking into account (4.22), we may conclude that in this particular combination the addition of one external line does not spoil the reduction from a quadratic divergence to a logarithmic divergence.

It will be interesting to make explicit checks for other three- (and higher) point vertex functions with two loops as well. However without a clever method to combine the different contributions this seems to be out of the question.

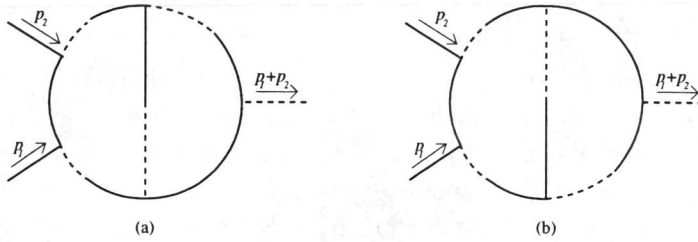


**Figure 4.4:** Two-loop contributions to the classical 3-point vertex function in the real-time formalism that combined yield a logarithmic degree of divergence.

### 4.3.4 Other gauges

To verify the general argument in section 4.3.1 that two-loop diagrams are logarithmically divergent, we have estimated in sections 4.3.2 and 4.3.3 the degree of divergence of some two-loop diagrams in the Feynman gauge. Here we want to argue that the estimates in the Feynman gauge extend to general Coulomb gauges [31].

The retarded gauge propagator in a general Coulomb gauge with gauge parameter  $\alpha_C$  reads

$$\Delta_{\mu\nu} = \frac{1}{K^2} T_{\mu\nu}(\mathbf{k}) + \delta_{\mu 0} \delta_{\nu 0} \frac{1}{k^2} + \alpha_C \frac{K_\mu K_\nu}{k^4}, \quad (4.26)$$

with the transverse projector  $T_{ij}(\mathbf{k}) = \delta_{ij} - k_i k_j / k^2$ ,  $T_{00} = T_{0i} = T_{i0} = 0$ .

First we realize that the external momentum dependence in the transverse projector may be neglected  $T_{\mu\nu}(\mathbf{p} - \mathbf{k}) \sim T_{\mu\nu}(\mathbf{k})$  when the integration momentum  $\mathbf{k}$  is large. In the power counting of a diagram we may estimate  $T_{\mu\nu} \sim 1$ , and we see that a diagram with all transverse propagators has the same degree of divergence as the same diagram in the Feynman gauge. Since the 00-component and the gauge dependent part of the propagator cannot give a soft denominator like (4.20), we can also neglect the external momenta in these components; they are then estimated as  $k^{-2}$ . Therefore diagrams containing these components of the propagator will not have a larger degree of divergence. We conclude that the degree of divergence of a certain diagram is the same in the Feynman gauge as in a general Coulomb gauge. We stress that this does not necessarily imply that the logarithmically divergent contribution is gauge independent as is the case for the linear divergences, this remains a subject for further study.

Finally we like to remark that in general covariant gauges it is not expected that individual diagrams obey the power counting of section 4.3.1, but rather the sum of the diagrams with a certain number of loops.

#### 4.4 Discussion

The important result of this chapter is that the divergence of two-loop diagrams was at most logarithmic. This is fortunate, since otherwise it would not be possible to use perturbation theory in the calculation of the effect of hard modes on soft modes even in a quantum theory. Consider for instance, the hard-mode contribution to a two-loop self-energy diagram at soft momentum. If the classical limit would give a superficial linear divergence instead of a logarithmic one, it would schematically read  $g^4 T^2 \Lambda / P$ . The  $T^2$  comes from the two classical distributions functions, the linear divergence gives  $\Lambda$ , to make the dimensions correct we need an energy scale in the denominator this can only be given by the external momentum. In the quantum theory we would have a similar contribution with  $\Lambda \sim T$  (see remark 4. in section 2.4), which gives  $g^4 T^3 / P$ . For soft momenta  $P \sim g^2 T$  this is as large as the HTL contribution. Hence the occurrence of a linear divergence at two loops in a classical theory would invalidate the perturbative treatment of the hard modes even in a quantum theory. Fortunately, we have found in our two-loop calculations only superficial logarithmic divergences.

The result that superficial divergence decreases per loop is also an essential property that allows one to introduce counterterms to reduce the cut-off dependence of the classical theory. We will discuss this further in the next chapter, where we will make use of this result.

Here we would like suggest that the classical log divergences point to an effective low-energy theory beyond the HTL approximation. Consider for instance the effective action for soft modes with momenta  $P < \Lambda_{\text{int}}$ , with  $\Lambda_{\text{int}}$  an intermediate scale  $\omega_{\text{pl}} < \Lambda_{\text{int}} < T/\hbar$ . In a classical or high-temperature expansion, the effective action for the soft modes would look like

$$\Gamma_{\text{eff}} = g^2 T \left( \frac{T}{\hbar} - c_1 \Lambda_{\text{int}} \right) \bar{\Gamma}_{\text{HTL}} + (g^2 T)^2 \log \left( \frac{c_2 T}{\hbar \Lambda_{\text{int}}} \right) \bar{\Gamma}_{\text{log}} + S_{\text{cl}} + \mathcal{O} \left( g^2 \hbar, \frac{\hbar \Lambda_{\text{int}}}{T}, \frac{\omega_{\text{pl}}}{\Lambda_{\text{int}}} \right), \quad (4.27)$$

with  $c_1, c_2$  constants that depend on the regularization. The HTL action is proportional to  $\hbar^{-1}$ , while the term proportional to  $\log(c_2 T / \hbar \Lambda_{\text{int}})$  corresponds to the classical log divergences. In this way they may provide a natural extension beyond HTL's. A consistent scheme to include hard mode contributions beyond hard thermal loops, thus seems to be to include the hard mode contributions that diverge in the classical limit.

In any case, the inclusion of linear and logarithmic divergences in the

classical theory as counterterms or as hard-mode contributions will give a current in the equation of motion for the gauge field (similar as the HTLs enter as a current in Maxwell's equation, see (3.18-3.20). For consistency, it is necessary that this current is conserved. In the next section, we will show that the log divergent part of the self-energy is transverse. This implies that the current that generates this logarithmic part is conserved.

#### 4.5 Transversality of the log divergent part of the self-energy

In the following we will verify that the logarithmic divergent part of the classical retarded self-energy is transverse.

We start with a short review of the Ward identity for the self-energy at non-zero temperature [18,119]. For the full retarded propagator  $D_{R,\text{full}}^{\mu\nu}$  in the covariant gauge with gauge parameter  $\alpha$ , the Ward identity reads

$$P_\mu P_\nu D_{R,\text{full}}^{\mu\nu} = -\alpha. \quad (4.28)$$

This identity is the same at zero and non-zero temperature.

At zero temperature the self-energy  $\Pi^{\mu\nu}$  must be a linear combination of the two available tensors  $g^{\mu\nu}$  and  $P^\mu P^\nu$ . Using the relation between the self-energy and the full propagator, the Ward identity (4.28) gives an equation for the self-energy. The result is that the self-energy at zero temperature is transverse.

At non-zero temperature the self-energy tensor can also depend on the four velocity  $u^\mu$  of the plasma (we will always take  $u^\mu = (1, 0, 0, 0)$ ). Hence the self-energy can be expressed in four tensors, for instance  $g^{\mu\nu}$ ,  $P^\mu P^\nu$ ,  $u^\mu u^\nu$ , and  $u^\mu P^\nu + P^\mu u^\nu$ . More convenient are the dimensionless tensors  $T^{\mu\nu}$ ,  $L^{\mu\nu}$ ,  $C^{\mu\nu}$ , and  $D^{\mu\nu}$ , detailed in [119]. We express the self-energy in these tensors

$$\Pi^{\mu\nu} = \Pi_T T^{\mu\nu} + \Pi_L L^{\mu\nu} + \Pi_C C^{\mu\nu} + \Pi_D D^{\mu\nu}. \quad (4.29)$$

Important is that  $T$  and  $L$  are transverse with respect to the four momentum  $P^\mu$  (3.13), whereas  $C$  and  $D$  are not:

$$P_\mu T^{\mu\nu} = P_\mu L^{\mu\nu} = 0, \quad P_\mu C^{\mu\nu} \neq 0, \quad P_\mu D^{\mu\nu} \neq 0. \quad (4.30)$$

Hence the self-energy is transverse when  $\Pi_C = \Pi_D = 0$ .

From (4.28) and the decomposition (4.29) the Ward identity for the self-energy can be derived, see e.g. [119],

$$[\Pi_C(P)]^2 = [P^2 + \Pi_L(P)] \Pi_D(P). \quad (4.31)$$

This identity holds for linear gauges that do not break rotational invariance. At non-zero temperature the Ward identity does not imply that the self-energy is transverse. Indeed an explicit calculation shows that already at one loop the self-energy is not transverse [82]. It is a very special feature of the hard thermal loop self-energy that it is transverse:  $P_\mu \Pi_{HTL}^{\mu\nu} = 0$ .

We will simplify the Ward identity (4.31) for the divergent parts of the self-energy. We take  $P^2 \neq 0$ .

Let us start at one loop. Since  $\Pi_C = 0$  at tree-level, it starts at  $\mathcal{O}(g^2)$ . From the Ward identity (4.31) with  $P^2 \neq 0$ , it follows that  $\Pi_D$  starts at  $\mathcal{O}(g^4)$ . Since the two-loop contribution,  $\Pi_D^{2l}$  is superficially log divergent, it can at most contain one linear subdivergence. Hence, the one-loop contribution to  $\Pi_C$  cannot contain a linear divergence. Therefore the linear divergent part of the one-loop self-energy is transverse:

$$P^\mu \Pi_{\mu\nu}^{1l,\text{lin}} = 0. \quad (4.32)$$

From the correspondence between linear divergences and HTL's and the transversality of the HTL self-energy, this was already known. The above argument may be viewed as a particularly simple (re-)derivation of the result that the HTL self-energy is transverse.

Now we turn to the logarithmic divergences at two loops. We start again with the  $D$ -component. We split the two-loop self-energy in a logarithmic divergent part, a part that contains a linear subdivergence and a finite part

$$\Pi_D^{2l} = \Pi_D^{2l,\text{log}} + \Pi_D^{2l,\text{sublin}} + \Pi_D^{2l,\text{fin}}. \quad (4.33)$$

We insert (4.33) in the Ward identity (4.31). Since at one loop there is no logarithmic divergence and  $P^2 \neq 0$ , we get

$$\Pi_D^{2l,\text{log}} = 0. \quad (4.34)$$

We saw already that  $\Pi_C$  does not contain a linearly divergent part, therefore we get as a bonus

$$\Pi_D^{2l,\text{sublin}} = 0. \quad (4.35)$$

Next, we consider  $\Pi_C$ . Analogous to (4.33), we write

$$\Pi_C^{2l} = \Pi_C^{2l,\text{log}} + \Pi_C^{2l,\text{sublin}} + \Pi_C^{2l,\text{fin}}. \quad (4.36)$$

We use the Ward identity at  $\mathcal{O}(g^8)$ , for which we may write

$$\left( \Pi_C^{2l,\text{log}} + \Pi_C^{2l,\text{sublin}} + \Pi_C^{2l,\text{fin}} \right)^2 + 2\Pi_C^{1l,\text{fin}}\Pi_C^{3l} = P^2\Pi_D^{4l} + \Pi_L^{1l}\Pi_D^{3l} + \Pi_L^{2l}\Pi_D^{2l}. \quad (4.37)$$

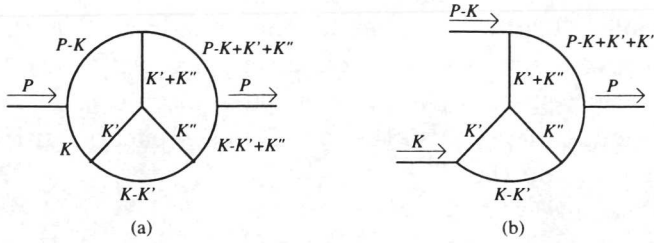


**Figure 4.5:** A three-loop diagram (a) with the two-loop subdiagram (b)

We now focus on the terms that may contain a double logarithmic divergence. Then we get the equation

$$\left(\Pi_C^{2l, \log}\right)^2 + 2\Pi_C^{1l, \text{fin}}\Pi_C^{3l} = P^2\Pi_D^{4l} + \Pi_L^{1l}\Pi_D^{3l}. \quad (4.38)$$

Here we used that  $\Pi_D^{2l}$  does not contain a logarithmic divergence, such that the last term in (4.37) cannot contribute to (4.38). Let us consider the products of one- and three-loop contributions. Since at one loop there are no logarithmic divergences, the three-loop diagrams must contain a double logarithmic divergence for these products to contribute. Schematically the expression for a three-loop diagram is

$$\Pi^{3l}(P) = g^6 T^3 \int dK dK' dK'' f^{3l}(K, K', K'', P). \quad (4.39)$$

The integral over  $K'$  and  $K''$  can be viewed as a two-loop (sub)diagram or an expression for two disjunct one-loop (sub)diagrams, with external lines depending on the momenta  $P, K$ . Consider, for example the three-loop diagram in Fig. 4.5. In the case that the integration over  $K'$  and  $K''$  corresponds to a two-loop diagram it can at most give a single logarithmic divergence ( $\log \Lambda$ ). When it does, the integration over  $K$  cannot give an extra  $\log \Lambda$ , since the superficial degree of divergence of the total diagram is  $-1$ . In the other case that the integration over  $K'$  and  $K''$  does not give a logarithmic divergence, the integration over  $K$  may give one  $\log \Lambda$ . Hence a three-loop diagram can at most give a single logarithmic divergence. Therefore the product of one- and three-loop diagrams cannot contribute in (4.38).

The above argumentation can be repeated for the four-loop contribution to the self-energy. The result after integration over three of the four momenta can be viewed as a three-loop diagram or an expression for a disjunct

two- and one-loop diagram, or three disjunct one-loop diagrams. Therefore it can at most give a single logarithmic divergence. And since the four-loop contribution to the self-energy is finite the integration over  $K$  cannot give an extra log divergence. Hence, also the four-loop self-energy cannot contribute in (4.38). Thus, we find that

$$\Pi_C^{2l,\log} = 0. \quad (4.40)$$

We conclude that the logarithmic divergent part of the two-loop classical self-energy is transverse

$$P^\mu \Pi_{\mu\nu}^{2l,\log} = 0. \quad (4.41)$$

We stress once more that at non-zero temperature this a special property, that should not generally be expected.

## 4.6 Conclusion

Classical thermal field theories contain ultraviolet divergences. In an analysis of classical vertex functions, we found that at one loop only linear divergences occur, which come from classical HTL's, i.e. the classical equivalences of the HTL's in the quantum theory. Furthermore we argued that for  $n$ -point vertex functions with arbitrary  $n$ , the degree of divergence decreases with the number of loops. This implies that two-loop contributions are (superficially) logarithmically divergent and higher loops are superficially finite. This may be compared with static dimensional reduction, where the  $L$ -loop contribution to the self-energy has also a degree of divergence  $2 - L$ . The difference is that in the static limit higher-point vertex functions are less divergent than the self-energy. Indeed, the static theory is a superrenormalizable field theory and a finite number of counterterms, like a one- and two-loop mass counterterm, suffices.

The consequences of this are the following. Since three and higher-loop diagrams are superficially finite, these are infrared dominated. Therefore, they are in principle calculable in the classical theory. The loophole is of course the possible occurrence of divergences in (one or two-loop) subdiagrams. To deal with these divergences, counterterms have to be introduced. In the scalar case the divergences occur only in the self-energy and are momentum independent, therefore a mass renormalization is sufficient to obtain a cut-off independent theory. This may be useful for a numerical approach

to time-dependent problems, such as the dynamics of the phase transition and/or topological defects in a (complex) scalar field theory. In  $SU(N)$  gauge theories the divergences are momentum dependent, nevertheless a renormalization of the plasmon frequency takes care of the linear divergences [56,98]. This will be the subject of the next chapter, where also lattice generalizations are discussed. Two-loop divergences cannot yet be handled, since we do not know what their precise form is. It is interesting to study them, not only for the introduction of counterterms, but also to see if they have the same nice properties as the one-loop divergences (classical HTL's), such as gauge invariance and a conserved energy for the effective theory. In this respect it is promising that we have found that the logarithmic divergent part of the self-energy is transverse.

#### 4.A Gauge invariant cut-off in the classical theory

We argue that in classical gauge theories it is possible to introduce a (continuum) momentum cut-off without breaking gauge invariance. The basic ingredient is the result of Landshoff and Rebhan [77,78] that in general linear gauges it is possible to formulate a (quantum) real-time theory in which only the two physical degrees of freedom of the gauge field acquire a thermal part. This implies that a change in the distribution function

$$n(k^0) \rightarrow n(k^0)f(k/\Lambda), \quad (4.1)$$

with  $f$  some function, does not break gauge invariance. Introducing a cut-off in this way will not affect the Slavnov-Taylor identities. This has been employed in a Wilson renormalization group approach to hot (quantum)  $SU(N)$  gauge theories [17,41].

If we take the classical limit of (4.1) and choose  $f$  as the step function, we get

$$n_{\text{cl}}(k^0) \rightarrow n_{\text{cl}}(k^0)\theta(\Lambda - k), \quad (4.2)$$

which as (4.1) does not break gauge invariance. It is for instance straightforward to check that the HTL's calculated with distribution function (4.2) satisfy the same abelian-like Ward identities as usual. Finally we should remark that the regularization (4.2) is sufficient to render the theory ultraviolet finite, since each loop introduces one distribution function.<sup>5</sup>

---

5. In the quantum theory the cut-off in (4.1) acts only on thermal fluctuations. A zero-temperature regularization and renormalization is still necessary to avoid divergences coming from the zero-temperature quantum fluctuations.

#### 4.B Classical one-loop $SU(N)$ self-energy: explicit calculation

We present in this appendix the calculation of the classical self-energy in  $SU(N)$  gauge theory, in particular the  $\Pi_{ii}$  part, in the Feynman gauge. The starting point is given by (4.6) in the main text. After changing variables from  $\mathbf{k} \rightarrow -\mathbf{k} - \mathbf{p}$  in the part that is proportional to  $n_{\text{cl}}(\omega_{\mathbf{p}+\mathbf{k}})$ , we find

$$\Pi_{ii,\text{cl}}^{ab}(P) = \delta^{ab} g^2 N \Pi_{\text{cl}}(P), \quad (4.3)$$

with

$$\Pi_{\text{cl}}(P) = \int \frac{d^3k}{(2\pi)^3} \frac{\hbar n_{\text{cl}}(\omega_{\mathbf{k}})}{\omega_{\mathbf{k}}} \left\{ 6 + \frac{A_{ii}}{(p^0 + \omega_{\mathbf{k}})^2 - \omega_{\mathbf{p}+\mathbf{k}}^2} + \frac{A_{ii}}{(p^0 - \omega_{\mathbf{k}})^2 - \omega_{\mathbf{p}+\mathbf{k}}^2} \right\}, \quad (4.4)$$

and  $A_{ii} = 4k^2 + 4\mathbf{k} \cdot \mathbf{p} + 5p^2 - 6p_0^2$ . We have combined  $\hbar$  with  $n_{\text{cl}}(\omega_{\mathbf{k}})$ , which is an  $\hbar$ -independent combination.

The angular integrations can be performed, and

$$\begin{aligned} \Pi_{\text{cl}}(p^0, p) = & \int dk \frac{k \hbar n_{\text{cl}}(k)}{\pi^2} \left\{ 1 + \frac{p^0}{p} \ln \frac{p_+}{p_-} - \frac{k}{2p} [L_+(k) - L_-(k)] \right\} \\ & - \int dk \frac{k \hbar n_{\text{cl}}(k)}{8\pi^2 p} \left\{ \frac{3p^2 - 4p_0^2}{k} [L_+(k) - L_-(k)] + 4p^0 [L_+(k) + L_-(k)] \right\}. \end{aligned} \quad (4.5)$$

Motivated by Weldon [118], we used here the notation

$$p_{\pm} = \frac{1}{2}(p^0 \pm p), \quad L_{\pm}(k) = \ln \frac{k \pm p_+}{k \pm p_-}. \quad (4.6)$$

The result (4.5) agrees with the expression obtained by Weldon in the appendix of [118], except of course that the distribution function is classical in our case.

The remaining radial integral in the first line of (4.5) is linearly divergent. For the first two terms this is obvious, and for the third term one can use  $L_+(k) - L_-(k) = 2p/k + \mathcal{O}(k^{-3})$ . In fact, the divergence in this term cancels against the first term. The integrals in the second line are convergent. To regulate the divergences, we use the distribution function with a momentum cut-off  $\hbar n_{\text{cl}}(k) = T/k \theta(\Lambda - k)$ . The final result requires the evaluation of four integrals, which read (recall that  $p^0$  contains a small positive imaginary part)

$$\int dk k \hbar n_{\text{cl}}(k) = T\Lambda, \quad (4.7)$$

$$\int dk k^2 \hbar n_{cl}(k) [L_+(k) - L_-(k)] = T (2p\Lambda + \frac{1}{2} \pi i p p^0), \quad (4.8)$$

$$\int dk \hbar n_{cl}(k) [L_+(k) - L_-(k)] = T \pi i \ln \frac{p_+}{p_-}, \quad (4.9)$$

$$\int dk k \hbar n_{cl}(k) [L_+(k) + L_-(k)] = -T \pi i p. \quad (4.10)$$

The second and fourth integral are straightforward using partial integration, and the third one can be performed by complex contour integration while being careful around  $k = 0$ . Note that these integrals are much simpler than in the quantum case, because of the simple  $k$  dependence of the classical distribution function.

Putting all the results together, we find for the classical one-loop retarded self energy

$$\Pi_{ii,cl}^{ab}(P) = N \delta^{ab} g^2 \left[ \frac{T \Lambda p^0}{\pi^2 p} \ln \frac{p_+}{p_-} + \frac{T}{4\pi} \left( i p^0 - \frac{3p^2 - 4p_0^2}{2p} i \ln \frac{p_+}{p_-} \right) \right], \quad (4.11)$$

which is presented in (4.10).

### 4.C Two loop naively linear divergent contributions

#### Diagram b

In this appendix we give the results for the naively linearly divergent contributions to the classical two-loop self-energy. We start with the classical limit of the self-energy diagram (b) in fig. 4.1, presented in (4.18), and use the shorthand notation of (4.19). There are three naively linearly divergent contributions and we shall denote these with (b1), (b2), and (b3).

We start with contribution (b1), obtained by taking  $s_3 = s'$ ,  $s_2 = -s$  and setting the external  $p^0, \mathbf{p}$  to zero in the energy denominators with three loop-energies. We then find

$$\begin{aligned} \Pi_{ij,cl}^{(b1)}(P) = & \frac{1}{2} (g^2 \hbar)^2 \int \frac{d^3 k}{(2\pi)^3} \int \frac{d^3 k'}{(2\pi)^3} (k)_{ij}^4 \sum_{ss's_1} \frac{-s_1}{2^5 \omega \omega' \omega_1 \omega_2 \omega_3} \times \\ & \frac{1}{p^0 + s'(\omega' + \omega_3)} \frac{n_{cl}(s\omega_2) - n_{cl}(s\omega)}{p^0 + s(\omega - \omega_2)} \times \\ & \left[ \frac{n_{cl}(s_1\omega_1) - n_{cl}(s'\omega_3)}{-s'\omega' - s\omega + s_1\omega_1} - \frac{n_{cl}(s_1\omega_1) + n_{cl}(s'\omega')}{s'\omega' - s\omega + s_1\omega_1} \right]. \quad (4.12) \end{aligned}$$

The difference between distribution functions  $[n_{\text{cl}}(s\omega_{\mathbf{p}-\mathbf{k}}) - n_{\text{cl}}(s\omega_{\mathbf{k}})]$  reduces the degree of divergence by one compared to the naive estimate, which is from linear to logarithmic. Note that the other difference between distribution functions  $[n_{\text{cl}}(s_1\omega_{\mathbf{k}-\mathbf{k}'} - n_{\text{cl}}(s'\omega_{\mathbf{p}-\mathbf{k}'})]$ , does not reduce the degree of divergence any further, since  $\mathbf{k}$  is not a (small) external momentum, but is integrated over.

A similar contribution is obtained by taking  $s_2 = s$  and  $s_3 = -s'$  and again setting  $p^0, \mathbf{p} = 0$  in the same energy denominators. We obtain

$$\begin{aligned} \Pi_{ij,\text{cl}}^{(\text{b}2)}(P) = & \frac{1}{2}(g^2\hbar)^2 \int \frac{d^3k}{(2\pi)^3} \int \frac{d^3k'}{(2\pi)^3} (k)_{ij}^4 \sum_{ss's_1} \frac{-s_1}{2^5\omega\omega'\omega_1\omega_2\omega_3} \times \\ & \frac{1}{p^0 + s'(\omega' - \omega_3)} \frac{n_{\text{cl}}(s'\omega_3) - n_{\text{cl}}(s'\omega')}{p^0 + s(\omega + \omega_2)} \times \\ & \left[ -\frac{n_{\text{cl}}(s_1\omega_1) + n_{\text{cl}}(s\omega_2)}{s'\omega' + s\omega + s_1\omega_1} + \frac{n_{\text{cl}}(s_1\omega_1) - n_{\text{cl}}(s\omega)}{s'\omega' - s\omega + s_1\omega_1} \right]. \quad (4.13) \end{aligned}$$

Again a difference between distribution functions appears that reduces the degree of divergence to a logarithmic one.

The third naively linearly divergent contribution to consider is of a different type. It is obtained from the classical limit of (4.18) by setting  $s = -s_2$  and  $s' = -s_3$  and taking the linear term in  $p^0, \mathbf{p}$  in an expansion of the energy denominator with  $\omega_1 = \omega_{\mathbf{k}-\mathbf{k}'}$ . The zeroth order term in this expansion gives rise to a naively quadratic divergence and was already discussed in the main text. The first-order term reads

$$\begin{aligned} \Pi_{ij,\text{cl}}^{(\text{b}3)}(P) = & \frac{1}{2}(g^2\hbar)^2 \int \frac{d^3k}{(2\pi)^3} \int \frac{d^3k'}{(2\pi)^3} (k)_{ij}^4 \sum_{ss's_1} \frac{-s_1}{2^5\omega\omega'\omega_1\omega_2\omega_3} \\ & \frac{1}{p^0 + s'(\omega' - \omega_3)} \frac{1}{p^0 + s(\omega - \omega_2)} \frac{1}{(s'\omega' - s\omega + s_1\omega_1)^2} \\ & \left\{ s'(\mathbf{p} \cdot \hat{\mathbf{k}}') [n_{\text{cl}}(s\omega_2) - n_{\text{cl}}(s\omega)] [n_{\text{cl}}(s'\omega_3) + n_{\text{cl}}(s_1\omega_1)] \right. \\ & \quad - s(\mathbf{p} \cdot \hat{\mathbf{k}}) [n_{\text{cl}}(s'\omega_3) - n_{\text{cl}}(s'\omega')] [n_{\text{cl}}(s\omega_2) - n_{\text{cl}}(s_1\omega_1)] \\ & \quad + p^0 n_{\text{cl}}(s_1\omega_1) \left( [n_{\text{cl}}(s\omega) - n_{\text{cl}}(s\omega_2)] + [n_{\text{cl}}(s'\omega') - n_{\text{cl}}(s'\omega_3)] \right) \\ & \quad \left. + p^0 n_{\text{cl}}(s_1\omega_1) [n_{\text{cl}}(s\omega)n_{\text{cl}}(s'\omega_3) - n_{\text{cl}}(s\omega_2)n_{\text{cl}}(s'\omega')] \right\}. \quad (4.14) \end{aligned}$$

We emphasize again that the region of phase space where  $s'\omega' - s\omega + s_1\omega_1$  vanishes is excluded in this expansion. The first three terms between curly

brackets all have a factor which is the difference between distribution functions. The fourth term is different, but also here the factor with distribution functions vanishes when the external momentum is taken to zero (i.e. when  $\omega_2 \rightarrow \omega, \omega_3 \rightarrow \omega'$ ). Hence this factor contributes a power  $\Lambda^{-3}$  instead of  $\Lambda^{-2}$ , and it brings down the degree of divergence. We conclude that the degree of divergence is reduced from linear to logarithmic in contribution (b3) as well.

### Diagram c

The final diagram that needs to be examined is diagram (c) in fig. 4.1. The quantum expression is

$$\begin{aligned} \Pi_{ij}^{(c)}(P) = & (g^2 \hbar)^2 \int \frac{d^3 k}{(2\pi)^3} \int \frac{d^3 k'}{(2\pi)^3} (k)_{ij}^2 \sum_{ss's_1s_2} \frac{ss's_1s_2}{2^4 \omega \omega' \omega_1 \omega_2} \frac{1}{p^0 - s\omega - s_2 \omega_2} \\ & \left\{ \frac{1}{s\omega + s'\omega' - s_1 \omega_1} \left( [n(s\omega) + 1][n(s'\omega') + 1]n(s_1 \omega_1) \right. \right. \\ & \quad \left. \left. - n(s\omega)n(s'\omega')[n(s_1 \omega_1) + 1] \right) \right. \\ & \left. + \frac{1}{p^0 - s_2 \omega_2 + s'\omega' - s_1 \omega_1} \left( [n(s'\omega') + 1]n(s_1 \omega_1)n(s_2 \omega_2) - \right. \right. \\ & \quad \left. \left. n(s'\omega')[n(s_1 \omega_1) + 1][n(s_2 \omega_2) + 1] \right) \right\}, \quad (4.15) \end{aligned}$$

where in this case  $\omega_1 = \omega_{\mathbf{p}-\mathbf{k}-\mathbf{k}'}$  and we inserted  $(k)_{ij}^2$  to indicate the two powers of momentum that come from the two three-point vertices.

We take the classical limit of (4.15). The contribution with  $s_2 = -s$  is naively linearly divergent, it reads

$$\begin{aligned} \tilde{\Pi}_{ij,cl}^{(c)} = & (g^2 \hbar)^2 \int \frac{d^3 k}{(2\pi)^3} \int \frac{d^3 k'}{(2\pi)^3} (k)_{ij}^2 \sum_{ss's_1} \frac{-s's_1}{2^4 \omega \omega' \omega_1 \omega_2} \frac{1}{p^0 - s\omega + s\omega'} \\ & \frac{1}{s\omega + s'\omega' - s_1 \omega_{\mathbf{k}+\mathbf{k}'}} [n(s\omega) - n(s\omega_2)][n(s_1 \omega_1) - n(s'\omega')]. \quad (4.16) \end{aligned}$$

Again the first difference between distribution functions reduces the degree of divergence to a logarithmic one.



## 5 Counterterms for linear divergences

### 5.1 Introduction

In the previous chapter we have demonstrated that diagrams in a classical field theory contain linear divergences at one loop and logarithmic divergences at two loops. This indicates that certain quantities will not be calculable in a classical theory and the breakdown of the classical approximation. Examples we have encountered are the tadpole mass (2.12) and the plasmon frequency (4.5). Unfortunately, the divergences are not strictly confined to these quantities, but they also affect (superficially) finite quantities.

An illuminating and important example is given by the typical time scale for the non-perturbative modes with momenta  $p \sim g^2 T$ . One may recall from (3.86) that this time scale for a quantum theory is

$$t \sim \frac{\omega_{\text{pl}}^2}{p^3}. \quad (5.1)$$

The derivation in section 3.8 made use of the transverse propagator with the HTL self-energy inserted. Here we shall estimate this time scale for a classical theory (without HTL's) with cut-off  $\Lambda$ . Remember that the dominant (linearly divergent) contributions correspond exactly to the quantum HTL's except for the value of the plasmon frequency, see section 4.2.1. This implies that the estimate (5.1) can be used, except that we have to insert the classical plasmon frequency  $\omega_{\text{pl,cl}}^2 \sim g^2 T \Lambda$  (4.5). This yields [12]

$$t \sim \frac{\omega_{\text{pl,cl}}^2}{p^3} \sim g^{-4} \frac{\Lambda}{T^2}. \quad (5.2)$$

Because this time scale diverges, the Chern-Simons diffusion rate is proportional to  $\Lambda^{-1}$  (following the same reasoning as from (3.86) to (3.87)).

The cut-off dependence arises because the hard modes affect the soft modes in an essential way. Diagrammatically, this corresponds to superficially finite diagrams that acquire a cut-off dependence through divergent

subdiagrams. The aim is now to improve the classical theory such that linear divergences are absent. In terms of the example above, the goal is to obtain an effective classical theory that yields the correct (quantum) time scale. This implies that the HTL's have to be included in the classical theory; this was the subject of chapter 3. But in addition it requires the inclusion of counterterms for the classical divergences.

Counterterms for classical divergences are different from counterterms at zero temperature, since classical divergences are non-local and extend to diagrams with any number of external legs. For real-time classical gauge theories, counterterms were first studied by Bödeker, McLerran, and Smilga [25]. They derived an effective theory by integrating out modes with momenta  $k > \Lambda_{\text{int}}$ , where  $\Lambda_{\text{int}}$  is an intermediate cut-off:  $gT < \Lambda_{\text{int}} < T$ . In the HTL approximation this yielded the usual HTL's with subtractions linear in the cut-off  $\Lambda_{\text{int}}$ . These subtractions were interpreted as counterterms. Their treatment was not gauge invariant and, therefore, gauge invariance of the effective theory was broken by the counterterms. Later it was argued that in a gauge invariant approach the subtraction should be confined to the one-loop plasmon frequency [3, 56]. We will confirm this conjecture here. Furthermore, on the basis of the results of the previous chapter we may conclude that no linear divergences will appear beyond one loop. A useful result that we will use in the reasoning is the fact that classical linear divergences are the classical analogues of HTL's. This allows us to use the known facts on HTL's, see chapter 3.

For practical calculations the implementation of counterterms for classical lattice theories is of some interest. After an introduction, the main part of this chapter will be devoted to this topic. We will find that exact lattice counterterms prevent a matching of the quantum HTL's to the continuum. Approximate counterterms may be given by a lattice generalization of the model proposed by Iancu [56]. These approximate counterterms go beyond the counterterm that was used by Bödeker, Moore and Rummukainen [29].

## 5.2 Cut-off dependence

To start, we will consider a general formulation of the problem of classical divergences in a  $SU(N)$  theory given by the Yang-Mills equations of motion

$$D_{\mu}^{ab} F^{\mu\nu b} = j_{\text{HTL}}^{\nu a}, \quad (5.3)$$

with a cut-off  $\Lambda$  to make the theory finite. The notation is the same as in chapter 3, except that the non-Abelian HTL source (3.65) generated by

hard thermal loops is now denoted by  $j_{\text{HTL}}$ . The inclusion of the HTL-corrections in the classical theory was motivated by the need to resum diagrams that are dominated by soft momenta in the integration over internal momenta; see chapter 3. However, in an effective classical theory, we also have to deal with the Rayleigh-Jeans divergences, which are not removed by a HTL resummation. In the previous chapter we have determined the general structure of these divergences in perturbation theory. Here we will study the ensuing cut-off dependence in the equation of motion. In particular we will be concerned with the question whether classical divergences can be removed by counterterms.

Let us first simplify to a purely classical theory without any source.

$$D_{\mu}^{ab} F^{\mu\nu b} = 0 . \quad (5.4)$$

To study the cut-off dependence of this theory it is useful to reduce the theory with cut-off  $\Lambda$  to an effective theory with (smaller) cut-off  $\Lambda'$  by integrating out the modes with momenta  $\mathbf{k}$ :  $\Lambda' < |\mathbf{k}| < \Lambda$ . This generates extra interactions in the equations of motion which we collect in a source

$$D_{\mu}^{ab} F^{\mu\nu b} = \delta j^{\nu a} . \quad (5.5)$$

From the preceding chapter we know that the leading behavior of these interactions is

$$\delta j^{\nu a} = g^2 T (\Lambda - \Lambda') j_{\text{lin}}^{\nu a} + (g^2 T)^2 \log \left( \frac{\Lambda}{\Lambda'} \right) j_{\text{log}}^{\nu a} + \mathcal{O}(1/\Lambda) . \quad (5.6)$$

Here we have used the result that linear divergences occur at one loop and log divergences at two loops. The current  $j_{\text{lin}}^{\nu a}$  generates the linear divergences in a similar manner as the induced source in the Vlasov equations generates the HTL's (3.69). Also contributions from linear subdivergences occur. These are however suppressed when  $(\Lambda - \Lambda')/\Lambda \ll 1$ . For instance consider  $n$  HTL self-energy insertions into a certain loop; this gives an extra factor  $[g^2 T (\Lambda - \Lambda')]^n / \Lambda^{2n}$  compared to the loop without HTL insertions.

Equations (5.5) and (5.6) show that no matter what the momentum scale of interest is, the (dynamics of the) gauge fields will be sensitive to the cut-off. The time-scale (5.2) is an example of this sensitivity. Let us remark here that for static quantities the cut-off dependence is less severe. Especially the dimensionally reduced theory (3.80) valid for the non-perturbative length scale  $1/g^2 T$  is cut-off independent [63].

### 5.3 Effective theory with counterterms

The simple nature of the cut-off dependence (5.6) suggests that the divergences can be removed by a subtraction of linear and logarithmic terms. In the Vlasov equation (5.3) including HTL corrections, we propose to do this as follows

$$D_{\mu}^{ab} F^{\mu\nu b} = j_{\text{HTL}}^{\nu a} - j_{\text{ct}}^{\nu a}, \quad (5.7)$$

with a counterterm for the linear divergences of the form  $j_{\text{ct}}^{\nu a} = g^2 T \Lambda j_{\text{lin}}^{\nu a}$ .

Let us discuss the diagrams that this theory generates in perturbation theory. Firstly, there are classical diagrams, that is, diagrams that are constructed from classical propagators and tree-level vertices. The Feynman rules for the case of a scalar theory have been given in section 2.7 and one-loop and two-loop divergent diagrams relevant to  $SU(N)$  gauge theories have been studied in the previous chapter. Secondly, there are diagrams that contain HTL self-energy insertions and/or HTL vertices. The HTL vertices are of the general form (3.70), and the HTL self-energy has been worked out in detail in (3.10), (3.14), and (3.15). Finally, also diagrams with self-energy insertions and vertices from the counterterm current  $j_{\text{ct}}^{\nu a}$  occur. The counterterm current is chosen to be equal to the linearly divergent current generated in the classical theory. It subtracts all linearly divergent one-loop vertex functions (without HTL resummation). These vertex functions have been discussed in section 4.2.1, where it was shown that they equal HTL vertex functions, except that the plasmon frequency is the classical one (4.5).

Since HTL's and classical counterterms are non-local and may contain any number of fields, see sections 3.2, 3.7, and 4.2.1, one might expect that these terms themselves give rise to new (and perhaps even worse) divergences. However, we shall now argue that such new terms are at most superficially logarithmically divergent. Consider a diagram in the effective theory (5.7) with some interactions from  $j_{\text{lin}}^{\nu a}$ . Such vertices come from linearly divergent diagrams (with more loops) in the purely classical theory. For such diagrams the power counting of the previous chapter applies. Hence, we know that its superficial degree of divergence is at most logarithmic, with a linear sub-divergence. The logarithmic divergence must be subtracted by a logarithmic counterterm. However, an explicit form cannot be given without actually doing the calculations. In the remainder of this chapter we shall confine ourselves to linear counterterms leaving the logarithmic problem to further research.

We find by this reasoning that diagrams with vertices from  $j_{\text{lin}}^{\nu a}$  do not generate new linear divergences. The same may be argued for diagrams that

contain vertices from the HTL source  $j_{\text{HTL}}^{\nu a}$ , since these vertices may be seen as classical diagrams with a cut-off of the order of the temperature.

The subtraction of linear divergences as in (5.7) may be compared to the standard method of (HTL) resummations in the quantum theory. Then one uses the action

$$S = S_{\text{cl}} + \Gamma_{\text{HTL}} - \Gamma_{\text{ct}} = S_{\text{resum}} - \Gamma_{\text{ct}}, \quad (5.8)$$

where the counterterm action  $\Gamma_{\text{ct}}$  is in fact equal to the HTL action  $\Gamma_{\text{HTL}}$ , but is treated as a counterterm to the resummed action represented by the first two terms. In the simplest case, this amounts to the introduction of the HTL self-energy into the (resummed) propagator. The counterterm action corrects for overcounting in the resummed theory, because otherwise the resummed action would generate HTL's which are already included in  $\Gamma_{\text{HTL}}$ .

Now consider the classical case. The classical diagrams that are generated by the resummed action in (5.8) give rise to linearly and logarithmically divergent terms controlled by a cut-off  $\Lambda$ , and finite terms. The linear divergences are the classical analogues of HTL's and should as such be incorporated in the effective theory. However, in the resummed action they have already been taken into account explicitly. Therefore, any linear divergence that appears should be subtracted by the counterterm action in (5.8). The classical equations of motion (5.7) are then just the variational equations of the action (5.8). In a manner of speaking, we could say that (5.7) constitutes a classical resummation of HTL's.

We should mention here that these arguments do not ensure that (5.7) provides a consistent theory. This requires that current and energy conservation as well as stability of the system need to be checked separately. We will find that these requirements (especially the stability of the system) limit the applicability of counterterms.

## 5.4 Continuum

Let us consider what this means for a classical theory on the continuum. We have noticed already that the HTL's and classical linear divergences are the same except for a proportionality factor, see section 4.2. Therefore the two sources on the right hand side of (5.7) can be combined. This yields a HTL source whose strength is  $\Lambda$ -dependent

$$\begin{aligned} j_{\text{HTL,ct}}^{\nu a} &= j_{\text{HTL}}^{\nu a} - j_{\text{ct}}^{\nu a} \\ &= 3\omega_{\text{pl}}^2(\Lambda) \int \frac{d\Omega}{4\pi} V^\nu W^a(x, \mathbf{v}). \end{aligned} \quad (5.9)$$

The  $W^a$ -fields satisfy the standard equation (3.66). The  $\Lambda$ -dependent plasmon frequency is given by the difference between the quantum (4.4) and classical plasmon frequency (4.5)

$$\begin{aligned}\omega_{\text{pl}}^2(\Lambda) &= -\frac{1}{3\pi^2}g^2N \int_0^\infty dk k^2 [n'(k) - n'_{\text{cl},\Lambda}(k)] \\ &= \frac{1}{9}g^2NT \left( T - \frac{6}{\pi^2}\Lambda \right),\end{aligned}\quad (5.10)$$

where the cut-off is introduced according to

$$n_{\text{cl},\Lambda}(k) = \frac{T}{k} \Theta(\Lambda - k). \quad (5.11)$$

Thus we find that a subtraction in the plasmon frequency suffices to renormalize the classical linear divergences, confirming the proposal of [3, 56].

We like also to mention that the subtraction in the plasmon frequency can be found from first principles [97]. Then one starts from the quantum theory and integrates out all modes except the classical ones with momentum  $k < \Lambda$ <sup>1</sup>, in the HTL approximation. This yields precisely the HTL's with a subtraction in the plasmon frequency. From consistency it then follows that this should provide the correct counterterm. (This is only straightforward for one-loop diagrams. At two loops it may be that non-local (non-divergent) vertices need to be included into the effective classical theory for the subtractions to match the divergences [59].). This mechanism for generation of the one-loop counterterm we have already encountered in the simple case of scalar  $\lambda\phi^4$ -theory in section 2.3. Namely, the counterterm for the linear divergence in the classical (zero-mode) contribution to the tadpole (2.12) was generated by the non-zero mode contribution (2.13).

Since the subtraction only enters the plasmon frequency, the system has the same properties as the HTL equations. The current is conserved. Also there is a conserved energy (the non-Abelian generalization of (3.29))

$$E = \frac{1}{2} \int d^3x \left[ (\mathbf{E}^a)^2 + (\mathbf{B}^a)^2 + 3\omega_{\text{pl}}^2(\Lambda) \int \frac{d\Omega}{4\pi} W^a(x, \mathbf{v}) W^a(x, \mathbf{v}) \right]. \quad (5.12)$$

We note that for  $\omega_{\text{pl}}^2(\Lambda) < 0$  the energy is not bounded. This implies that the system is unstable. For  $\omega_{\text{pl}}^2(\Lambda) > 0$ , the cut-off has to satisfy  $\Lambda < \pi^2 T/6$ .

---

1. This analysis is performed in perturbation theory in a fixed gauge. The difficulty is to divide the modes in soft (classical) and hard modes, while preserving BRS invariance. But this can be done [97].

Hence the we cannot interpret  $\Lambda$  as a true UV-cut-off, but only as an intermediate cut-off. Therefore contributions that are proportional to inverse powers of  $\Lambda$  cannot be made to vanish by sending the cut-off to infinity. But for  $\Lambda \sim T$  they are suppressed by powers of the coupling.

As an example we estimate the part of classical one-loop self-energy proportional to  $\Lambda^{-1}$ , denoted as  $\Pi_{1,\text{cl}}$ , for soft momenta  $p_0 \sim p \sim gT$ . Since we consider a one-loop contribution, the expression will contain one classical distribution function. Hence, the one-loop self-energy is proportional to  $T$ . Combined with a dimensional analysis, we obtain  $\Pi_{1,\text{cl}} \sim g^2 T p^2 \Lambda^{-1} \sim g^4 T^2$ , for  $\Lambda \sim T$ . The part suppressed by inverse powers of the cut-off is of order  $g^2$  compared to the HTL contribution. When we consider a classical diagram that is not divergent, we should compare the suppressed part (proportional to an inverse power of  $\Lambda$ ) to the unsuppressed classical contribution. Then we find that it is of order  $g$ . Hence, even though the cut-off cannot be send to infinity, to leading order in the coupling  $g$ , suppressed contributions may be neglected.

## 5.5 Perturbative renormalization on a lattice

### 5.5.1 Static

Before turning to the HTL equations of motion, we shortly review the static classical theory on a lattice, as far as the linear divergences are concerned. The appropriate classical theory is the dimensionally reduced theory that we did already encounter in (3.79)

$$L_{DR} = \int d^3x \left[ \frac{1}{4} F_{ij}^a F^{ija} + \frac{1}{2} (D_i^{ab} A_0^b)^2 + \frac{1}{2} \mu_0^2 (A_0^a)^2 + \frac{1}{4} \lambda_0 (A_0^a A_0^a)^2 \right]. \quad (5.13)$$

We now consider this theory on a lattice. Ideally, one would like to mimic the continuum theory as best as possible. This means that the thermal corrections that one has to include, should be calculated in the continuum, whereas the counterterms for the divergences need to be calculated on the lattice.

Consider for instance the Debye mass. It contains the only linear divergence in the static 3d theory. A counterterm for this divergence may be introduced in the mass of the temporal gauge field [63, 87]

$$\mu_0^2 = m_D^2 - m_{\text{cl,lat}}^2, \quad (5.14)$$

with the continuum HTL contribution

$$m_D^2 = -2g^2 N \int \frac{d^3k}{(2\pi)^3} n'(k) = \frac{1}{3} g^2 N T^2, \quad (5.15)$$

and the classical mass (for a simple cubic lattice with lattice spacing  $a$ )

$$m_{\text{cl,lat}}^2 = -2g^2 N \int \frac{d^3 p}{(2\pi)^3} n'(\Omega_{\mathbf{p}}) \approx 0.51g^2 N T a^{-1}. \quad (5.16)$$

The momentum  $\mathbf{p}$  is restricted to the first Brillouin zone  $|p_i| \leq \pi/a$  and the energy  $\Omega_{\mathbf{p}}$  is

$$\Omega_{\mathbf{p}}^2 = \frac{4}{a^2} \left[ \sin^2 \left( \frac{p_x a}{2} \right) + \sin^2 \left( \frac{p_y a}{2} \right) + \sin^2 \left( \frac{p_z a}{2} \right) \right]. \quad (5.17)$$

The mass (5.16) is the linearly divergent contribution to the Debye mass on the lattice. Its subtraction in (5.14) ensures that no linear divergences are present in the static theory with the mass counterterm included. The continuum HTL contribution (5.15) to the mass (5.14) provides the finite renormalization. It ensures that the leading-order Debye screening in this effective lattice model is the same as in the continuum.

### 5.5.2 Real-time

The above approach may be extended to a real-time classical theory. We consider again the equation of motion for the gauge fields

$$D_{\mu}^{bc} F^{\mu\nu c} = j_{\text{HTL,ct}}^{\nu b}, \quad (5.18)$$

but now space is a simple cubic lattice with lattice spacing  $a$ . A simple subtraction in the plasmon frequency will not suffice to remove the linear divergences, as it did for the continuum. Therefore we start anew from (5.7). Similar to the static mass (5.14), that consists of the continuum HTL Debye mass with the classical lattice mass subtracted, we construct a source to contain a continuum HTL contribution with a classical lattice contribution subtracted

$$j_{\text{HTL,ct}}^{\nu b} = j_{\text{HTL}}^{\nu b} - j_{\text{ct}}^{\nu b}. \quad (5.19)$$

To this end, we introduce two particle distribution functions  $\delta N(x, \mathbf{k})$  and  $\delta N_{\text{ct}}(x, \mathbf{p})$  for particles with energies  $E_{\mathbf{k}} = |\mathbf{k}|$  and  $\Omega_{\mathbf{p}}$  respectively. The idea is that the particle distribution function  $\delta N$  generates the continuum HTL source  $j_{\text{HTL}}^{\nu b}$ , and  $\delta N_{\text{ct}}$  generates the counterterms for the linear lattice divergences in the current  $j_{\text{ct}}^{\nu b}$ . The particle distribution function  $\delta N$  satisfies the equation (the non-Abelian generalization of (3.20))

$$V^{\mu} D_{\mu}^{bc} \delta N^c(x, \mathbf{k}) = g \mathbf{v} \cdot \mathbf{E}^b(x) n'(k), \quad (5.20)$$

with  $V^\mu = (1, \mathbf{k}/k)$ . It contributes to the HTL current as

$$j_{\text{HTL}}^{\nu b}(x) = 2gN \int \frac{d^3 k}{(2\pi)^3} V^\nu \delta N^b(x, \mathbf{k}). \quad (5.21)$$

To obtain an effective lattice theory free of linear divergences, the current  $j_{\text{ct}}^{\nu b}$  should subtract the linear classical lattice divergences. To achieve this, the current  $j_{\text{ct}}^{\nu b}$  is chosen equal to the induced source of the classical lattice Vlasov theory. The latter generates classical lattice HTL's which are exactly the linear divergences that need to be subtracted (remember that classical HTL's correspond to linear divergences). In the classical lattice Vlasov theory the distribution function satisfies the equation [12]

$$V_{\text{lat}}^\mu D_\mu^{bc} \delta N_{\text{ct}}^c(x, \mathbf{p}) = g \mathbf{v}_{\text{lat}} \cdot \mathbf{E}^b(x) n'_{\text{cl}}(\Omega_{\mathbf{p}}), \quad (5.22)$$

with the four-velocity on the lattice  $V_{\text{lat}}^\mu = (1, \mathbf{v}_{\text{lat}})$  with

$$v_{\text{lat}}^i = \partial_{p_i} \Omega_{\mathbf{p}} = \frac{1}{a\Omega_{\mathbf{p}}} \sin(ap_i), \quad (5.23)$$

and  $|\mathbf{v}_{\text{lat}}| \neq 1$  in general. The counterterm current is then given by

$$j_{\text{ct}}^{\mu b}(x) = 2gN \int \frac{d^3 p}{(2\pi)^3} V_{\text{lat}}^\nu \delta N_{\text{ct}}^b(x, \mathbf{p}). \quad (5.24)$$

Here the integration over  $\mathbf{p}$  is restricted to the first Brillouin zone  $|p_i| < \pi/a$ .

As in the continuum, it is useful to define a field  $W^b(x, \mathbf{v})$  that satisfies (3.66)

$$\partial_t W^b(x, \mathbf{v}) + \mathbf{v} \cdot \mathbf{D}^{bc} W^c(x, \mathbf{v}) = \mathbf{v} \cdot \mathbf{E}^b, \quad (5.25)$$

in the  $A_0^b = 0$  gauge. Since the lattice velocity (5.23) is not restricted to the speed of light, we have to allow for general velocities  $\mathbf{v}$  in (5.25). Hence, the  $W^b$ -field lives on a 6+1 dimensional space instead of the 5+1 dimensional space that is sufficient in the continuum case. The current (5.19) reads

$$j_{\text{HTL,ct}}^{\nu b}(x) = 3\omega_{\text{pl}}^2 \int \frac{d\Omega}{4\pi} V^\nu W^b(x, \mathbf{v}) - 2g^2 N T a^{-1} \int \frac{d^3 \hat{p}}{(2\pi)^3} \hat{\Omega}_{\mathbf{p}}^{-2} V_{\text{lat}}^\nu W^b(x, \mathbf{v}_{\text{lat}}). \quad (5.26)$$

with the dimensionless quantities  $\hat{p}_i = ap_i$ ,  $\hat{\Omega}_{\mathbf{p}} = a\Omega_{\mathbf{p}}$  and the integration restricted to  $|\hat{p}_i| < \pi$ . It may be verified that the induced current (5.26) is covariantly conserved:  $D_\mu^{bc} j_{\text{HTL,ct}}^{\mu c} = 0$ , because.

The first term on the right hand side of (5.26) is the continuum contribution for which the  $k$ -integration decouples and has been performed. In the second term on the right hand side of (5.26), the integration cannot be simplified since the velocity not only depends on the direction of the momentum  $\mathbf{p}$ , but also on its magnitude. The lattice contribution requires fields that depend also on the magnitude of the velocity  $|\mathbf{v}_{\text{lat}}| < 1$ . This in contrast to the calculation of the continuum contribution to the induced current a field  $W(x, \mathbf{v})$  depending on the direction of  $\mathbf{v}$  only is sufficient, and a subtraction in the plasmon frequency renders the effective classical theory free of linear divergences. In section 5.6.2 we will study the question whether, for the calculation of the Chern-Simons diffusion rate, we may approximate the induced current with fields that only depend on the direction of the velocity.

Just as the usual HTL equations, the equations (5.25) and (5.26) (or equivalently (5.20), (5.22) and (5.19)), together with the equation for the gauge fields, define a perturbation theory. Taking retarded initial conditions the retarded propagator (and higher-order retarded vertex functions) can be obtained, as in [22]. The classical KMS condition then fixes the entire propagator, including its thermal part. Using perturbation theory we may verify that also the time-dependent counterterms are correct. We calculate the retarded propagator to one-loop order. In a general linear gauge it takes the form

$$D_{\text{cl}}^{\mu\nu}(Q) = \left[ g^{\mu\nu} Q^2 - Q^\mu Q^\nu + F^\mu F^\nu + \Pi_{\text{cl}}^{\mu\nu}(Q) + \Pi_{\text{HTL,ct}}^{\mu\nu}(Q) \right]^{-1}, \quad (5.27)$$

with  $F^\mu$  the gauge fixing vector and  $\Pi_{\text{cl}}^{\mu\nu}$  the classical self-energy and  $\Pi_{\text{HTL,ct}}^{\mu\nu}$  the counterterm self-energy introduced in the induced source (5.26). The classical self-energy to one-loop order reads [25, 26]

$$\Pi_{\text{cl}}^{\mu\nu}(Q) = 2g^2 N a^{-1} \int \frac{d^3 \hat{p}}{(2\pi)^3} n'_{\text{cl}}(\Omega_{\mathbf{p}}) \left[ -\delta^{\mu 0} \delta^{\nu 0} + \frac{V_{\text{lat}}^\mu V_{\text{lat}}^\nu q_0}{q_0 + i\epsilon - \mathbf{v}_{\text{lat}} \cdot \mathbf{q}} \right]. \quad (5.28)$$

At this order the classical self-energy contains no contribution from the induced source. The linearized induced source

$$j_{\text{HTL,ct}}^\mu(x) = \int d^4 x' \Pi_{\text{HTL,ct}}^{\mu\nu}(x, x') A_\nu(x') \quad (5.29)$$

defines the retarded self energy

$$\Pi_{\text{HTL,ct}}^{\mu\nu}(Q) = \Pi_{\text{HTL}}^{\mu\nu}(Q) - \Pi_{\text{cl}}^{\mu\nu}(Q), \quad (5.30)$$

with the continuum HTL self-energy

$$\Pi_{\text{HTL}}^{\mu\nu}(Q) = 3\omega_{\text{pl}}^2 \left[ -\delta^{\mu 0} \delta^{\nu 0} + \int \frac{d\Omega}{4\pi} \frac{V^\mu V^\nu}{q_0 + i\epsilon - \mathbf{v} \cdot \mathbf{q}} \right]. \quad (5.31)$$

Inserting the self-energy (5.30) in the propagator (5.27), the linear divergent classical self-energy in (5.27) is compensated by the subtraction in (5.30). The resulting self-energy in the propagator (5.27) is the correct (continuum) HTL self-energy (5.31). Furthermore one may note that in the static limit the self-energy (5.30) reduces to the counterterm mass (5.14), as it should.

Unfortunately the system defined by (5.25), (5.26) is unsuitable for numerical implementation [90]. This follows from the conserved energy of the system

$$E = \int d^3x \frac{1}{2} \left[ (\mathbf{E}^b)^2 + (\mathbf{B}^b)^2 + 3\omega_{\text{pl}}^2 \int \frac{d\Omega}{4\pi} W^b(x, \mathbf{v}) W^b(x, \mathbf{v}) - 2g^2 N T a^{-1} \int \frac{d^3\hat{p}}{(2\pi)^3} \hat{\Omega}_{\mathbf{p}}^{-2} W^b(x, \mathbf{v}_{\text{lat}}) W^b(x, \mathbf{v}_{\text{lat}}) \right], \quad (5.32)$$

with  $\mathbf{B}$  the chromo-magnetic field and  $b$  the adjoint index. The energy is unbounded from below and this means that the system is unstable. Perturbatively there is no problem, the effect of the counterterm particle distribution function is precisely neutralized by the hard modes of the classical gauge fields. However in a non-perturbative lattice simulation the evolution of the particle density and the hard modes will differ, which means that after some time the (wrong) effect of the counterterm particle distribution function is no longer compensated by the hard modes, and the fields will (exponentially) blow up.

## 5.6 Two stable lattice models

### 5.6.1 Model with lattice dispersion relation

The goal is now to obtain a model that is defined on the lattice, that is stable and can be used to calculate IR-sensitive real-time properties of a non-Abelian plasma without linear divergences. Such a model should meet the following three requirements:

1. In the small lattice spacing limit the continuum HTL equations of motion should be obtained.
2. Counterterms for the linear divergences (on the lattice) should be included.

### 3. The energy must be bounded from below.

As a reminder, the model considered in the previous section failed to have bounded energy. To obtain a model with a bounded energy one may consider a model where the modes inducing the finite renormalization have the same dispersion relation as the counterterm modes. In this section we focus on a model where both the counterterm modes and the modes generating the finite renormalization satisfy a lattice dispersion relation. Perhaps we should warn the practical-minded readers that the model considered below will not allow for a useful continuum limit. Those readers may be more interested in the next section, where the other possibility of enforcing the continuum dispersion relation on the counterterm modes is explored

To obtain HTL equations where the both types of modes satisfy a lattice dispersion relation, we do not match to a continuum quantum theory as in the previous section, but to a quantum theory on the lattice, with a (small) lattice spacing  $a_S$ . The trick is that we can then combine the required generation of quantum HTL's and classical counterterms into one distribution function  $\delta\tilde{N}(x, \hat{p})$ , where  $\hat{p}$  is the dimensionless lattice momentum. With this distribution function the Vlasov equations (in the  $A_0^b = 0$  gauge) become

$$D_\mu^{bc} F^{\mu\nu c}(x) = j^{\nu b}(x) = 2gN \int \frac{d^3\hat{p}}{(2\pi)^3} V_{\text{lat}}^\nu \delta\tilde{N}^b(x, \hat{p}), \quad (5.33)$$

$$\partial_t \delta\tilde{N}^b(x, \hat{p}) - \mathbf{v}_{\text{lat}} \cdot \mathbf{D}^{bc} \delta\tilde{N}^c(x, \hat{p}) = -g\mathbf{v}_{\text{lat}} \cdot \mathbf{E}^b(x) \partial_{\hat{\Omega}_{\hat{p}}} \tilde{N}(\hat{\Omega}_{\hat{p}}), \quad (5.34)$$

with  $x = (t, \mathbf{x})$ , where the time  $t$  is continuous and the position  $\mathbf{x}$  is an element of a cubic lattice with (large) lattice spacing  $a_L$ . The dimensionless momentum  $\hat{p}$  is restricted to the first Brillouin zone  $|\hat{p}_i| < \pi$ , the dimensionless energy is  $\hat{\Omega}_{\hat{p}} = 2\sqrt{\sum_i \sin^2(\hat{p}_i/2)}$  and the velocity is  $v_{\text{lat}}^i = \partial_{\hat{p}_i} \hat{\Omega}_{\hat{p}}$ .

The lattice spacing has been scaled out of the above equations and enters only in the equilibrium distribution function  $\tilde{N}$ . The distribution function  $\tilde{N}$  should contain a contribution that generates, after solving (5.34), the quantum HTL source and a contribution that generates the counterterms for the classical divergences. The important step is now to allow for different lattice spacings  $a_L, a_S$  in the the different parts of the equilibrium distribution function

$$\tilde{N}(\hat{\Omega}_{\hat{p}}) = a_S^{-2} n^S(\hat{\Omega}_{\hat{p}}) - a_L^{-2} n_{\text{cl}}^L(\hat{\Omega}_{\hat{p}}), \quad (5.35)$$

with

$$n^S(\hat{\Omega}_{\hat{p}}) = \frac{1}{e^{\hat{\Omega}_{\hat{p}}/(a_S T)} - 1},$$

$$n_{\text{cl}}^L(\hat{\Omega}_{\hat{\mathbf{p}}}) = \frac{Ta_L}{\hat{\Omega}_{\hat{\mathbf{p}}}}, \quad (5.36)$$

and  $T$  the temperature of the system.

To see that the model (5.33) and (5.34) contains the counterterms for the linear divergences it is useful to introduce the field

$$\tilde{W}^b(x, \hat{\mathbf{p}}) = \delta\tilde{N}^b(x, \hat{\mathbf{p}}) / \left(-g\tilde{N}'(\hat{\Omega}_{\hat{\mathbf{p}}})\right), \quad (5.37)$$

where  $\tilde{N}'(\hat{\Omega}_{\hat{\mathbf{p}}}) = \partial_{\hat{\Omega}_{\hat{\mathbf{p}}}} \tilde{N}(\hat{\Omega}_{\hat{\mathbf{p}}})$ . It satisfies the equation

$$\partial_t \tilde{W}^b(x, \hat{\mathbf{p}}) - \mathbf{v}_{\text{lat}} \cdot \mathbf{D}^{ab} \tilde{W}^c(x, \hat{\mathbf{p}}) = \mathbf{v}_{\text{lat}} \cdot \mathbf{E}^b(x). \quad (5.38)$$

The source can be split into a part generating the finite quantum HTL source and a part subtracting the linear divergent classical source

$$j_{\text{ind}}^{\nu b} = j_{\text{fin}}^{\nu b} - j_{\text{ct}}^{\nu b}. \quad (5.39)$$

In terms of the field  $\tilde{W}$  these sources read

$$j_{\text{fin}}^{\nu b} = 2g^2 N \int \frac{d^3 p_S}{(2\pi)^3} V_{\text{lat}}^\nu n'(\Omega_S) \tilde{W}^b(x, \mathbf{p}_S a_S), \quad (5.40)$$

$$j_{\text{ct}}^{\nu b} = 2g^2 N \int \frac{d^3 p_L}{(2\pi)^3} V_{\text{lat}}^\nu n'_{\text{cl}}(\Omega_L) \tilde{W}^b(x, \mathbf{p}_L a_L), \quad (5.41)$$

with  $\mathbf{p}_S = a_S^{-1} \hat{\mathbf{p}}$ ,  $\Omega_S = a_S^{-1} \hat{\Omega}_{\hat{\mathbf{p}}}$  and similar for  $\mathbf{p}_L, \Omega_L$ . Both sources (5.40) and (5.41) are covariantly conserved.

Written in dimensionful quantities we recognize the source  $j_{\text{ct}}$  (5.41) as the classical HTL source on a lattice with lattice spacing  $a_L$ . The difference with the perturbative model of the previous section is the choice of the finite renormalization. The source  $j_{\text{fin}}$  (5.40) is the quantum HTL source on a lattice with lattice spacing  $a_S$ . To extract continuum results from this model we should require  $a_S^{-1} \gg T$ . Also  $a_L$  cannot be too large, since the relevant field configurations for the sphaleron rate have size  $(g^2 T)^{-1}$ . Therefore we should at least require  $a_L^{-1} \gg g^2 T$ . However, as Bödeker [27] has shown, modes of spatial size  $(gT)^{-1}$  give corrections of  $\mathcal{O}(1)$ ; to take these corrections into account requires a smaller lattice spacing  $a_L^{-1} \gg gT$ .

To ensure the stability of the model (5.33) and (5.34) we demand that the energy,

$$E = \int d^3 x \frac{1}{2} \left[ (\mathbf{E}^b)^2 + (\mathbf{B}^b)^2 + 2N \int \frac{d^3 \hat{\mathbf{p}}}{(2\pi)^3} \delta\tilde{N}^b(x, \hat{\mathbf{p}}) \delta\tilde{N}^b(x, \hat{\mathbf{p}}) / \tilde{N}'(\hat{\Omega}_{\hat{\mathbf{p}}}) \right], \quad (5.42)$$

**Table 5.1:** The maximum value of  $a_S^{-1}/T$  given the ratio  $a_L/a_S$ . This follows from the requirement that the energy is bounded from below.

$a_L/a_S$	1.1	1.5	2	5	10	20	25	50	100	1000
$\max(a_S^{-1})/T$	0.31	0.64	0.86	1.36	1.68	1.97	2.06	2.33	2.59	3.42

is bounded from below. This leads to the requirement

$$-\tilde{N}'(\hat{\Omega}_{\hat{\mathbf{p}}}) > 0. \quad (5.43)$$

For  $\hat{\mathbf{p}} = 0$ , this requirement implies  $a_S < a_L$ , which is in accordance with the general idea that the classical theory is matched to a quantum theory with a smaller lattice spacing.

The function  $-\tilde{N}'(\hat{\Omega}_{\hat{\mathbf{p}}})$ , with  $a_S < a_L$ , decreases from plus infinity at  $\hat{\Omega}_{\hat{\mathbf{p}}} = 0$ , to its minimum below zero, after which it increases and asymptotically reaches zero. The maximum value of the dimensionless energy is  $\hat{\Omega}_{\hat{\mathbf{p}}} = 2\sqrt{3}$ . Demanding that

$$-\tilde{N}'(2\sqrt{3}) > 0, \quad (5.44)$$

together with  $a_S < a_L$  is sufficient for (5.43) to hold for any  $\hat{\mathbf{p}}$ . In this way, we obtain a maximum value for  $a_S^{-1}$  given the ratio  $a_L/a_S$ . In table 5.1 the smallest possible lattice spacings  $a_S$  are listed for some values of the ratio  $a_L/a_S$ .

The conclusion is that it is possible to match a real-time classical lattice theory, with lattice spacing  $a_L$ , to a real-time quantum lattice theory at smaller lattice spacing  $a_S$ . But that this is restricted by the constraint that the energy must be bounded from below. Given the lattice spacing of the classical theory this restricts the lattice spacing of the quantum theory to which can be matched.

We see from table 5.1 that in order to obtain continuum-like HTL contributions, the ratio  $a_L/a_S$  should be very (exponentially) large. Since we want  $a_L^{-1} \gg gT$ , the coupling  $g$  should be chosen extremely small. For instance, if we fix  $a_S^{-1} = 2.59T$ , then stability requires  $a_L/a_S \geq 100$ , so  $a_L^{-1} \leq 2.59 \cdot 10^{-2}T$  and  $g \ll 2.59 \cdot 10^{-2}$ .

The very small coupling that is required to reach the continuum limit makes this model useless for practical purposes. It is interesting to

note, however, that matching to a quantum lattice model is not a problem. Rather, the problem is to match lattice with the continuum than classical with quantum. In the next section we will discuss an approximate matching of lattice classical to continuum quantum that may be useful for numerical calculations.

### 5.6.2 Model with a continuum dispersion relation

The other approach that we want to investigate is a model where we enforce the continuum dispersion relation on the counterterm modes. Such a model has the advantage that instead of a 6+1d field  $\delta N$ , a 5+1d auxiliary field  $W^b(x, \hat{\mathbf{v}}_{\text{lat}})$ , that depends only on the direction of the velocity  $\hat{\mathbf{v}}_{\text{lat}} = \mathbf{v}_{\text{lat}}/|\mathbf{v}_{\text{lat}}|$ , can be used. The counterterms that we obtain in this model are not exact, but for the calculation of the Chern-Simons diffusion rate they provide a reasonable approximation.

The model that we consider is given by the replacement of the induced source (5.26) by the expression

$$j_{\text{app}}^{\nu b}(x) = 3\omega_{\text{pl}}^2 \int \frac{d\Omega}{4\pi} V^\nu W^b(x, \mathbf{v}) - 2g^2 N T a^{-1} \int \frac{d^3 \hat{\mathbf{p}}}{(2\pi)^3} \hat{\Omega}_{\mathbf{p}}^{-2} |\mathbf{v}_{\text{lat}}| \tilde{V}_{\text{lat}}^\nu W^b(x, \hat{\mathbf{v}}_{\text{lat}}), \quad (5.45)$$

with  $\tilde{V}_{\text{lat}}^\nu = (1, \hat{\mathbf{v}}_{\text{lat}})$ . We use this construct since it reproduces the induced vector current for a field configuration with  $W^b(x, \hat{\mathbf{v}}_{\text{lat}}) = W^b(x, \mathbf{v}_{\text{lat}})$ . And the vector current is essential in the dynamics of the soft fields. The density is then determined by requiring current conservation  $D_\mu^{bc} j_{\text{app}}^{\mu c} = 0$ . As a consequence the induced density  $j_{\text{HTL,ct}}^{0b}$  in (5.26) is not correctly reproduced by the density  $j_{\text{app}}^{0b}$ . This can be understood as follows, changing the velocity of the particles and requiring current conservation either the vector current or the density can remain unaltered. The expression (5.45) is the lattice equivalent of the approximation for the induced source used by Iancu in [56].

We may also write (5.45) as

$$j_{\text{app}}^{\nu b}(x) = \int \frac{d\Omega}{4\pi} m^2(\mathbf{v}) V^\nu W^b(x, \mathbf{v}), \quad (5.46)$$

with the velocity dependent mass

$$m^2(\mathbf{v}) = 3\omega_{\text{pl}}^2 - 2g^2 N T a^{-1} \int \frac{d^3 \hat{\mathbf{p}}}{(2\pi)^3} \hat{\Omega}_{\mathbf{p}}^{-2} |\mathbf{v}_{\text{lat}}| \delta^S(\mathbf{v} - \hat{\mathbf{v}}_{\text{lat}}). \quad (5.47)$$

The second term contains a linear divergence in the direction  $\mathbf{v} = (1, 1, 1)/\sqrt{3}$  [90] and logarithmic divergences in directions  $\mathbf{v} = (1, 1, s)/\sqrt{2 + s^2}$  with  $-1 < s < 1$  (and directions related by symmetry). Therefore, the mass and the energy are not strictly positive. To obtain a bounded energy some averaging over the direction of the velocity  $\mathbf{v}$  should be performed. This can be achieved by expanding the field  $W^b(x, \mathbf{v})$  in spherical harmonics

$$W^b(x, \mathbf{v}) = \sum_{lm} W_{lm}^b(x) Y_{lm}(\mathbf{v}), \quad (5.48)$$

and keeping a finite number terms. The induced source can then be written as

$$j_{\text{app}}^\nu(x) = \sum_{lm} a_{lm}^\nu W_{lm}(x), \quad (5.49)$$

with coefficients

$$a_{lm}^\nu = \int \frac{d\Omega}{4\pi} m^2(\mathbf{v}) V^\nu Y_{lm}(\mathbf{v}). \quad (5.50)$$

Given the lattice spacing  $a$ , the requirement that the energy is bounded from below, puts an upper bound  $l_{\text{max}}$  on allowed values of  $l$ . It was found in [29] that the Chern-Simons diffusion rate is insensitive to  $l_{\text{max}}$  for even  $l_{\text{max}}$ . In the following we will therefore focus on the approximation made in (5.45).

As was already mentioned, the approximation (5.45) changes the charge density. For instance, for the coefficient  $a_{00}^0$  we have

$$a_{00}^0 = m_D^2 - 2g^2 NT a^{-1} \int \frac{d^3\hat{p}}{(2\pi)^3} \hat{\Omega}_{\mathbf{p}}^{-2} |\mathbf{v}_{\text{lat}}|. \quad (5.51)$$

Comparing (5.51) with (5.16), we see that the expression (5.45) does not correctly reproduce the counterterm for the Debye mass. This implies that the current is not suitable to describe the behavior of fields at length scale  $(gT)^{-1}$ .

To see whether the approximation (5.45) is valid for fields at the length scale  $(g^2T)^{-1}$ , we consider the spatial components of the counterterm self-energy generated by the source (5.45) (for  $l_{\text{max}} \rightarrow \infty$ )

$$\Pi_{\text{app}}^{ij}(q_0, \mathbf{q}) = \Pi_{\text{HTL}}^{ij}(q_0, \mathbf{q}) - \Pi_{\text{app,ct}}^{ij}(q_0, \mathbf{q}), \quad (5.52)$$

with

$$\Pi_{\text{app,ct}}^{ij}(q_0, \mathbf{q}) = 2g^2 NT a^{-1} \int \frac{d^3\hat{p}}{(2\pi)^3} \hat{\Omega}_{\mathbf{p}}^{-2} |\mathbf{v}_{\text{lat}}| \frac{\hat{v}_{\text{lat}}^i \hat{v}_{\text{lat}}^j q_0}{q_0 + i\epsilon - \hat{v}_{\text{lat}} \cdot \mathbf{q}}, \quad (5.53)$$

which should be compared with the classical self-energy (5.28). It is important to realize that the relevant fields for the Chern-Simons diffusion rate we are interested in, have typical momenta of order  $q_0 \sim g^4 T$ ,  $q \sim g^2 T$  [12], see section 3.9. For the gauge fields that are relevant for the Chern-Simons diffusion rate  $q_0 \ll |q|$  and we may neglect  $q_0$  in the denominator of the counterterm (5.53) and the classical self-energy (5.28). We then note that these two expressions are equal and that they cancel. For these fields the effective theory is finite and reproduces the HTL contributions.

However, as was realized by Bödeker [27], interactions between semi-hard and soft fields give corrections to the dynamics of the soft fields which are not suppressed by powers of  $g$ . On the contrary, even  $\log(1/g)$  enhanced contributions arise, resulting in the Chern-Simons diffusion rate [27]

$$\Gamma_{CS} = \left[ \kappa_1 \log \frac{1}{g} + \kappa_2 \right] g^{10} T^4. \quad (5.54)$$

The counterterms in the approximated source (5.45) and the classical HTL's do not cancel for the semi-hard modes (with momenta  $q_0, q \sim gT$ ). Therefore the semi-hard modes are sensitive to the cut-off  $a^{-1}$ .

The leading log contribution arises from the IR-sensitive part of the contribution of the semi-hard modes with momenta  $k_0 \ll k \sim \mu$ , with  $\mu \sim g^2 T$  an IR cut-off. For these momenta the approximation is correct to leading order. Therefore a calculation of the Chern-Simons diffusion rate with approximation (5.45) produces the correct leading-log contribution, that is the coefficient  $\kappa_1$  in (5.54) is independent of the lattice spacing.

The  $\mathcal{O}(1)$  correction from the semi-hard modes does depend on the cut-off. An estimate of the cut-off dependence can be obtained from a comparison of the classical HTL self-energy (5.28) with the counterterm (5.53). To be explicit, we compare the diagonal components at zero spatial momentum

$$\Pi_{\text{cl}}^{ii}(q_0, \mathbf{q} = 0) = 2g^2 N T a^{-1} \int \frac{d^3 \hat{p}}{(2\pi)^3} \hat{\Omega}_{\mathbf{p}}^{-2} |\mathbf{v}_{\text{lat}}|^2 = 0.26 g^2 N T a^{-1}, \quad (5.55)$$

$$\Pi_{\text{app}}^{ii}(q_0, \mathbf{q} = 0) = 2g^2 N T a^{-1} \int \frac{d^3 \hat{p}}{(2\pi)^3} \hat{\Omega}_{\mathbf{p}}^{-2} |\mathbf{v}_{\text{lat}}| = 0.34 g^2 N T a^{-1}. \quad (5.56)$$

Comparing the difference between (45) and (46) with the HTL self-energy at zero spatial momentum  $\Pi_{\text{HTL}}^{ii}(q_0, \mathbf{q} = 0) = 3\omega_{\text{pl}}^2 = g^2 T^2/3$ , we obtain an estimate for the maximal error of about 25% for  $a^{-1} = T/\hbar$ . However, the semi-hard modes that give the  $\mathcal{O}(1)$  correction have space-like momenta  $q_0 < |q|$  [28]. For these modes we expect (5.53) to be a better approximation to the classical self-energy (5.28).

Besides the mismatch between classical HTL's and the counterterms from (5.45), the lattice spacing dependence of  $\kappa_2$  depends on the magnitude of the  $\mathcal{O}(1)$  correction from the semi-hard modes. Especially when the soft modes dominate the contribution to  $\kappa_2$  this model is suitable for a calculation of the Chern-Simons diffusion rate.

## 5.7 Conclusion

In this chapter, we studied the linear divergences in classical  $SU(N)$  gauge theories at finite temperature. Counterterms for these divergences can be incorporated in an (induced) source. Although the divergences are non-local the equations of motion including these counterterms can be given in a local form by introducing auxiliary fields. In the continuum a subtraction in the plasmon frequency is sufficient to render the classical theory free of linear divergences. For a lattice theory this is not the case.

We have presented two lattice models that are stable. The first matches the classical lattice model to a real-time quantum lattice theory with a small lattice spacing  $a_S$ . The requirement that the energy is bounded, presents a lower bound on  $a_S$ , given the lattice spacing  $a_L$  of the classical model. To obtain the continuum limit  $a_L$  has to be extremely large, which requires an unrealistically small coupling  $g$  to keep the interesting excitations on the lattice. In the second model we argued that the restriction to auxiliary fields depending on the direction of the velocity allows for a reasonable approximation (5.45) for the calculation of quantities dominated by fields with momenta  $(q_0, q) \sim (g^4 T, g^2 T)$ , such as the Chern-Simons diffusion rate.

## 6 Baryon-number generation in the broken phase

### 6.1 Introduction

One of the important cosmological observations that may provide information about physics beyond the standard model is given by the matter anti-matter asymmetry in the universe [19, 73]. Quantitatively the asymmetry may be expressed by the ratio between the baryon-number density and the photon density [101]

$$\frac{n_B}{n_\gamma} = (1.55 - 4.45) \times 10^{-10}. \quad (6.1)$$

The problem is to explain the observation (6.1) without assuming a special initial state for the universe<sup>1</sup>.

In the introduction of this thesis we have already described the standard scenario for electroweak baryogenesis. This scenario requires the electroweak phase-transition to be strongly first-order. For experimentally allowed Higgs masses this requirement is not satisfied by the standard model [64, 107]. Hence the standard scenario does not provide an explanation of the observed baryon asymmetry within the standard model. Extensions of the standard model, such as the minimal supersymmetric standard model, may allow for a phase-transition strong enough to generate (sufficient) baryons. However with the increasing experimental lower bound on the Higgs mass, for such models the parameter space consistent with the observed baryon asymmetry becomes quite small [37, 39]. This has triggered the search for alternative scenario's for baryogenesis at the electroweak scale. For instance, recently scenario's have been studied where baryon production occurs at the end of inflation during or after preheating [47, 51, 74].

---

1. To state the problem completely we have to specify the value of some conserved charges [69]. We do not assume special initial conditions and take for the difference between baryon and lepton number  $B - L = 0$ , hypercharge  $Y = 0$  and isospin  $T_3 = 0$ .

We study a different scenario. It requires the electroweak phase-transition to be weakly first-order. Therefore, this scenario will not provide an explanation of the observed asymmetry (6.1) within the standard model also. But, for extended models the allowed Higgs mass lies below that for the standard scenario.

The scenario discussed here is based on the following. At high temperatures, there is an effective potential for the baryon number given by the free energy at given baryon number,  $F(B)$ . Before the phase transition in the symmetric phase this potential is symmetric and quadratic for small baryon-number densities, we write  $F(B) = \alpha B^2$ . In equilibrium the expectation value of the baryon number vanishes:  $\langle B \rangle = 0$ . During the phase transition, when the particles acquire a mass by the Higgs mechanism, the potential will change to  $F(B) = \alpha' B^2$ , with  $\alpha' < \alpha$ . Also in the broken phase the baryon-number expectation value vanishes in equilibrium. But, the point is that when C and CP-violation is present the baryon-number expectation value may acquire a non-zero value after the transition before it relaxes to its equilibrium value zero. If the Higgs expectation value has grown enough to effectively stop baryon-number violating processes before this relaxation, the baryon-number will remain at its non-zero value and baryons will have been created.

To handle baryon-number violation in a non-equilibrium situation is extremely complicated (at least when linear response theory does not apply). Therefore most of this chapter deals with a simpler situation, namely with a system in equilibrium without potential  $F(B) = 0$ . In this case, the expectation value  $\langle B \rangle$  is constant. We assume that initially it is zero, then for all times the expectation value vanishes. However, the distribution function of the baryon number may develop an asymmetry. We will show this happens indeed. In particular, we will argue that the position of the maximum of the distribution will not remain at  $B = 0$ , but move as  $B \sim \delta t$ , with  $\delta$  the strength of the CP-violation. (The analysis is based on an expansion in  $\delta$ , it may well be that the  $\mathcal{O}(\delta^2)$  contribution will change this behavior. But for  $t \sim \delta^{-1}$  we expect this linear increase or decrease in time.) To keep the expectation value equal to zero this means that the tail of the distribution function is much larger in the direction opposite of which the peak moves.

Let us now sketch how such an asymmetric developing distribution may lead to the a temporary non-zero baryon-number expectation value when the effective potential is included. We consider an initial distribution that is peaked more sharply around  $B = 0$  than the equilibrium distribution (the situation after the first-order phase transition in the above described

scenario). Then the peak of the distribution will start to move (say towards positive baryon-number), and there will develop a long tail in the negative baryon-number direction. After some time the effect of the potential will manifest itself for the tail. Then it can no longer compensate for the peak at positive baryon-number. As a consequence the expectation value of the baryon-number will grow. This continues until the peak of the distribution feels the potential, after which the expectation value will decrease and finally reach its equilibrium value zero. As mentioned above, to generate a lasting non-zero baryon number the baryon-changing processes should be effectively stopped before equilibrium is reached.

Before we will study the above ideas in more detail, we will review first some of the basics of (electroweak) baryogenesis. In the next section we will first discuss general requirements for baryon-number generation first which were formulated by Sakharov.

## 6.2 Sakharov requirements

In 1967 Sakharov was the first to address the problem of baryon number generation [108]. He noted that there are three requirements to be met:

1. baryon-number non-conservation,
2. C- and CP-violation,
3. departure from equilibrium.

Since we are interested in the possibility of baryogenesis at the electroweak scale, we consider if and how these requirements may be satisfied in the standard model.

1. baryon-number non-conservation

As was discovered by 't Hooft [54] baryon-number is not conserved. This is due to the anomaly equation

$$\partial_\mu j_B^\mu = \frac{3g^2}{32\pi^2} F_{\mu\nu}^a \tilde{F}^{\mu\nu a}, \quad (6.2)$$

with baryon current  $j_B^\mu$ , the SU(2) field strength  $F_{\mu\nu}^a$ , its dual  $\tilde{F}_{\mu\nu}^a = \frac{1}{2}\epsilon_{\mu\nu\rho\sigma} F^{\rho\sigma}$ , and gauge coupling  $g$ . Together with the vacuum structure of the SU(2)-Higgs sector of the standard model. (The contribution of the U(1)-fields to the anomaly equation is not given in (6.2). Since, due to the trivial vacuum structure of the U(1)-fields, such a contribution cannot lead to a permanent change in baryon-number.) A transition from one (classical) vacuum to the

next in the positive (negative) Chern-Simons direction yields a change in baryon-number of  $+3(-3)$ . In the broken phase these vacua are separated by energy barriers. At zero temperature, transitions from one vacuum to another occur through instanton processes, and the rate of baryon-number non-conservation is very much suppressed. At high temperatures however, the system can go over the barrier due to thermal fluctuations. Then the transition rate is proportional to the Boltzmann factor  $\exp -\beta E_{\text{sph}}$ , where  $E_{\text{sph}}$  is the energy of the minimal energy configuration at the barrier, called the sphaleron. This sphaleron energy is  $E_{\text{sph}} = \text{"number"} \times 4\pi v/g$ , with  $v$  is the expectation value of the Higgs field. The "number" depends on the Higgs mass, for typical values of about 100 – 300 GeV the "number" is approximately 2. At zero temperature the Higgs vacuum expectation value  $v \approx 250$  GeV determines the sphaleron energy  $E_{\text{sph}} \approx 10$  TeV. In the next section we will discuss sphaleron transitions in more detail.

## 2. C- and CP-violation

In the standard model C symmetry is violated. In our scenario (as in most scenario's for electroweak baryogenesis) C-violation is included through the relation (6.2).

Also CP-violation is present in the standard model, namely in the CKM-matrix. However an order of magnitude estimate of CP-violation in the CKM-matrix indicates that it is too small to account for the observed matter-antimatter asymmetry [106,111]. In extensions of the standard model, such as the minimal supersymmetric standard model and the two Higgs doublet model, the amount of CP-violation may be sufficient. We will use the effective action approach and include CP-violation through the following nonrenormalizable dimension-eight operators

$$S_{CP} = \int d^4x \frac{1}{M^4} \left[ \delta_{CP}^1 (D_\rho \phi)^\dagger (D^\rho \phi) - \delta_{CP}^2 \frac{1}{4} F_{\rho\sigma}^a F^{\rho\sigma a} \right] \frac{3g^2}{32\pi^2} F_{\mu\nu}^b \tilde{F}^{\mu\nu b}, \quad (6.3)$$

where the mass  $M$  and the coefficients  $\delta_{CP}^1, \delta_{CP}^2$  can (in principle) be expressed in the parameters of a fundamental theory. The action (6.3) contains the lowest-dimensional operators in the SU(2)-Higgs effective action that contribute to the asymmetry (6.1). We will see that the dimension-six operator  $\phi^\dagger \phi F_{\mu\nu}^a \tilde{F}^{\mu\nu a}$  does not contribute to the baryon asymmetry in the scenario that we study here.

## 3. departure from equilibrium.

We first recall the reasoning for the necessity for a departure from equilibrium. There are basically two arguments for this. One states that if we start with an initial state with zero baryon-number and end up in a state with non-zero baryon number, somewhere between the final and initial state the system must have been out of equilibrium (see e.g. [106]). Another, stronger statement is that in equilibrium the baryon-number expectation value is zero (see e.g. [105]). The argument runs as follows. The equilibrium value of the baryon number  $B$  is given by

$$\langle B \rangle_{\text{eq}} = \text{Tr} e^{-\beta H} B, \quad (6.4)$$

where we have assumed that conserved charges (such as the difference between lepton- and baryon-number) are zero. Note that we did not include a chemical potential for the baryon-number, since it is not a conserved quantity. Using the fact that the Hamiltonian  $H$  is CPT-even and that  $B$  is CPT-odd, the manipulations

$$\begin{aligned} \text{Tr} e^{-\beta H} B &= \text{Tr} e^{-\beta H} [\text{CPT}][\text{CPT}]^{-1} B \\ &= \text{Tr} [\text{CPT}] e^{-\beta H} [\text{CPT}]^{-1} B \\ &= \text{Tr} e^{-\beta H} [\text{CPT}]^{-1} B [\text{CPT}] \\ &= -\text{Tr} e^{-\beta H} B \end{aligned} \quad (6.5)$$

show that

$$\langle B \rangle_{\text{eq}} = 0. \quad (6.6)$$

The standard scenario for electroweak baryogenesis assumes that the electroweak phase-transition was strongly first-order. This provides then the necessary departure from equilibrium.

In the scenario that we study here, the departure from equilibrium is introduced by the change in the effective potential for the baryon-number during the weakly first-order phase-transition. The required strength of the phase transition for our scenario to work is determined by the time-scale that the baryon-number expectation value differs from zero after the phase transition, because the stronger the transition the faster sphaleron transitions are effectively stopped and baryon-number is conserved.

### 6.3 Sphaleron transitions

Since sphaleron transitions form the crucial physical process in scenarios for electroweak baryogenesis, we will review these first.

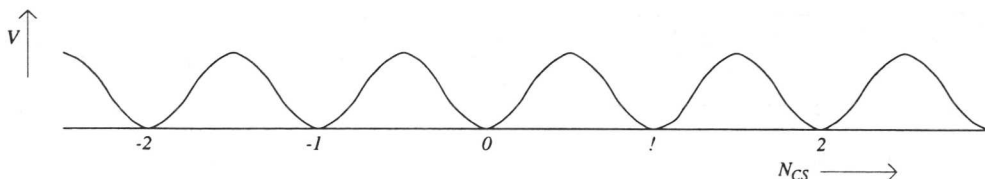


**Figure 6.1:** The potential of  $N_{CS}$  without baryons.

The anomaly equation relates the baryon number  $B$  to the Chern-Simons number  $N_{CS}$

$$\begin{aligned} B(t) - B(0) &= 3 [N_{CS}(t) - N_{CS}(0)] \\ &= \frac{3g^2}{32\pi^2} \int_0^t dt \int d^3x F_{\mu\nu}^a \tilde{F}^{\mu\nu a}. \end{aligned} \quad (6.7)$$

This equation relates the change in baryon number to the time evolution of the gauge fields. The practical implication is that  $B$ -changing processes can be studied by focusing on the gauge field dynamics. And we will do so in the following.

Here, we will take the baryon density equal to zero, in the next section we will review the effect of a non-zero baryon density.

The potential of the Chern-Simons number along the minimal-energy path<sup>2</sup> is sketched in fig. 6.1. The different (classical) vacua are separated by an energy barrier. As already mentioned in the introduction, at zero-temperature the transitions from one vacuum to another occur through tunneling and are very much suppressed. At high temperatures however the system can go over the barrier. The transition rate is [9, 69, 75]

$$\Gamma_{\text{sph}} \sim \exp -\beta E_{\text{sph}}, \quad (6.8)$$

in the broken phase.

The physical picture is that once in a while the mode along the Chern-Simons direction gets thermally activated and can cross the energy barrier. After the transition to the neighboring vacuum at the right or left, this mode gets damped and loses its energy to the other modes. Subsequently, another transition will take place after some time. When the temperature is small compared to the energy barrier between different vacua ( $T \ll E_{\text{sph}}$ ), it is

2. The sphaleron has zero modes [9], for example those related to simple translations and rotations. Therefore there is not a unique minimal energy path.

expected that subsequent transitions are uncorrelated. This implies that the system follows a random walk and one expects that

$$\langle [N_{CS}(t) - N_{CS}(0)]^2 \rangle = V\Gamma_{\text{sph}}t, \quad (6.9)$$

with  $V$  the volume of the system. The sphaleron rate equals the Chern-Simons diffusion rate.

In section 6.4 we will show that in the presence of CP-odd operators, the probabilities for a transition to the right or left differ, with the effect that the most probable value of  $N_{CS}$  grows linearly in time.

### 6.3.1 Including a baryon density

The non-conservation of baryon-number, although required for baryogenesis, poses also a serious problem. Namely, a once created baryon asymmetry may be washed out by sphaleron transitions. To discuss this issue, we review the sphaleron rate in the presence of a baryon density [9, 69].

A useful starting point is the free energy at a given baryon number [69]

$$F(B) = \frac{237}{216} \frac{B^2}{VT^2}, \quad (6.10)$$

where we assumed that the difference between baryon and lepton number  $B - L = 0$  and that the baryon density is small:  $B/V \ll T^3$ . Equation (6.10) holds when the temperature is much larger than the masses of the fermions. The coefficient  $\alpha$  used in the introduction as coefficient of the quadratic part of the potential  $F(B)$  in the symmetric phase may be read off from (6.10). The other coefficient  $\alpha'$  differs by a mass correction, as will be discussed later on.

As before, it is assumed that, in the broken phase, the sphaleron transitions are slow, so that after a transition the system is thermalized (in that baryon sector) before the next transition. Then one may use (6.10) as an effective potential that generates a force towards  $B = 0$ . Hence, at non-zero baryon-density the rate towards positive  $N_{CS}$ ,  $\Gamma^\uparrow$ , will differ from the rate towards negative  $N_{CS}$ ,  $\Gamma^\downarrow$ . The rate equation reads

$$\dot{B} = 3V (\Gamma^\uparrow - \Gamma^\downarrow), \quad (6.11)$$

with

$$\Gamma^{\uparrow(\downarrow)} = \Gamma_{\text{sph}} \left[ 1 - (+) \frac{3}{2} \beta \partial_B F(B) \right], \quad (6.12)$$

where we defined the discretized derivative  $\partial_B F(B) = [F(B+3) - F(B)]/3$ . The number 3 in (6.11) and the discretized derivative comes from the fact that the baryon number is changed by that amount in one transition. From (6.10), (6.11), and (6.12), one obtains the result [69]

$$\dot{B} = -\frac{237}{24} \Gamma_{\text{sph}} \frac{B}{T^3}. \quad (6.13)$$

It follows that an initial baryon number will (exponentially) decrease in time.

As already mentioned in the introduction, in the standard scenario for electroweak baryogenesis the baryon asymmetry is generated at the electroweak phase-transition. To avoid the wash out of baryon number, it is required that  $\Gamma_{\text{sph}}$  is sufficiently small after the phase transition. Since the sphaleron energy is proportional to the Higgs expectation value  $v$ , it is required that  $v$  is sufficiently large directly after the phase transition. This can be translated in a model-dependent upper-bound on the Higgs mass. For the standard model the requirement of a first-order phase transition allows for a Higgs mass  $m_H \lesssim 72$  GeV [64, 107]. Also requiring that a generated asymmetry is not washed out, one can bring down the upper bound to 45 GeV [24]. Since, the experimental lower bound on the Higgs mass is now 106 GeV, this scenario will not work within the Standard model. For the minimal supersymmetric standard model (MSSM) the upper bound on the Higgs mass reads 116 GeV (this upper bound depends on the allowed values for the mass of the heavy stop. If one restricts this mass to values below 1 TeV one can bring down the upper bound on the Higgs mass to 107 GeV) [37, 39]. A thorough discussion of the allowed parameter space in the MSSM may be found in references [37, 39].

#### 6.4 Effect of CP-violation on the rate

The Chern-Simons number  $N_{CS}$  is a CP-odd operator. Therefore the inclusion of the CP-odd operators in (6.3) may break the symmetry between sphaleron transitions towards positive and negative Chern-Simons number. We study the effect of the CP-violating operators in (6.3) on the motion along a particular path, that goes from a vacuum to the sphaleron. We use the path of Manton [83] and parameterize it by the time-dependent coordinate  $\Theta$  (in [83] this coordinate is called  $\mu$ ). This path is not the minimal energy path which was constructed in [5]. But we expect that the precise path will not be important for the following rather general arguments and

that the final result is sufficient as an order of magnitude estimate. We use the following parameterization for the fields

$$\text{gauge} \quad A_\mu^a \sigma^a = \frac{-2i}{g} f(r) [\partial_\mu U(\Theta)] U^{-1}(\Theta), \quad (6.14)$$

$$\text{Higgs} \quad \phi = \frac{1}{2} \sqrt{2} v h(r) U(\Theta) \begin{pmatrix} 0 \\ 1 \end{pmatrix}, \quad (6.15)$$

with the  $\Theta$ -dependent SU(2)-matrix

$$U(\Theta) = \frac{1}{r} \begin{pmatrix} z & x + iy \\ -x + iy & z \end{pmatrix} \sin \Theta + \begin{pmatrix} i & 0 \\ 0 & -i \end{pmatrix} \cos \Theta. \quad (6.16)$$

The functions  $f$  and  $h$  satisfy the boundary conditions

$$\begin{aligned} f &\rightarrow 0 & h &\rightarrow 0 & r &\rightarrow 0, \\ f &\rightarrow 1 & h &\rightarrow 1 & r &\rightarrow \infty. \end{aligned} \quad (6.17)$$

The parameterization (6.14), (6.15) is a non-static generalization of the fields considered in [71, 83]. It is convenient, since the field strength vanishes for  $r \rightarrow \infty$ . As is verified in appendix 6.A, this parametrization yields the correct Chern-Simons number for the sphaleron configuration.

We use Ansatz b of Klinkhamer and Manton [71] for the functions  $f$  and  $h$

$$f(\rho) = \begin{cases} \frac{\rho^2}{A(A+4)} & \rho \leq A \\ 1 - \frac{4}{A+4} \exp[\frac{1}{2}(A - \rho)] & \rho \geq A \end{cases}, \quad (6.18)$$

$$h(\rho) = \begin{cases} \frac{\sigma B + 1}{B(\sigma B + 2)} \rho & \rho \leq B \\ 1 - \frac{B}{\sigma B + 2} \frac{1}{\rho} \exp[\frac{1}{2}(A - \rho)] & \rho \geq B \end{cases}, \quad (6.19)$$

with  $\rho = gvr$  and  $\sigma = (\lambda/2g^2)^{\frac{1}{2}}$ . The parameters  $A, B$  are determined by minimizing the energy for the static field configuration at  $\Theta = \frac{1}{2}\pi$ . Then the static fields provide a very good approximation for the sphaleron configuration at  $\Theta = \frac{1}{2}\pi$  [71]. In this way the parameters depend only on the Higgs mass at zero temperature. We take  $M_H = 230$  GeV for which  $A = 1.15$  and  $B = 1.25$  [71] (the parameters depend only slightly on the Higgs mass;

also for a Higgs mass of about 100 GeV the following calculations are expected to provide a reasonable estimate).

Now that the dynamics has been restricted to the path described by (6.19) and (6.18) we may rewrite the SU(2)-Higgs action  $S$  and the CP-violating action (6.3) in terms of the coordinate  $\Theta$

$$S = \frac{4\pi v}{g} \int dt \left[ (a_1 + a_2 \sin^2 \Theta) \frac{\dot{\Theta}^2}{(gv)^2} - (a_3 \sin^2 \Theta + a_4 \sin^4 \Theta) \right], \quad (6.20)$$

$$S_{CP} = \frac{4\pi v^2}{M^4} \int dt (b_1 \delta_{CP}^1 + b_2 \delta_{CP}^2 + b_3 \delta_{CP}^2 \sin^2 \Theta) \dot{\Theta}^3 \sin^2 \Theta, \quad (6.21)$$

where we have neglected total time-derivatives. Had we included the dimension-six operator  $\phi^\dagger \phi F \tilde{F}$ , it would only have given a total time-derivative. The coefficients  $a_1, a_2, a_3, a_4, b_1, b_2,$  and  $b_3$  are given by the integrals

$$a_1 = \int_0^\infty d\rho \rho^2 \left[ (\partial_\rho f)^2 + \frac{1}{2} h^2 (1-f)^2 \right] = 2.51, \quad (6.22)$$

$$a_2 = 8 \int_0^\infty d\rho f^2 (1-f)^2 = 1.35, \quad (6.23)$$

$$a_3 = \int_0^\infty d\rho \left[ 4(\partial_\rho f)^2 + \frac{1}{2} (\partial_\rho h)^2 + h^2 (1-f)^2 - 2fh(1-f)(1-h) + f^2(1-h)^2 \right] = 1.58, \quad (6.24)$$

$$a_4 = \int_0^\infty d\rho \left[ 2f^2(1-f)^2 + 2fh(1-f)(1-h) - f^2(1-h)^2 + \frac{1}{4}(1-h^2)^2 \right] = 0.53, \quad (6.25)$$

$$b_1 = \frac{9}{2} \int_0^\infty d\rho h^2 (\partial_\rho f) f (1-f)^3 = 0.14, \quad (6.26)$$

$$b_2 = 9 \int_0^\infty d\rho (\partial_\rho f)^3 f (1-f) = 0.096, \quad (6.27)$$

$$b_3 = 72 \int_0^\infty d\rho \frac{1}{\rho^2} (\partial_\rho f)^3 f (1-f)^3 = 0.23. \quad (6.28)$$

In terms of the coordinate  $\Theta$  the CP-transformation is simply

$$\Theta \rightarrow -\Theta. \quad (6.29)$$

The action  $S_{CP}$  (6.21) is CP-odd and CPT-even. The effect of these CP-odd operators on sphaleron transitions is studied in the next section.

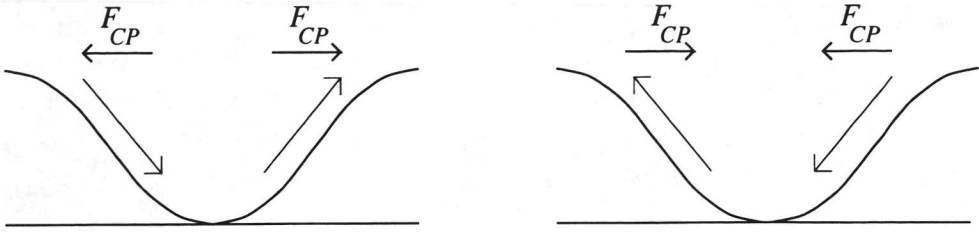


**Figure 6.2:** The force  $F_{CP}$  for a motion to the right (left figure) and a motion to the left (right figure).

### 6.4.1 Asymmetry

The CP-odd action (6.21) introduces a velocity-dependent force in the equations of motion. For the moment we ignore the  $\sin \Theta$ -dependence in the action (6.21), and denote this force as

$$F_{CP} = -\delta \dot{\Theta} \ddot{\Theta}, \quad (6.30)$$

with  $\delta$  a positive coefficient that can be expressed in the parameters in the CP-odd action (6.21). This force points in the direction of motion when the system moves from the vacuum towards the sphaleron at  $N_{CS} = +\frac{1}{2}$ , whereas the force is opposite to the direction of motion when the motion is towards the sphaleron at  $N_{CS} = -\frac{1}{2}$ , see fig 6.2. As a consequence, the system will find it easier to cross the barrier to the right than to the left. Therefore, the probability of crossing the barrier to the right,  $P^\uparrow$ , is larger than the probability of crossing the barrier to the left,  $P^\downarrow$ . This difference in probabilities implies that the diffusion of the Chern-Simons number will evolve in an asymmetric manner. This, however, does not imply that the Chern-Simons number develops a non-zero expectation value. Indeed, from the fact that the average velocity vanishes in equilibrium, it follows that it will not. The asymmetry will manifest itself in the distribution function of the Chern-Simons number and expectation values such as  $\langle N_{CS}^3 \rangle$ . In a non-equilibrium situation, the asymmetric evolution may result in a non-zero expectation value of  $N_{CS}$ . In the following, we will estimate the asymmetry in the probabilities.

To obtain a quantitative estimate for the effect of the CP-odd terms on the motion over the barrier, we consider the shift in the energy caused by the extra CP-violating terms (6.21)

$$E_{CP}(\Theta, \dot{\Theta}) = \frac{8\pi v^2}{M^4} (b_1 \delta_{CP}^1 + b_2 \delta_{CP}^2 + b_3 \delta_{CP}^2 \sin^2 \Theta) \dot{\Theta}^3 \sin^2 \Theta. \quad (6.31)$$

Especially the typical energy shift at the sphaleron configuration is important. To calculate this energy shift, we need the typical velocity  $\dot{\Theta}$ . To zeroth-order in  $\delta_{CP}^1$  and  $\delta_{CP}^2$  the velocity has a Gaussian distribution at the sphaleron and we find

$$\langle \dot{\Theta}^2 \delta(\Theta - \frac{1}{2}\pi) \rangle = \frac{(gv)^3 T}{4\pi v^2 (a_1 + a_2)}, \quad (6.32)$$

where the  $\delta$ -function enforces that the average over the velocity is taken at the sphaleron configuration. With this estimate for the velocity we find for the typical energy shift

$$\delta E_{\text{sph}} = \frac{1}{\sqrt{\pi} v M^4} (b_1 \delta_{CP}^1 + b_2 \delta_{CP}^2 + b_3 \delta_{CP}^2) \left[ \frac{(gv)^3 T}{(a_1 + a_2)} \right]^{\frac{3}{2}}, \quad (6.33)$$

which provides a quantitative measure for the amount of CP-violation.

As an estimate for  $P^\uparrow$  we may take the probability that a configuration at the barrier moves in the positive Chern-Simons direction

$$P^\uparrow = \langle \delta(\Theta - \frac{1}{2}\pi) H(\dot{\Theta}) \rangle / \langle \delta(\Theta - \frac{1}{2}\pi) \rangle, \quad (6.34)$$

where  $H(\dot{\Theta})$  is the Heaviside function. In a similar manner  $P^\downarrow$  can be calculated. We get

$$P^{\uparrow(\downarrow)} = \frac{1}{2} + (-)0.80 \beta \delta E_{\text{sph}}. \quad (6.35)$$

In the estimate for these probabilities in the presence of CP-violating interactions (6.3) an uncertainty arises from the path that we have chosen, because the fields (6.14) and (6.15) do not satisfy the (SU(2)-Higgs) equations of motion. However, for  $\Theta = \frac{1}{2}\pi$ ,  $\dot{\Theta} = 0$  these fields do provide a very good approximation to the solution of the (static) field equations [71]. Hence, we expect that close to the sphaleron and for small velocities  $\dot{\Theta} \ll gv$ , the estimates (6.33) and (6.41) provide a reasonable approximation. The parametric dependence on  $g$ ,  $v$ ,  $M$ , and  $T$  is expected to be correct.

The asymmetry in the probabilities of moving left or right at the sphaleron configuration implies that there is a difference in the average velocity of configurations that move left or right. To consider the average velocity along the  $\Theta$ -trajectory at the sphaleron for configurations that move to the right is

$$v^\uparrow = \langle |\dot{\Theta}| H(\dot{\Theta}) \delta(\Theta - \frac{1}{2}\pi) \rangle / \langle H(\dot{\Theta}) \delta(\Theta - \frac{1}{2}\pi) \rangle \quad (6.36)$$

For configurations moving in the opposite direction the average velocity is

$$v^\downarrow = \langle |\dot{\Theta}| H(-\dot{\Theta}) \delta(\Theta - \frac{1}{2}\pi) \rangle / \langle H(-\dot{\Theta}) \delta(\Theta - \frac{1}{2}\pi) \rangle \quad (6.37)$$

From the observation that the flux vanishes (this is discussed in section 6.4.4)

$$\langle \dot{\Theta} \delta(\Theta - \frac{1}{2}\pi) \rangle = \langle |\dot{\Theta}| H(\dot{\Theta}) \delta(\Theta - \frac{1}{2}\pi) \rangle - \langle |\dot{\Theta}| H(-\dot{\Theta}) \delta(\Theta - \frac{1}{2}\pi) \rangle = 0, \quad (6.38)$$

it follows that the asymmetry in the probabilities (6.35) results in a difference in the average velocities (6.36) and (6.37). In particular, when  $\delta E_{\text{sph}} > 0$  we have

$$v^\downarrow > v^\uparrow. \quad (6.39)$$

Further, we note that the asymmetry in the velocities and probabilities vanishes at  $\Theta = 0$ , but is everywhere else of the same sign. This means that if we consider the time evolution of the probability distribution it will not only spread due to diffusion, but also develop an asymmetry. Namely, since the average velocity towards negative Chern-Simons numbers is larger, the tail of the distribution in the negative Chern-Simons direction will be longer than the tail in the positive direction.

As mentioned in the introduction of this chapter, we will argue that the peak of the distribution will increase linearly in time. We should remark here, that the above derived asymmetry in the the probabilities is not sufficient to conclude that this will happen. This may be illustrated by the following simple model. Consider a particle on a one-dimensional lattice, that has a probability of 2/3 of moving one step to the right and a probability 1/3 of moving two steps to the left. In this way the average flux is zero, as it should in equilibrium, see subsection 6.4.4. It is easy to derive that for this simple system the peak of the probability distribution function remains located at the initial position of the particle.

The notion that the peak of the distribution moves, is based on the argument presented in the next section. Here we conjecture that the velocity of the peak is proportional to the asymmetry in the probabilities. We write

$$\langle N_{\text{CS}}(t) - N_{\text{CS}}(t_{\text{in}}) \rangle_{\text{mp}} = V \left( \Gamma^\uparrow - \Gamma^\downarrow \right) (t - t_{\text{in}}), \quad (6.40)$$

with  $V$  the volume. The brackets  $\langle \dots \rangle_{\text{mp}}$  denote the peak of the distribution function. The difference in rates towards negative or positive Chern-Simons number is expected to be proportional to the difference in the probabilities (6.35)

$$\Gamma^\uparrow(\downarrow) = \Gamma_{\text{sph}} [1 + (-) c\beta\delta E_{\text{sph}}], \quad (6.41)$$

where  $c$  is a coefficient of order one.

### 6.4.2 Alternative derivation

Here we present the argument that the asymmetry in the distribution function will manifest itself also through a linear increase of the most probable Chern-Simons number.

We define an effective force for the random walk by averaging the force (6.30) over one transition

$$\bar{F}_{CP} = \frac{1}{\pi} \int_0^\pi d\Theta F_{CP}. \quad (6.42)$$

Inserting (6.30) we get

$$\begin{aligned} \bar{F}_{CP} &= -\frac{\delta}{\pi} \int_0^\pi d\Theta \dot{\Theta} \ddot{\Theta} \\ &= -\frac{\delta}{\pi} \int_{t_b}^{t_e} dt \dot{\Theta}^2 \ddot{\Theta}, \end{aligned} \quad (6.43)$$

where  $t_b$  is time that the system starts its barrier-crossing motion, and  $t_e$  is the time it ends in the other vacuum. We find

$$\bar{F}_{CP} = -\frac{\delta}{3\pi} (v_e^3 - v_b^3), \quad (6.44)$$

where  $v_b$  is the velocity at the beginning of the motion and  $v_e$  is the velocity at the end. When the temperature is much smaller than the sphaleron energy,  $T \ll E_{\text{sph}}$ , the velocity  $v_b$  is much larger than the average velocity. Due to damping from the coupling to other degrees of freedom  $v_e$  will be closer to the average velocity, and (in most transitions) smaller than  $v_b$ . Hence,

$$\bar{F}_{CP} > 0. \quad (6.45)$$

Note that in this derivation the damping by the modes plays an essential role. It may be remarked that the difference between the velocities  $v_b$  and  $v_e$  is only present sufficiently deep in the broken phase, where  $T \ll E_{\text{sph}}$ . Here the velocity  $v_b$  has to be exceptionally large to cross the barrier. Especially in the symmetric phase it is to be expected that on average the begin velocity and end velocity on average are equal (in the symmetric phase the begin- and endpoint of a crossing is not even well-defined). Therefore, we expect that in the symmetric phase the rates  $\Gamma^\uparrow$  and  $\Gamma^\downarrow$  are equal.

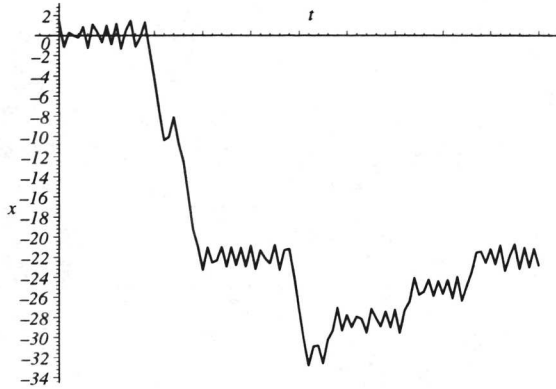


**Figure 6.3:** A numerical solution of the equations of motion that follow from the Lagrangian (6.46) at an energy equal to six.

### 6.4.3 Numerical check

In this section we present a numerical analysis to verify the linear growth of the Chern-Simons number (6.40). We consider the model system

$$L = \frac{1}{2} \left[ \dot{x}^2 + \frac{1}{6} \dot{x}^3 + \frac{1}{36} \dot{x}^4 \right] - 2 \sin(x)^2 + \sum_{i=1}^2 L_{\text{od}}(\dot{x}_i, x_i) - V_{\text{int}}(x, x_i). \quad (6.46)$$

Here the coordinate  $x$  plays the role of Chern-Simons number. The  $\dot{x}^3$ -term is the analog of the CP-violating operator. We have also included a  $\dot{x}^4$ -term so that the energy is bounded for large velocities. The coefficient of this term is sufficiently large that the Lagrangian is convex and a Hamiltonian analysis is possible. The other degrees of freedom  $x_i$ ,  $i = 1, 2$ , introduce the necessary damping. The Lagrangian of these degrees of freedom and the interaction potential reads

$$L_{\text{od}}(\dot{x}_i, x_i) = \frac{1}{2} \dot{x}_i^2 - \frac{1}{2} x_i^2, \quad (6.47)$$

$$V_{\text{int}}(x, x_i) = \frac{1}{30} \left[ \sin(x)^2 + \sum_{i=1}^2 x_i^2 \right]^2. \quad (6.48)$$

In fig. 6.3 a numerical solution to the equations of motion is shown for an energy equal to six. We see the expected behavior: there are transitions from one vacuum to another, and in between transitions the system oscillates around the local minimum of the potential. Of interest is the long-time

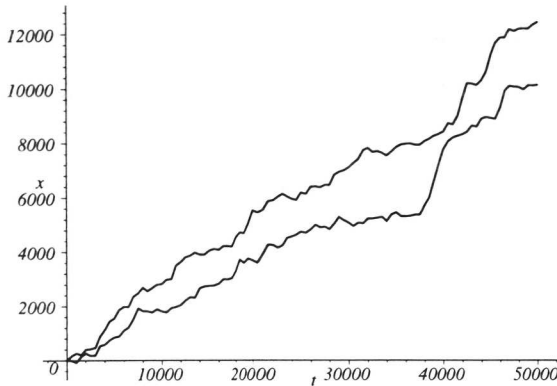


**Figure 6.4:** Two solutions to the equations of motion that follow from the Lagrangian (6.46) at an energy equal to six.

behavior of the system. From (6.40) we expect a linear growth of the angle  $x$ . In fig. 6.4 the long-time behavior of two solutions is shown both with an energy equal to six. The initial conditions of the two solutions are chosen such, that they interchange under the transformation  $x \rightarrow -x$ . Therefore without the  $\dot{x}^3$ -term in the Lagrangian the solution curves should interchange under  $x \rightarrow -x$  (which indeed they do). We see that with the (equivalent of a CP-odd)  $\dot{x}^3$ -term in the Lagrangian, the angle  $x$  grows linearly in time, even though the fluctuations in  $x$  are quite large. This is in qualitative agreement with (6.40).

We have also performed a more quantitative analysis of the model system (6.46). We solved numerically the equations of motion for 20 different initial conditions with the energy fixed, and the same initial conditions for  $x, p$ :  $x_{\text{in}} = 1.3$ ,  $p_{\text{in}} = 0$ . We let the system evolve for  $t = 200,000$ . For each initial condition the final value of  $x$  is positive, and the average (over initial conditions) differs from 0 by  $10\sigma$ . Hence, for these initial conditions  $x$  grows in time. When we would have taken a thermal average over initial conditions however, the average of  $x$  should remain equal to 0. That we find such a clear increase of the average of  $x$  implies that the system is not ergodic or, at least, that the equilibration time is much larger than 200,000. This conclusion is further supported by simulations where we started with a large part of the energy in the  $x$  and  $p$  coordinates. Then we found that the system moves over the barriers, without slowing down, and without energy redistribution. Also, when we start out with a small amount of energy for the coordinates  $x, p$ , the system stays in one vacuum for extremely long times.

The main point is the following. When the system is not trapped in one vacuum or moves without slowing down over the, that it makes transitions from one vacuum to another in a random fashion, the coordinate  $x$  increases in time. This implies that for thermal initial conditions the peak of the distribution will move towards larger values, in agreement with the arguments in sections 6.4.1 and 6.4.2.

#### 6.4.4 Some remarks on an asymmetric distribution function

Let us first present the argument why in equilibrium the expectation value  $\langle N_{CS}(t) - N_{CS}(0) \rangle$  remains zero, or at least will not grow linear in time. We use again the coordinate  $\Theta$  along the Chern-Simons direction, with conjugate momentum  $p_\Theta$ , and Hamiltonian  $H$ . The Hamiltonian is periodic in  $\Theta$  with period  $\pi$ . To argue that the Chern-Simons number expectation value is zero we should show that  $\langle \Theta \rangle = 0$ .

An argument similar as used in section 6.2 to show that the baryon-number expectation value vanishes (6.6), cannot be given. Since it would rely on the phase-space average

$$\langle \Theta \rangle = Z^{-1} \int dp_\Theta \int_{-\infty}^{\infty} d\Theta \Theta e^{-\beta H}. \quad (6.49)$$

However this quantity is not well defined, since the equilibrium distribution function,  $\exp -\beta H$ , is not normalizable on the full real axis  $\Theta \in ]-\infty, \infty[$ .

Hence we should restrict the equilibrium distribution to a finite interval, for instance  $\Theta \in ]-\frac{1}{2}\pi, \frac{1}{2}\pi]$ . Then we cannot calculate the expectation value of the winding number. But we can calculate the average of its velocity

$$\begin{aligned} \langle \dot{\Theta} \rangle &= \int dp_\Theta \int_{-\frac{1}{2}\pi}^{\frac{1}{2}\pi} d\Theta \dot{\Theta} e^{-\beta H} \\ &= \int dp_\Theta \int_{-\frac{1}{2}\pi}^{\frac{1}{2}\pi} d\Theta \frac{\partial H}{\partial p_\Theta} e^{-\beta H} = 0. \end{aligned} \quad (6.50)$$

The phase space average of the velocity vanishes, also when the kinetic energy is complicated. For an ergodic system this implies that

$$\lim_{t \rightarrow \infty} \frac{1}{t} \int_0^t dt' \dot{\Theta} = 0. \quad (6.51)$$

Hence,  $\Theta$  can not grow linearly in time.

Other asymmetric functions like  $\Theta^3$  may be non-static in equilibrium. The thermal average of the time-derivative  $3\Theta^2\dot{\Theta}$  seems to vanish in a similar manner as for (6.50). However the thermal average is not well defined when  $\Theta$  is not bounded. For the same reason the quantity  $\Theta^2$  may be non-static, as expected for systems where diffusion plays a role. From the argument below (6.38), we infer that  $\langle\Theta^3\rangle$  becomes negative and grows in time.

#### 6.4.5 Fokker-Planck equation

Here we will derive the Fokker-Planck equation for systems with a complicated kinetic energy, as we have encountered in section 6.4. This allows us to verify that the time-evolution of the distribution function may result in an asymmetry.

It may be useful to specify a typical Hamiltonian for the coordinate  $x$  along the Chern-Simons direction and its conjugate momentum  $p$

$$H = \frac{1}{2} (p^2 - \delta p^3 + \delta^2 p^4) + V(x). \quad (6.52)$$

In terms of the velocity the kinetic energy reads

$$\frac{1}{2} (\dot{x}^2 + \delta \dot{x}^3 + \delta^2 \dot{x}^4) + \mathcal{O}(\delta^3). \quad (6.53)$$

The contribution  $+\delta \dot{x}^3$  corresponds to the CP-violating term.

The degree of freedom, that represents the Chern-Simons number, interacts with other modes of the plasma with coordinates  $x_i$ . We assume interactions of the form  $V_{\text{int}}(x, x_i)$  (no interactions involving the momentum  $p$ ). We include this interaction with the other modes by a damping term and a stochastic force in the equations of motion

$$\dot{p} = -\partial_x V(x) - \sigma \dot{x} + \xi, \quad (6.54)$$

$$\dot{x} = v(p) = p - \frac{3}{2} \delta p^2 + 2\delta^2 p^3, \quad (6.55)$$

with

$$\begin{aligned} \langle \xi(t) \rangle &= 0 \\ \langle \xi(t) \xi(t') \rangle &= T \sigma \delta(t - t'). \end{aligned} \quad (6.56)$$

The subtlety in the introduction of the damping and the stochastic force lies in the use of the velocity instead of the momentum in the damping term.

This is motivated as follows. For interactions including only the position  $x$  and not the momentum  $p$ , integrating out the other modes generates a memory kernel involving  $x$  at earlier times. For a slowly varying  $x$  this may be approximated by a damping term. The point is now that this memory kernel involves only the position, and is independent of the kinetic part of the Hamiltonian. Therefore, in a local approximation of the memory kernel time-derivatives of  $x$  naturally occur. This motivates the use of the velocity instead of the momentum in the damping term in (6.54)

From the stochastic equation (6.54) with velocity (6.55), we can derive the Fokker Planck equation using standard methods, see for instance paragraph 3.2 of [120]. The result is

$$\dot{P} = \partial_p \{ T\sigma \partial_p P + [\partial_x V + \sigma v(p)] P \} - v(p) \partial_x P, \quad (6.57)$$

with the probability distribution  $P = P(x, p, t)$ .

We note that the static solution of the Fokker-Planck equation (6.57) is the equilibrium distribution  $\exp -\beta H$ , as expected.

The equilibrium distribution is invariant under the transformations

$$x \rightarrow -x \quad (6.58)$$

and, to order  $\delta$ ,

$$p \rightarrow -p + \delta p^2 + \mathcal{O}(\delta^2). \quad (6.59)$$

But these transformations are not a symmetry of the Fokker-Planck equation (even when the transformations are applied together). This implies that an initial equilibrium distribution restricted to the interval  $x \in [-\frac{1}{2}\pi, \frac{1}{2}\pi]$  may develop an asymmetry. Which according to the arguments in section 6.4.1 will happen indeed.

## 6.5 Baryon-number generation

In this section we study the evolution of the baryon-number expectation value after the phase transition. The basic idea is, as discussed in the introduction, that during the phase-transition the effective potential changes: from  $F(B) \sim \alpha B^2$  to  $F(B) \sim \alpha' B^2$  with  $\alpha' < \alpha$ . The asymmetric evolution of the distribution function of the baryon-number/Chern-Simons number may lead, in this non-equilibrium situation, to a (temporary) non-zero baryon-number expectation value, for a simple example see appendix 6.B. The argument is as follows. When the distribution function spreads, to adjust

itself to the new potential, the tail in the negative baryon-number direction will become larger than the tail in the positive baryon-number direction, as discussed below (6.38). Therefore, the distribution function “feels” the potential in the negative baryon-number direction first. Then the tail in the negative direction can no longer compensate for the positive part of the distribution function. This results in a positive value of the baryon-number expectation value. To generate a lasting asymmetry, it is necessary that the baryon-number is frozen out, before it relaxes back to its equilibrium value, which is zero. Here, we calculate the maximum (largest deviation from equilibrium) baryon-number expectation value possible in this scenario. Then we include a suppression factor to account for the smallness of the deviation from equilibrium. Finally, we estimate the time that the expectation value is non-zero. Which gives a bound on the strength of the phase transition.

To estimate the maximum baryon-number the peak of the distribution function can reach, we superimpose the effect of a non-zero baryon density on the asymmetry of the sphaleron rates, see (6.12) and (6.41). Combining these effects, we find for the rates

$$\Gamma^{\uparrow(\downarrow)}(n_B) = \Gamma_{\text{sph}} \left[ 1 - (+) 0.80 \frac{n_B}{n_\gamma} + (-) c \frac{\delta E_{\text{sph}}}{T} \right], \quad (6.60)$$

where  $n_\gamma = 0.24 T^3$  is the photon density. Similar as in (6.11) the rate equation reads

$$\frac{dn_B}{dt} = 3 \left[ \Gamma^\uparrow(n_B) - \Gamma^\downarrow(n_B) \right]. \quad (6.61)$$

This equation is not CPT-invariant. As explained in section 6.4.2 this is due to the effect of damping. From the rate equation with (6.60) we find the stationary (and stable) solution

$$\left. \frac{n_B}{n_\gamma} \right|_{\text{max}} = 1.25c \frac{\delta E_{\text{sph}}}{T}. \quad (6.62)$$

This provides a maximum that the baryon number can grow in an effective potential  $F(B)$  (6.10).

This maximum value will only be reached for a maximal deviation from equilibrium initially. That is when the initial distribution is much sharper peaked than the equilibrium distribution. In our scenario, after the weakly first-order phase transition, the distribution is not that sharply peaked and we expect a suppression. When we parameterize, as in the introduction, the initial distribution as  $\exp -\alpha B^2$  and the equilibrium distribution as  $\exp -\alpha' B^2$ ,

the suppression factor  $(1 - \alpha'/\alpha)$  may be expected (we find this suppression factor in simple examples, see for instance the one in appendix 6.B). The difference between  $\alpha$  and  $\alpha'$  arises from the mass that the baryons acquire in the broken phase due to the Higgs mechanism. The largest contribution to the difference comes from the top quark mass  $m_t(v_{\text{pt}})$  after the phase transition, (we have indicated the dependence on the Higgs expectation value after the phase transition,  $v_{\text{pt}}$ ). The suppression factor may be estimated as  $(1 - \alpha'/\alpha) \sim m_t(v_{\text{pt}})^2/T^2$ . The precise relation may be calculated by the methods employed in [76]. For the phase-transition temperature  $T \sim 100$  GeV and a typical Higgs expectation value after a weakly first-order phase-transition  $v_{\text{pt}} \sim 70$  GeV, we may estimate  $m_t(v_{\text{pt}})^2/T^2 \sim 0.1$ .

Let us estimate the baryon asymmetry that may be generated in this scenario. We evaluate the maximal baryon-asymmetry (6.62) at the temperature  $T^* \approx v(T^*) \approx 100$  GeV, at which the baryon-number is frozen out [106]. From (6.22)-(6.28), (6.33), and (6.62), we obtain for the resulting baryon-number at  $T = T^*$

$$\left. \frac{n_B}{n_\gamma} \right|_{T=T^*} = (2 \delta_{CP}^1 + 4 \delta_{CP}^2) \times 10^{-4} \left( \frac{100 \text{ GeV}}{M} \right)^4, \quad (6.63)$$

where we have used  $c = 1$  and included the suppression factor  $(1 - \alpha'/\alpha) \sim 0.1$ . The baryon-photon ratio is not constant under expansion of the universe. The relation between the ratio at  $T = T^*$  and now ( $T = T_{\text{now}}$ ) is given by

$$\left. \frac{n_B}{n_\gamma} \right|_{\text{now}} = \frac{g_{*S}(T_{\text{now}})}{g_{*S}(T^*)} \left. \frac{n_B}{n_\gamma} \right|_{T=T^*}, \quad (6.64)$$

with  $g_{*S}$  the (effective) number of particle species contributing to the entropy at a given temperature [73]. We get from  $g_{*S}(T_{\text{now}})/g_{*S}(T^*) = 0.037$  the final result

$$\left. \frac{n_B}{n_\gamma} \right|_{\text{now}} = (7 \delta_{CP}^1 + 16 \delta_{CP}^2) \times 10^{-6} \left( \frac{100 \text{ GeV}}{M} \right)^4. \quad (6.65)$$

In the standard model the magnitude of  $\delta_{CP}^1, \delta_{CP}^2$  is too small (about  $10^{-20}$ ) to explain the observed matter anti-matter asymmetry (6.1). However, for extensions of the standard model  $\delta_{CP}^1, \delta_{CP}^2$  can be as large as  $10^{-3}$  and we see that (6.65) may explain the observed baryon-number excess (6.1), at least when the new mass-scale  $M$  is not too large.

A remaining question is, how long after the phase transition the baryon asymmetry will remain at a substantial fraction of the maximum (6.62). This is important since this time scale determines the window of Higgs expectation

values  $v_{\text{pt}}$  for which the scenario may explain the observed baryon asymmetry (6.1). For instance, if this time scale is short  $v_{\text{pt}}$  should be very close to  $v(T^*)$  to prevent the relaxation back to the equilibrium value  $\langle B \rangle = 0$ .

The typical time scale for a sphaleron transition is  $t_{\text{sph}} \sim (\Gamma_{\text{sph}})^{-1} T^3$ . The time scale to develop the asymmetry is longer, since it is inversely proportional to the asymmetry in the rates  $t_{\text{as}} \sim (\Gamma^\uparrow - \Gamma^\downarrow)^{-1} T^3$ . We do not expect that there is another time scale for the relaxation back to equilibrium, since  $t_{\text{as}}$  determines the time after which the asymmetry starts to “feel” the quadratic potential. The required Higgs expectation value may be obtained by comparing the time scale  $t_{\text{as}}$  to the time scale for sphaleron transitions at the point baryon number freezes out:  $t_{\text{as}} = t_{\text{sph}}(T^*)$ . At the freeze out temperature the sphaleron rate is  $\Gamma_{\text{sph}}(T^*) \sim \exp(-45)$  [111]. We use

$$\Gamma^\uparrow - \Gamma^\downarrow \sim 10^{-6} \Gamma_{\text{sph}}. \quad (6.66)$$

The required Higgs expectation value after the phase transition is determined by

$$10^{-6} \Gamma_{\text{sph}}|_{v=v_{\text{pt}}} > \exp(-45), \quad (6.67)$$

which leads to

$$v_{\text{pt}} > 70 \text{ GeV}. \quad (6.68)$$

This is somewhat lower than the required  $v_{\text{pt}}$  for the standard scenario (see the introduction of this thesis) where the baryons must be frozen out immediately after the transition, this demands  $v_{\text{pt}} > 100 \text{ GeV}$ .

## 6.6 Conclusion

We have shown that in the absence of a baryon density, the dimension-eight CP-odd operators in (6.3) introduce an asymmetry in the diffusion of the Chern-Simons number. This implies that the distribution function of the Chern-Simons number will become asymmetric. We have argued that this effect may lead to baryon-number generation after a weakly first-order electroweak transition. The estimated baryon asymmetry may, depending on the strength of the CP-violation, be sufficient to agree with the observed asymmetry (6.1).

## 6.A Chern-Simons number of the sphaleron

In this appendix we calculate the difference between the Chern-Simons number of the vacuum and sphaleron configuration. The difference in Chern-Simons number is

$$\Delta N_{CS} = \frac{1}{32\pi^2} \int_0^{t_f} dt \int d^3x F_{\mu\nu}^a \tilde{F}^{\mu\nu a}, \quad (6.69)$$

where at the initial time  $t = 0$  the system starts at a classical vacuum, it ends at  $t = t_e$  at a sphaleron.

We calculate the r.h.s. of (6.69) for a (general) motion from a vacuum to a sphaleron along the  $\Theta$ -path. Since we do not evaluate (6.69) for general paths the calculation presented here is not so much a (re-)derivation of the Chern-Simons number of the sphaleron [71], but rather a check on the field parameterization (6.14), (6.15). Using this parameterization, we may rewrite the r.h.s. of (6.69) and we get

$$\Delta N_{CS} = \frac{12}{\pi} \int_0^{t_f} dt \dot{\Theta} \sin^2 \Theta \int_0^\infty dr (\partial_r f) f(1-f). \quad (6.70)$$

We note that the time and spatial integration are factorized. For the spatial integration it is sufficient to know the boundary values of the function  $f$  (6.17). The result is

$$\int_0^\infty dr (\partial_r f) f(1-f) = \frac{1}{6}. \quad (6.71)$$

The time integral can also be easily performed

$$\int_0^{t_f} dt \dot{\Theta} \sin^2 \Theta = \int_0^{\frac{1}{2}\pi} d\Theta \sin^2 \Theta = \frac{1}{4}\pi. \quad (6.72)$$

where we have chosen a path from a vacuum to the nearest sphaleron in the positive  $N_{CS}$  (the value of the integral for paths to other sphalerons differs by an integer times  $\pi/2$ ). The resulting Chern-Simons number is

$$\Delta N_{CS} = \frac{1}{2}, \quad (6.73)$$

in agreement with [71].

### 6.B Simple example of asymmetry generation

We consider a particle in a harmonic potential with Hamiltonian

$$H = \frac{1}{2}(p^2 - \delta p^3 + \delta^2 p^4) + \alpha' x^2, \quad (6.74)$$

which at the initial time  $t = 0$  its position and momentum are distributed according to

$$\rho_{\text{in}} = N \exp -\beta \left[ \frac{1}{2}(p^2 - \delta p^3 + \delta^2 p^4) + \alpha x^2 \right], \quad (6.75)$$

with  $N$  a normalization factor. In the case  $\alpha = \alpha'$ , the system is in equilibrium, and the expectation value of  $x$  vanishes at all later times. When  $\alpha \neq \alpha'$ , we find to first order in  $\delta$

$$\langle x(t) \rangle = \frac{1}{2} \delta \frac{T}{\pi} \left( 1 - \frac{\alpha'}{\alpha} \right) \sin^3 \sqrt{\alpha'} t + \mathcal{O}(\delta^2). \quad (6.76)$$

As expected, the expectation value becomes non-zero, even though the equilibrium expectation value of the system (6.74) vanishes. Since we did not include damping the expectation value remains oscillating.

## Bibliography

- [1] G. Aarts and J. Smit, *Phys. Lett.* **B393** (1997) 395.
- [2] G. Aarts and J. Smit, *Nucl. Phys.* **B511** (1998) 451.
- [3] G. Aarts, in proceedings of *Strong and Electroweak Matter* (SEWM 97), Eger, Hungary, 21-25 May 1997, 267, hep-ph/9707440.
- [4] G. Aarts, B. Nauta, and C. van Weert, *Phys. Rev.* **D61** (2000) 105002.
- [5] T. Akiba, H. Kikuchi and T. Yanagida, *Phys. Rev.* **D38** (1988) 1937.
- [6] J. Ambjørn and A. Krasnitz, *Phys. Lett.* **B362** (1995) 97.
- [7] J. Ambjørn and A. Krasnitz, *Nucl. Phys.* **B506** (1997) 387.
- [8] T. Appelquist and R. Pisarski, *Phys. Rev.* **D23** (1981) 2305.
- [9] P. Arnold and L. McLerran, *Phys. Rev.* **D36** (1987) 581.
- [10] P. Arnold and Espinosa, *Phys. Rev.* **D47** (1993) 3546.
- [11] P. Arnold and C. Zhai, *Phys. Rev.* **D50** (1994) 7603.
- [12] P. Arnold, D. Son, and L. Yaffe, *Phys. Rev.* **D55** (1997) 6264.
- [13] P. Arnold, *Phys. Rev.* **D55** (1997) 7781.
- [14] P. Arnold, in proceedings of *Strong and Electroweak Matter* (SEWM 97), Eger, Hungary, 21-25 May 1997, 3, hep-ph/9706305.
- [15] P. Arnold, D. Son, and L. Yaffe, *Phys. Rev.* **D59** (1999) 105020.
- [16] A. Arrizabalaga, B. Nauta, and C. van Weert, accepted for *Phys. Lett.* **B**.
- [17] M. D'Attanasio and M. Pietroni, *Nucl. Phys.* **B498** (1997) 443.
- [18] M. Le Bellac, *Thermal Field Theory*, (Cambridge University Press, 1996).
- [19] L. Bergström and A. Goobar, *Cosmology and particle astrophysics* (Wiley-Praxis, 1999).
- [20] J. Blaizot and E. Iancu, *Phys. Rev. Lett.* **70** (1993) 3376.
- [21] J. Blaizot and E. Iancu, *Nucl. Phys.* **B390** (1993) 589.
- [22] J. Blaizot and E. Iancu, *Nucl. Phys.* **B417** (1994) 608.
- [23] J. Blaizot and E. Iancu, *Nucl. Phys.* **B421** (1994) 565.
- [24] A. Bochkarev, S. Kuzmin, and M. Shaposhnikov, *Phys. Lett.* **B244** (1990) 275.
- [25] D. Bödeker, L. McLerran, and A. Smilga, *Phys. Rev.* **D52** (1995) 4675.
- [26] D. Bödeker and M. Laine, *Phys. Lett.* **B416** (1998) 169.
- [27] D. Bödeker, *Phys. Lett.* **B426** (1998) 351.
- [28] D. Bödeker, *Nucl. Phys.* **B566** (2000) 402.
- [29] D. Bödeker, G. Moore, and K. Rummukainen, *Phys. Rev.* **D61** (2000) 056003.

- [30] D. Boyanovsky, H. de Vega, R. Holman, S. Prem Kumar, and R. Pisarski, *Phys. Rev.* **D58** (1998) 125009.
- [31] E. Braaten and R. Pisarski, *Nucl. Phys.* **B337** (1990) 569.
- [32] E. Braaten and R. Pisarski, *Phys. Rev. Lett.* **64** (1990) 1338.
- [33] E. Braaten and A. Nieto, *Phys. Rev.* **D51** (1995) 6990.
- [34] E. Braaten and A. Nieto, *Phys. Rev.* **D53** (1996) 3421.
- [35] F. Brandt, J. Frenkel, and J. Taylor, *Phys. Rev.* **D44** (1991) 1801.
- [36] W. Buchmüller and A. Jakovác, *Phys. Lett.* **B407** (1997) 39.
- [37] M. Carena, M. Quiros, and C. Wagner, *Nucl. Phys.* **B524** (1998) 3.
- [38] M. Carrington, T. Hansson, H. Yamagishi, and I. Zahed, *Annals Phys.* **190** (1989) 373.
- [39] J. Cline, G. Moore, *Phys. Rev. Lett.* **81** (1998) 3315.
- [40] A. Cohen, D. Kaplan, and A. Nelson, *Nucl. Phys.* **B349** (1991) 727.
- [41] D. Comelli and M. Pietroni, *Phys. Lett.* **B417** (1998) 337.
- [42] L. Dolan and R. Jackiw, *Phys. Rev.* **D9** (1974) 3320.
- [43] M. van Eijck, R. Kobes, and Ch. van Weert, *Phys. Rev.* **D50** (1994) 4097.
- [44] M. van Eijck, *Thermal field theory and the finite-temperature renormalization group*, thesis, University of Amsterdam (1995), Ch. 2, 3.
- [45] K. Farakos, K. Kajantie, K. Rummukainen, and M. Shaposhnikov, *Nucl. Phys.* **B425** (1994) 67.
- [46] R. Feynman and Vernon, *Ann. Phys.* **24** (1963) 118.
- [47] J. Garcia-Bellido, D. Grigoriev, A. Kusenko, and M. Shaposhnikov, *Phys. Rev.* **D60** (1999) 123504.
- [48] J. Garcia-Bellido and D. Grigoriev, *JHEP* **0001** (2000) 017.
- [49] C. Greiner and B. Müller, *Phys. Rev.* **D55** (1997) 1026.
- [50] D. Grigoriev and V. Rubakov, *Nucl. Phys.* **B299** (1988) 67.
- [51] D. Grigoriev, hep-ph/0006115.
- [52] F. Guérin, *Phys. Rev.* **D49** (1994) 4182.
- [53] P. Henning and R. Fauser, hep-ph/9605372.
- [54] G. 't Hooft, *Phys. Rev. Lett.* **37** (1976) 8.
- [55] C. Hu and B. Müller, *Phys. Lett.* **B409** (1997) 377.
- [56] E. Iancu, *Phys. Lett.* **B435** (1998) 152.
- [57] E. Iancu, in proceedings of the *5th International Workshop on Thermal Field Theories and Their Applications*, Regensburg, Germany, August 10-14, 1998, hep-ph/9809535.
- [58] C. Itzykson and J. Zuber, *Quantum Field Theory* (McGRAW-HILL, 1980).
- [59] A. Jakovác, *Nucl. Phys.* **B521** (1998) 219.

- [60] S. Jeon, *Phys. Rev.* **D52** (1995) 3591.
- [61] S. Jeon and L. Yaffe, *Phys. Rev.* **D53** (1996) 5799.
- [62] K. Kajantie and J. Kapusta, *Ann. Phys.* **160** (1985) 477.
- [63] K. Kajantie, M. Laine, K. Rummukainen, and M. Shaposhnikov, *Nucl. Phys.* **B458** (1996) 90.
- [64] K. Kajantie, M. Laine, K. Rummukainen, and M. Shaposhnikov, *Phys. Rev. Lett.* **77** (1996) 2887.
- [65] K. Kajantie, M. Laine, K. Rummukainen, and M. Shaposhnikov, *Phys. Lett.* **B423** (1998) 137.
- [66] N. van Kampen, *Stochastic processes in physics and chemistry* (North-Holland, 1981).
- [67] J. Kapusta, *Finite-Temperature Field Theory*, (Cambridge University Press, 1989).
- [68] L. Keldysh, *Zh. Eksp. Teor. Fiz.* **47** (1964) 1515 [*Sov. Phys. JETP* **20** (1965) 1018].
- [69] S. Khlebnikov and M. Shaposhnikov, *Nucl. Phys.* **B308** (1988) 885.
- [70] T. Kibble, *J. Phys.* **A9** (1976) 1387.
- [71] F. Klinkhamer and N. Manton, *Phys. Rev.* **D30** (1984) 2212.
- [72] R. Kobes, G. Kunstatter, and A. Rebhan, *Nucl. Phys.* **B355** (1991) 1.
- [73] E. Kolb and M. Turner, *The early universe*, (Addison-Wesley, 1989).
- [74] L. Krauss and M. Trodden, *Phys. Rev. Lett.* **83** (1999) 1502.
- [75] V. Kuzmin, V. Rubakov, and M. Shaposhnikov, *Phys. Lett.* **B155** (1985) 36.
- [76] M. Laine and M. Shaposhnikov, *Phys. Rev.* **D61** (2000) 117302.
- [77] P. Landshoff and A. Rebhan, *Nucl. Phys.* **B383** (1992) 607.
- [78] P. Landshoff and A. Rebhan, *Nucl. Phys.* **B410** (1993) 23.
- [79] K. Landsman and C. van Weert, *Phys. Rep.* **145** (1987) 141.
- [80] K. Landsman, *Nucl. Phys.* **B322** (1989) 489.
- [81] A. Linde, *Phys. Lett.* **B96** (1980) 289.
- [82] R. Kobes, G. Kunstatter, and K. Mak, *Z. Phys.* **C45** (1989) 129.
- [83] N. Manton, *Phys. Rev.* **D28** (1983) 2019.
- [84] G. Moore, *Nucl. Phys.* **B480** (1996) 657.
- [85] G. Moore and N. Turok, *Phys. Rev.* **D55** (1997) 6538.
- [86] G. Moore and N. Turok, *Phys. Rev.* **D56** (1997) 6533.
- [87] G. Moore, *Nucl. Phys.* **B523** (1998) 569.
- [88] G. Moore, C. Hu, and B. Müller, *Phys. Rev.* **D58** (1998) 045001.
- [89] G. Moore, in *Lattice '99*, Pisa, Italy, 1999.
- [90] G. Moore, private communications.
- [91] G. Moore and K. Rummukainen, *Phys. Rev.* **D61** (2000) 105008.

- [92] G. Moore, *JHEP* **0003** (2000) 006.
- [93] S. Nadkarni, *Phys. Rev.* **D27** (1983) 917.
- [94] V. Nair, *Phys. Rev.* **D50** (1994) 4201.
- [95] B. Nauta and C. van Weert, *Phys. Lett.* **B444** (1998) 463.
- [96] B. Nauta and C. van Weert, in proceedings of the *5th International Workshop on Thermal Field Theories and Their Applications*, Regensburg, Germany, August 10-14, 1998, hep-ph/9809378.
- [97] B. Nauta and C. van Weert, *Nucl. Phys.* **B571** (2000) 151.
- [98] B. Nauta, *Nucl. Phys.* **B575** (2000) 383.
- [99] B. Nauta, *Phys. Lett.* **B478** (2000) 275.
- [100] A. Nelson, D. Kaplan, and A. Cohen, *Nucl. Phys.* **B373** (1992) 453.
- [101] K. Olive, *Nucl. Phys. Proc. Suppl.* **80** (2000) 79.
- [102] G. Parisi, *Statistical Field Theory*, (Addison-Wesley Publishing Company, 1988).
- [103] A. Rajantie and M. Hindmarsh, *Phys. Rev.* **D60** (1999) 096001.
- [104] A. Rebhan, *Nucl. Phys.* **B430** (1994) 319.
- [105] A. Riotto and M. Trodden, *Ann. Rev. Nucl. Part. Sci.* **49** (1999) 35.
- [106] V. Rubakov and M. Shaposhnikov, *Phys. Usp.* **39** (1996) 461.
- [107] K. Rummukainen, M. Tsy-pin, K. Kajantie, M. Laine, and M. Shaposhnikov, *Nucl. Phys.* **B532** (1998) 283.
- [108] A. Sakharov, *JETP Lett.* **5** (1967) 24.
- [109] H. Schulz, *Nucl. Phys.* **B413** (1994) 353.
- [110] J. Schwinger, *J. Math. Phys.* **2** (1961) 407.
- [111] M. Shaposhnikov, *Nucl. Phys.* **B299** (1988) 797.
- [112] V. Silin, *Sov. Phys. JETP* **11** (1960) 1136.
- [113] J. Smit, *Nucl. Phys. Proc. Suppl.* **63** (1998) 89.
- [114] D. Son, hep-ph/9707351.
- [115] W. Tang and J. Smit, *Nucl. Phys.* **B482** (1996) 265.
- [116] W. Tang and J. Smit, *Nucl. Phys.* **B510** (1998) 401.
- [117] J. Taylor and S. Wong, *Nucl. Phys.* **B346** (1990) 115.
- [118] H. Weldon, *Phys. Rev.* **D26** (1982) 1394.
- [119] H. Weldon, *Annals Phys.* **271** (1999) 141.
- [120] J. Zinn-Justin, *Quantum Field Theory and Critical Phenomena*, (Clarendon, Oxford, 1989).

## Samenvatting

In deze samenvatting zal ik proberen op begrijpelijke wijze uit te leggen waar dit proefschrift over gaat en waarom dit (voor sommige mensen) interessant genoeg is om vier jaar aan te werken.

In dit proefschrift wordt onderzoek beschreven dat gedaan is naar het gedrag van elementaire deeltjes bij hoge temperatuur. Deze temperatuur is ongeveer  $10^{15} \text{ }^\circ\text{C} = 1.000.000.000.000.000 \text{ }^\circ\text{C}$ . Ter vergelijking, dit is ongeveer 60 miljoen keer zo heet als het binnenste van de zon. Om een eerste idee te krijgen wat er bij zo'n temperatuur gebeurt, kunnen we (in gedachten) een stof tot deze temperatuur verhitten, bijvoorbeeld een ijsblokje. Als dit verwarmd wordt tot boven de  $0 \text{ }^\circ\text{C}$  dan smelt het ijsblokje en ontstaat de vloeistof water. Op microscopisch niveau betekent dit dat de moleculen die op een vaste plaats zaten, nu langs elkaar kunnen bewegen. Bij een verdere verhoging van de temperatuur, tot boven het kookpunt van  $100 \text{ }^\circ\text{C}$ , raken de moleculen volledig los van elkaar, zodat ze vrij door de ruimte kunnen bewegen. Bij het nog verder verhogen van de temperatuur zullen de watermoleculen verder uiteenvallen in steeds kleinere eenheden, namelijk de moleculen in atomen, de atomen in electronen en atoomkernen, en de atoomkernen in protonen en neutronen. De protonen en neutronen vallen uiteindelijk uiteen in quarks en gluonen. De nu ontstane stof wordt het quark gluon plasma genoemd. Dit plasma ontstaat bij de extreem hoge temperatuur van ongeveer  $10^{12} \text{ }^\circ\text{C}$ , de hoogste temperatuur die momenteel in laboratoria bereikt kan worden. Dit jaar heeft men in de deeltjesversneller van CERN enkele keren het quark gluon plasma (voor zeer korte tijd) kunnen maken. De bovengenoemde quarks en gluonen zijn de kleinste of meest elementaire deeltjes die op dit moment bekend zijn.

Een belangrijke reden om het gedrag van deeltjes bij zulke hoge temperaturen te bestuderen is dat het vroege heelal zo heet is geweest. Er hebben toen een aantal belangrijke processen hebben plaatsgevonden die bepalend zijn geweest voor de ontwikkeling en huidige toestand van het heelal. Een voorbeeld is het opmerkelijke feit dat er nu materie is (ijsklontjes, bomen,

aarde, zon, etc.) in plaats van alleen straling (een mogelijke oorzaak hiervan wordt bestudeerd in hoofdstuk 6).

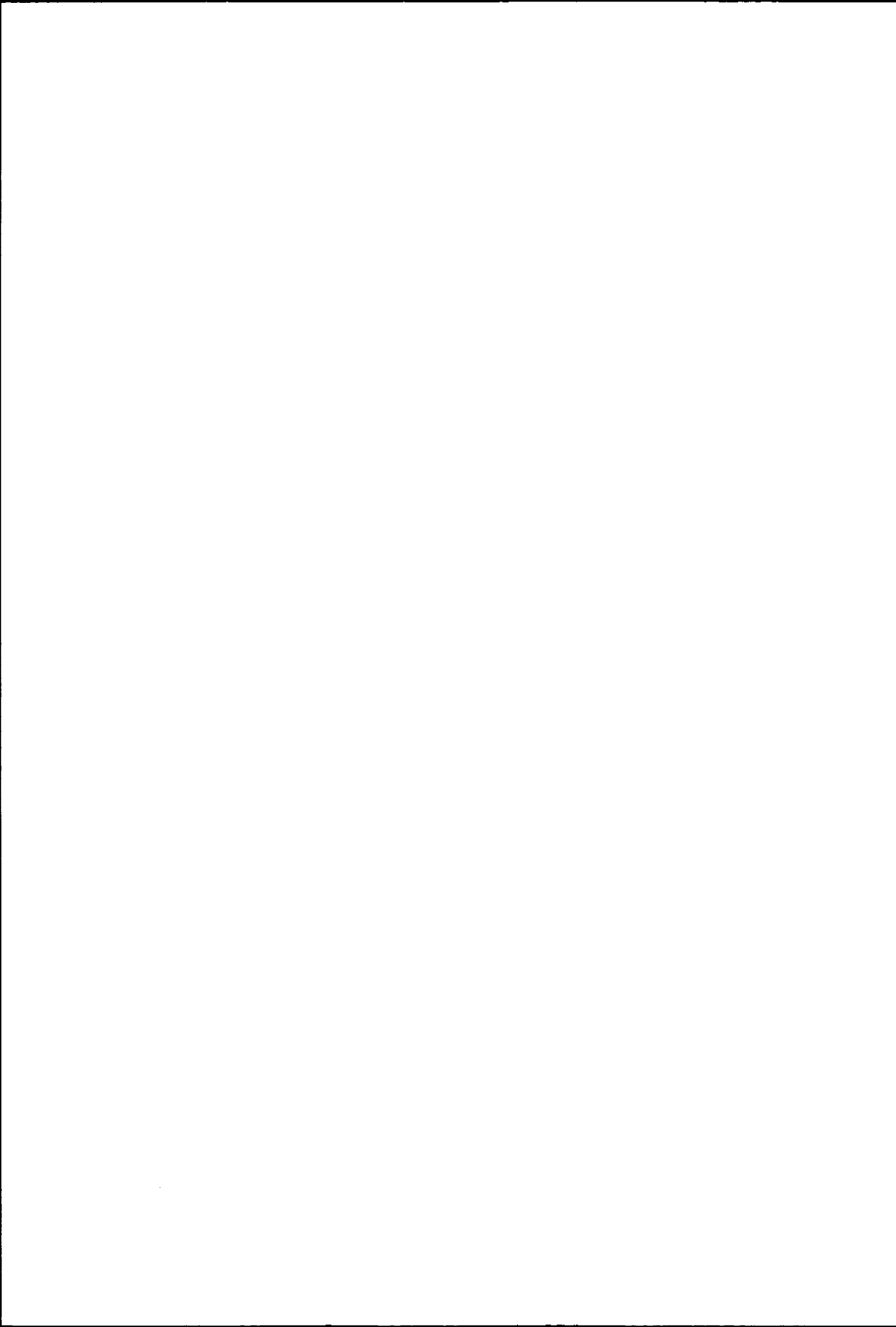
Als men deze processen bestudeert, worden vaak een aantal aannames gemaakt om het probleem te simplificeren. Een belangrijke simplificatie wordt ingegeven door op te merken dat in veel belangrijke processen in het vroege heelal alleen ijkvelden een rol spelen. Voorbeelden van ijkvelden zijn elektrische en magnetische velden. Men kan nu proberen om de processen alleen te beschrijven met ijkvelden, waarbij quarks en electronen (beide geen ijkvelden) worden weggelaten. Bij nadere bestudering blijkt echter dat, alhoewel quarks en electronen zelf geen rol spelen in het proces, ze wel een belangrijke invloed hebben op het gedrag van de ijkvelden. Dit betekent dat deze invloed toch in de beschrijving van de processen moet worden meegenomen. In hoofdstuk 3 wordt beschreven hoe deze invloed op natuurkundig en wiskundig correcte wijze verwerkt kan worden.

De bovenstaande situatie kan misschien met een meer alledaags (zeker in Nederland) voorbeeld verduidelijkt worden, namelijk regen. Hierbij is men geïnteresseerd in het gedrag van de druppels en niet van de lucht. Bij een gesimplificeerde beschrijving van het vallen van een druppel is het dan voor de hand liggend om in eerste instantie alle luchtmoleculen wegtelaten. De druppel is dan bolvormig en valt eenparig versneld naar de grond. Dit is niet correct aangezien door de wrijving met de lucht, de druppels met een constante snelheid vallen en ze de typische druppelvorm krijgen. Een betere beschrijving neemt dus de luchtweerstand mee. Dit is echter nog altijd veel simpeler dan een volledig model op te stellen waarin de beweging van alle luchtmoleculen is verwerkt.

een andere eigenschap van bepaalde processen is dat alleen ijkvelden met een grote golflengte een rol spelen. Vandaar is een tweede simplificatie om alleen ijkvelden te beschouwen met een golflengte groter dan een zekere minimale golflengte  $\lambda_{\min}$ . Hierbij heeft de minimale golflengte een willekeurige zelfgekozen waarde die, om de beschrijving werkelijk te simplificeren, groter wordt gekozen dan de onderlinge afstand van de deeltjes in het plasma. Omdat  $\lambda_{\min}$  willekeurig is, moeten de antwoorden die we vinden in een gesimplificeerde beschrijving (ook wel effectieve beschrijving genoemd) onafhankelijk zijn van  $\lambda_{\min}$ . Dit blijkt echter niet het geval te zijn. In hoofdstuk 4 wordt op systematische wijze de afhankelijkheid van vertex functies van  $\lambda_{\min}$  bestudeerd. Dit is niet alleen belangrijk om te bepalen waar fouten ( $\lambda_{\min}$ -afhankelijkheden) kunnen optreden, maar ook omdat een grote afhankelijkheid van  $\lambda_{\min}$  betekent dat hier de invloed van ijkvelden met korte golflengtes het grootst is. Dit begrip kan leiden tot een betere effectieve

beschrijving.

In hoofdstuk 5 wordt de belangrijkste invloed van ijkvelden met golflengtes korter dan  $\lambda_{\min}$  op ijkvelden met golflengtes langer dan  $\lambda_{\min}$  in de beschrijving meegenomen. Dit kan grotendeels op dezelfde wijze als waarop de electronen in hoofdstuk 3 werden geherintroduceerd. Het belangrijkste verschil is dat er nu voor moet worden gezorgd dat de uiteindelijke resultaten onafhankelijk van  $\lambda_{\min}$  zijn. Of en hoe dat mogelijk is, zijn dan ook het eigenlijke onderwerpen in hoofdstuk 5. Het blijkt dat het afhangt van de wijze waarop  $\lambda_{\min}$  wordt geïntroduceerd of een volledige  $\lambda_{\min}$ -onafhankelijke, correcte beschrijving kan worden gegeven.



## Dankwoord

Een aantal mensen hebben belangrijke directe of indirecte rol gespeeld bij de tot stand koming van dit proefschrift. Hen wil ik graag bedanken.

Allereerst bedank ik mijn promotor Chris van Weert. Chris, bedankt dat ik bij jou kon komen promoveren. Je brede natuurkundige kennis en aanwijzingen hebben me dikwijls gesteund en op het juiste spoor gezet. Ook je onvermoeibare(?) pogingen mij te leren duidelijk op te schrijven hoe een bepaalde berekening of formule tot stand gekomen is, heb ik gewaardeerd. De lezer kan aan de hand van dit proefschrift beoordelen in hoeverre deze pogingen succesvol zijn geweest.

Gert, jou wil ik bedanken voor het aanstekelijke enthousiasme waarmee je dit vakgebied benadert. Gesprekken met jou hadden altijd een motiverende uitwerking op mij. Natuurlijk wil ik je ook bedanken dat je met mij hebt willen samenwerken aan een artikel, welke een belangrijke basis vormde voor hoofdstuk 4. We hebben de afgelopen jaren samen een aantal workshops bezocht, vaak ook samen met Chris en Jan. Ik heb dat altijd heel gezellig gevonden.

Een andere mede-auteur die ik hier bedank is Alejandro. Je kritische vragen en opmerkingen hebben mij dikwijls geholpen bij het schrijven van dit proefschrift.

Ook wil ik graag Jan Smit bedanken voor menig kritische opmerking, die mij tot dieper nadenken aanspoorde. Ik heb veel geleerd van onze discussies.

Ik wil mijn ex-kamergenoot Mark bedanken voor het feit dat hij het bijna tot het laatst met mij in een kamer uitgehouden heeft. Mark, bedankt voor de gezelligheid, ik heb me altijd erg thuis gevoeld in onze gezamenlijke rommel. Ook alle andere instituut-genoten: bedankt voor de goede sfeer op ons instituut.

Mijn vrienden hebben tijdens mijn promotie-onderzoek voor veel ontspanning gezorgd. Dank jullie wel, ik heb erg veel plezier beleefd aan alle

spelletjes, wandelingen en etentjes.

Mijn paranimfen Johan en Steven wil ik speciaal bedanken. Ik hoop dat ik tijdens mijn verdediging niet op jullie hoeft terug te vallen, maar verwacht wel dat jullie je goed op je taak voorbereiden door dit boekje grondig te bestuderen.

Mijn moeder bedank ik voor haar warme belangstelling en steun.

Tenslotte wil ik Annemarie bedanken voor haar rol in mijn leven.

